Detection of Electric Arcs in 42-volt Automotive Systems

by

Joseph Luis

B.S., Electrical Engineering, Massachusetts Institute of Technology (2002)

Submitted to the Department of Electrical Engineering and Computer Science
in partial fulfillment of the requirements for the degree of

Master of Engineering in Electrical Engineering and Computer Science

at the

Massachusetts Institute of Technology

May 21, 2003

Author_____
Department of Electrical Engineering and Computer Science
May 21, 2003

Certified by_____
Markus Zahn
Professor of Electrical Engineering
Thesis Supervisor

Certified by_____
Dr. Thomas Keim
Principal Research Engineer
Thesis Supervisor

Accepted by_____
Arthur C. Smith
Chairman, Department Committee on Graduate Theses

Detection of Electric Arcs in 42-volt Automotive Systems

by
Joseph Luis

Submitted to the Department of Electrical Engineering and Computer Science
on May 21, 2003, in partial fulfillment of the
requirements for the degree of
Master of Engineering in Electrical Engineering and Computer Science

Abstract

The increasing demand of electrical power in today's automobile has led to the research and development of a new 42 V standard. One danger at this new voltage is stable electrical arcing. At the higher voltage, stable electric arcs do not self extinguish and can cause damage to the arcing conductors and cause a fire. This work evaluates possible methods to use to detect and stop electrical arcing before any major damage can occur to the vehicle and more importantly to the passengers. Electronic detection is proposed as the best approach. Arcing current of stable and unstable arcs at ~42 V and ~14 V are produced by the rebuilt apparatus of a previous MIT experiment that used a motor controlled mechanical switch to periodically energize a conductor to produce stable and unstable arcs. Fourier analysis is performed on the measured current waveforms to look for arc signatures in the frequency domain. Fourier analysis on the average of ten spectra of stable arcs showed that there were no consistent features universally present in stable arcs. Current waveforms of real electrical loads are also measured using electrical accessories (windows,door locks, seat adjustment, lights, sunroof, CD changer, radiator cooling fan) on an electrically operational 1997 Mercury Sable and the amplitudes of their frequency spectra are compared to the amplitude of the average arcing spectrum. It is determined that although some electrical loads have recognizable shapes in the frequency domain, the amplitudes of the spectra of the loads and the arcs are of the same order. It is concluded that additional research and development is needed for an improved electronic detection approach to detect and identify electric arcs in 42 V automotive systems.

Thesis Supervisor: Markus Zahn
Title: Professor of Electrical Engineering

Thesis Supervisor: Dr. Thomas Keim
Title: Principal Research Engineer

Acknowledgements

I would like to start by expressing my gratitude to my supervisors, Professor Markus Zahn and Dr. Thomas Keim, whose expertise, understanding, and patience, added considerably to my graduate experience. I would like to thank the MIT/Industry Consortium on Advanced Automotive Electrical/Electronic Components and Systems for giving me the opportunity to work on this project.

Also, I would like to thank Professor George Verghese for taking the time to discuss various aspects of the project. His advice always led to new findings. Alan Wu for explaining the control circuitry of his arcing project and Wayne Ryan for his help in modifying the experimental set-up and bypassing the ignition on the car in the lab.

I appreciate the help of the technical support engineers at National Instruments who spent countless hours on the phone with me to get my LabView code running smoothly.

Finally, I would like to thank my parents who have supported me through all my years at MIT. Without their encouragement I would not have gotten this far and I cannot thank them enough for everything they have done for me.

Contents

List of Figures

List of Tables

Chapter 1

Introduction

Today's automobile is more luxurious and contains more electrical components than ever before. Consequently, the power demands of the automobile are rapidly increasing. A variety of systems including anti-lock brakes, power windows, seat warmers, as well as stereo and navigation systems all require electrical power that was not needed in older vehicles. It has been predicted that by the year 2005, electrical components will demand an average power above 2kW [1]. In 1994, Mercedez Benz and MIT, along with seven other companies, met to develop a higher voltage bus. A 42 V bus was recommended. The MIT/Industry Consortium on Advanced Automotive Electrical/Electronic Systems, which is comprised of researchers at MIT as well as companies from the automotive industry, was formed soon after to investigate the switch to the higher voltage.

1.1 Arcing in a 42 V System

One potentially dangerous issue with the new 42 V bus is electric arcing. In the present 14 V system, current interruptions result in unstable arcs. However, if the voltage source were made high enough(greater than 15 V), a stable discharge would be produced [2]. The large amount of energy in the stable arcs as well as the extremely high temperatures reached can burn wire insulation as well as start fires. On automotive systems, melting insulation and fire can ignite fuel vapors, posing a threat to the passengers.

Arcing can occur anywhere on the wire harness. If the insulation of a wire becomes worn, for example from aging or damage during vehicle maintenance, so that an exposed wire makes contact with the chassis of the car, a parallel arc can occur. In effect, a short circuit is created between the two battery terminals resulting in a high current stable arc. If a wire is cut or if electric contacts separate, a stable series arc can occur. Circuit current is limited by the loads on the car but the high temperatures of the arc and the large amount of energy can still cause fire.

Fuses are presently used to protect the system in overcurrent situations. However, there is a possibility of creating high current stable but intermittent arcs that do not clear the

fuse because the RMS current is below the fuse rating. For example, if a car is on a bumpy road, a damaged wire may make repetitive contact with the chassis. This could create a stable arc during each contact separation but keep the RMS current low enough that the fuse protecting the circuit does not clear. This is a worst case scenario since instantaneous currents are high and the temperature of each arc causes damage to the insulation and melting of the contact materials.

Because of the danger of stable arcing in the 42 V bus, new connectors and other products that are less prone to stable arcing have been developed. Currently, no method exists that can prevent all stable arcs in electrical systems prone to stable arcing. Because of this, a detection method must be developed that can minimize the damage caused by stable arcing. This work focuses on the development of a detection method for arcs in the 42 V automotive system.

1.2 Previous Work

1.2.1 Arcing Energy

The importance of arcing at 42 V was first brought to the attention of the MIT/Industry Consortium by Yazaki Inc. A mechanical chopper was used to make periodic contact with a test wire. On separation, the contacts would create an arc. Battery voltages of 12 V and 36 V were used in the tests and the arcing created was compared. Results were dramatic. Arcing with a 36 V battery source created arcs that burned wire insulation, melted the test wire, and destroyed the blade used to make contact with the test wire. By contrast, arcs at 12 V did much less damage to the contacts.

Further work was done at MIT by extending Yazaki's experiment. A fuse was included in the test circuit and computer control of circuit current duration during contact showed that incidents of periodic arcing that did not clear the fuse could indeed occur [3]. Tests using 12 V and 36 V sources were performed and it was found that arcing energy was 10 to 100 times greater in the case of a 36 V source. Molten copper and steel from the contacts was seen only in the 36 V case, showing the possible dangers of an unprotected 42 V system. Arcing that did not clear the fuse was generally less intense than the arcs produced by the Yazaki work.

1.2.2 Arc Detection

A variety of work has been performed in the field of electric arc detection and is reviewed in detail in Chapter 3. The majority of this detection work has been done in 60 or 50 Hz AC systems and a lesser amount in DC systems.

Such research has been performed by B.D. Russell and his group at Texas A&M University in the detection of arc faults on power distribution feeders. They studied the changes in energy from cycle to cycle on the AC line of various frequency harmonics [4, 5, 6]. These changes in energy between cycles has enabled them to develop algorithms to detect arc faults in AC power systems. Another method of detecting arcs in AC systems was developed at the University of Manitoba in which the asymmetry between the current magnitudes of the positive and negative half cycles of the current are compared in order to determine that a fault is occurring [7].

Arc detection has been performed by detecting arc acoustic, electromagnetic, light, and heat radiation as well. At Schneider Electric Industries, work has been performed in AC systems in which the acoustic emission of a series arc is measured and characterized [8]. Thresholds of sound amplitude and sound duration are used to monitor sound on the busbar and determine when an arc occurs. The power systems research group at the University of Saskatchewan has combined acoustic, electromagnetic, and infrared radiation to produce a more reliable AC arc detection algorithm and to locate where an arc is occurring [9]. The detection of arcing faults by electromagnetic detection has also been performed at the University of Bath where electromagnetic radiation is used to detect and locate arc faults in AC power systems [10].

For detecting arcs in switch gear, busbar, and circuit breaker cubicle systems, The ABB Group has developed a product called the Arc Guard System. Using optical detectors and fiber optics, the Arc Guard System detects large changes in light intensity due to arcing and trips the breaker.

More relevant to automotive applications is arc detection work that has been performed in DC systems, specifically in the telecommunications 48 V DC power system. Research at Bell Communications Research has led to the detection of electric arcs by analyzing the frequency spectrum of the arc current and of normal current operation of the system [11, 12]. This spectrum analysis looks promising as the tested 48 V DC telecommunication system is similar to the proposed 42 V DC. Additional work has also been performed at Hendry Telephone Products in which the spectrum of the current is analyzed by the arc's fractal nature in order to develop proper filters and algorithms to detect arcing in the 48 V DC system [13]. Although slightly more complex, this may be a reasonable future approach

to take for the 42 V automotive system.

1.3 Thesis Scope

The goal of this research is to select and investigate a method of arc detection for use in the new 42 V automotive system. An evaluation of various detection methods and their feasibility in automotive systems is carried out. An electrical method of detection is selected because of its possible advantages in cost and in simplicity. Time and frequency domain analysis of circuit current during arcing events and normal operation is then performed. From the thesis research we conclude that Fourier analysis as well as energy monitoring may not be accurate enough for detecting and identifying arcs in 42 V automotive systems as arc current and normal operation curent have similar frequency spectra. Comparisons are made to previous work in DC systems which have successfully accomplished detection through Fourier analysis to determine the cause of our inability to produce similar results.

1.4 Thesis Organization

An overview of electric arc theory is presented in the following chapter. A discussion of detection methods researched in previous work and their comparisons follows in Chapter 3. An experimental setup that produces 42 V arcs is described in Chapter 4 and analysis of the data is then presented in Chapter 5. Measured circuit current during normal operation and during 14 V arcing on an electrically operational vehicle is presented and analyzed in Chapters 6 and 7. Conclusions and suggestions for future work follow in Chapter 8.

Chapter 2

Arc Physics

Before attempting to detect an arc, we should first understand the physics of arc discharges. Arc discharges can occur in many ways including electrical breakdown of gas between electrodes and by the separation of current-carrying electric contacts. The voltages in the new 42 V automotive system will not be great enough to cause breakdown of air and arc discharges will occur by the drawing apart of current carrying conductors. The following sections describe arc formation and arc characteristics of stable arcs that can occur in a 42 V system.

2.1 Arc Formation

Arcing at the new higher voltage will occur by the separation of energized conductors, creating either a series or a parallel arc. In a series arc, current-carrying electrodes separate, forming a stable arc. The electric load in series with the arcing wire limits the current. In parallel arcs, a current-carrying electrode is grounded, as can happen if a damaged wire touches the grounded chassis, and separation from the grounded electrode forms a parallel arc whose current is limited by the impedance of the chassis and the source.

As the electrodes separate, the surface area of contact becomes smaller. The current flowing in the circuit must then flow through the smaller area of much larger resistance and the current density at the electrodes increases. When the electrodes are near separation, the contact area is so small that the I^2R heating is enough to melt the electrode metals and a liquid metal bridge forms [14]. If the contacts continue to separate, the liquid bridge ruptures explosively. The rupturing is due to boiling at the hottest part of the bridge or because of insufficient surface tension forces in the system to maintain a stable liquid bridge of that length.

After rupture of the liquid bridge, the formation of a stable arc depends on the circuit characteristics, conductor material, as well as the speed at which the conductors are separating. If conditions are met for a stable arc to occur, a short arc follows [2, 14]. The short arc forms when the electrodes are at a distance of approximately 10^{-4}cm and lasts on the order

of 1μs. During this time, electrons fall freely between the cathode and the anode electrodes and rarely make any collisions because the distance between the cathode and the anode are on the order of the electronic mean free path [14]. At this point, the circuit current through the arcing electrodes is dominated by electrons emitted from the cathode that then hit the anode with the energy acquired in the transition from cathode to anode. Because the anode is receiving the majority of the energy of the arc during the short arc, the anode material evaporates at a faster rate. In systems of higher voltage, typically 400 V, the material from the cathode evaporates more quickly because of the Joule heating creating small points on the cathode that boil away [14]. However, in the case of the new automotive voltage, short arcs will be of the "anode" type, in which during short arcing the evaporation of electrode material comes mainly from the anode.

As the electrodes continue to separate, a transition from the short arc to the "long" column is made. Because the separation distance between the electrodes are no longer on the order of the electronic mean free path, electrons cannot freely fall from the cathode to the anode as in the short arc. Collisions now occur during the travel of electrons from the cathode to anode and cathode and anode fall regions develop as described in Section 2.2. The large amount of energy in the stable arc continues to cause damage to the electrodes. If the separation distance of the electrodes continues, the voltage required to sustain the stable arc increases and if the distance of the electrodes becomes large enough the arc will extinguish. If the electrodes stop moving and the stable arc is allowed to persist, the arc will continue until the electrode material is completely evaporated or the energy in the source falls below that necessary to maintain stable arcing conditions.

If the arcing electrodes once again contact each other after arcing, we have a periodic arcing condition. In a car, movement over bumps could cause arcing wires to make repetitive contact. Electrodes under these arcing conditions repeat the process of the rupturing of a liquid metal bridge, a short arc, and the formation of a stable long column. Because of this, major damage can be caused by periodic arcing. The extent of the damage depends on the source voltage and electrode materials. For example, on the 14 V bus, a short arc forms but a stable long column does not form. Periodic contact thus causes minor, if any, damage to the electrodes. At 42 V however, the stable long columns created by separating electrodes can cause major damage to electrodes.

2.2 Arc Regions

When the long column of a stable arc forms, current must be carried by the gas between the electrodes. For this to happen, the gas must become conducting by having charged

carriers either created in the gas or injected from the electrodes. At each of the electrodes there must also be a transition of the circuit current from the electrodes to the gas. This creates three main regions, the cathode fall, anode fall, and the long column with an electric potential distribution shown in Figure 2.1. The electrode column junction regions are particularly complex because of the necessary transitions of current from metal electrode to gas. Properties of each region are further described in the following sections.

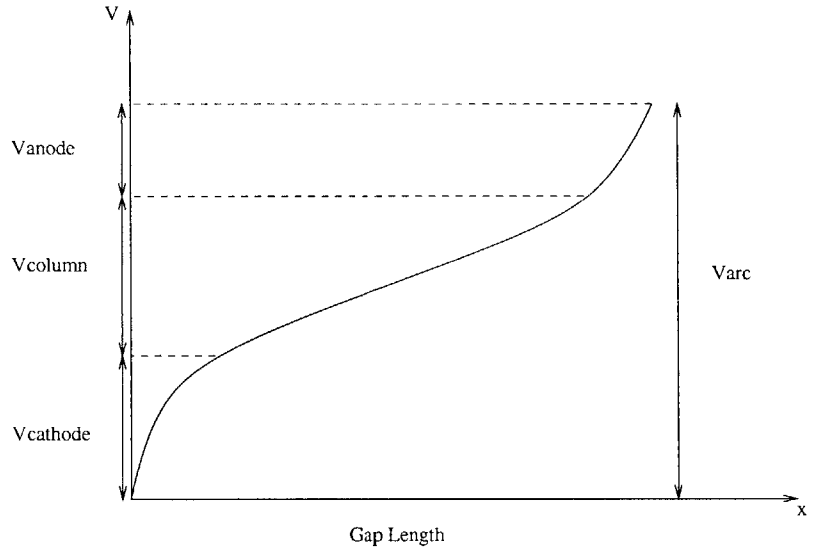

Figure 2.1: Potential distribution across arcing electrodes where generally $V_{anode} < V_{cathode}$

2.2.1 The Long Column

The arc consists of a quasi-neutral column of ionized gas containing electrons and negative and positive ions [14]. The literature pays particular attention to the electrons and positive ions, neglecting negative ions. Positive ions are formed in the gas by ionizing collisions with electrons or are injected into the column by the anode. This results in a high temperature arc and equilibrium is achieved when the rate of charge generation is balanced by the rate of recombination. The quasi-neutral arrangement of the charges in the charged gas are known as a plasma with the number density and charge per carrier of electrons and positive ions being respectively (n_e, -e) and (n_i, q_i). Quasi-neutrality requires that

$$-en_e + q_i n_i \approx 0 \tag{2.1}$$

where $e = 1.6 \times 10^{-19}$ Coulombs is the charge on an electron. The arc current is then related to the product of the each charge carrier's charge density and its respective velocity by

$$\bar{J}_{total} = -n_e e\bar{v}_e + n_i q_i \bar{v}_i \tag{2.2}$$

where $\bar{v}_e$ is the drift velocity of electrons, and $\bar{v}_i$ is the drift velocity of the positive ions. Because the mass of the positive ions is large compared to the mass of the electrons, $\bar{v}_e$ is much larger than $\bar{v}_i$. This shows that the current in the column is carried primarily by electrons and that the positive ions serve mainly to keep the region in a quasi-neutral state.

The fraction f of atoms that are ionized in terms of the temperature T in Kelvin, pressure P, and ionization potential V_i in volts is given by Saha's equation shown in Equation 2.3 where k is Boltzmann's constant [2, 14].

$$(\frac{f^2}{1-f^2})P = (3.16 \times 10^{-7})T^{2.5}e^{-\frac{eV_i}{kT}} \tag{2.3}$$

In summary, in a stable arc the column is a quasi-neutral region in which the current is carried primarily by electrons. The region is at an extremely high temperature and is in thermal and charge equilibrium.

2.2.2 Cathode Phenomena

At the cathode there exists a drop in potential known as the cathode fall and is shown in Figure 2.1 as $V_{cathode}$. Generally, the cathode fall is on the order of 10 V and is due to current flowing across the electrical-plasma interface and depends on the electrode material [14]. At the cathode, electrons are extracted and accelerated across a high electric field region into the positive column where they either ionize neutral particles or recombine with positive ions.

Electrons can be extracted in several ways. One way is the emission of electrons as a consequence of positive ions impinging on the cathode surface. However, this method is unlikely to be the main source of electrons since a cathode fall of hundreds of volts would be required to maintain a glow discharge [14].

Another method by which electrons can be emitted is thermionic emission from a hot enough cathode if emission is obtainable at temperatures below the boiling point of the cathode material [14]. The temperature at the cathode can be kept high by the energy received at the cathode from positive ions accelerated in the cathode fall.

Strong electric fields on the order of 10^7 V/cm at the cathode surface can also yield high electron emissions. If the current density at the cathode is large enough, a field of this magnitude can be produced by the space charge created by the incoming positive ions. If thin insulating layers are created at the surface of the cathode, positive ions can collect on this layer and also create high electric field strengths capable of pulling out electrons from the cathode.

Thus, there are a variety of ways in which electrons can be emitted to create the cathode fall region. One or more of the above mechanisms are present in arcing electrodes and exactly which mechanisms are occurring are difficult to specify.

2.2.3 Anode Phenomena

The conductor receiving electrons from the cathode is the anode. Except in special cases, the anode does not emit positive ions and the current carried at the anode is carried solely by electrons [2, 14]. Because of this, there will be a small region of negative space charge directly in front of the anode electrode and a potential fall V_{anode} is created. Unlike the cathode, both charge carriers are not produced in the anode region. In the cathode, electrons are emitted at the negative electrode surface and electrons and positive ions are produced at the column end of the cathode fall. However, at the anode, only positive ions are formed, making the anode potential fall smaller than the cathode fall.

Another difference at the anode is that the energy required to produce charge carriers is much less than at the cathode [14]. This is due to the fact that the anode current is carried by electrons and no positive ions enter the anode. If we look at the total arc current $I = I_e + I_i$, we see that at the cathode, there is a cathode current I_{ec} due to electrons and an I_{ic} due to positive ions flowing in the opposite direction. However, in the anode region, there only exists a current I_{ea} due to electrons. Thus, $\frac{I_i}{e}$ electrons and positive ions must be produced per second in the anode, compared to $\frac{I_e}{e}$ that must be produced in the cathode.

Since $I_e >> I_i$, there is less energy required to produce charge carriers in the anode [14].

2.3 Voltage and Current Minimums

In order to sustain a stable arc, the arc voltage must be greater than the minimum arc voltage V_m and the arc current must be greater than the minimum arc current I_m. Minimum stable arc voltages and currents for various electrode materials are shown in Table 2.1. The

Table 2.1: V_m and I_m for different cathode and anode materials [2]

Material	V_m**(V) (cathode)**	I_m**(A) (anode)**
Sb	10.5	-
Zn	10.5	0.1
Ag	12	0.4
Cu	13	0.43
Bronze	13.5	0.31
Sn	13.5	-
Al	14	-
Ni	14	0.4
Au	15	-
Steel	15	0.5
Pt	17.5	-
Carbon	20	0.03

minimum arc voltage V_m primarily depends on the cathode material due to the cathode potential fall dominating the arc voltage. The cathode fall depends on how easily electrons are emitted into the plasma column and this is a function of the cathode material. Notice that the voltage minimums required to sustain a stable arc are all lower than the new 42 V system.

The minimum arc current I_m is mainly a function of the anode material [2]. For all materials shown in Table 2.1, I_m is less than 1 A. As will be shown in Chapter 4, creating arcs using 3 12 V batteries results in current on the order of 100 A, much greater than I_m. Chapter 7 shows arcing on a 14 V system and although the current is around 45 A, the voltage of one battery is insufficient to sustain a stable arc.

2.4 V-I Characteristics

V_m and I_m create asymptotes by which we can begin to draw the VI characteristics of stable arcs. The shortest possible arc does not follow these straight asymptotes, however. Instead the shortest possible arc obeys Equation 2.4

$$(V - V_m)(I - I_m) = C \tag{2.4}$$

where C is a constant that depends on the material of the electrodes [2]. Thus the shortest possible arc follows a hyperbola. If the distance between the electrodes increases, the voltage-current characteristics change but continue to be related by hyperbola functions and obey the relationship

$$[V - V_m - V_{arc}(d, I)](I - I_m) = C(d) \tag{2.5}$$

where $V_{arc}(d, I)$ is the arc voltage as a function of gap length d and circuit current I and $C(d)$ is a constant that depends on the material of the electrodes as well as the gap length [2].

Figure 2.2 shows how the the voltage-current characteristics vary as a function of electrode gap length. Each curve represents the voltage and current relationship for a stationary stable arc for copper electrodes at a particular gap distance. To determine if a stable arc exists, a load line can be drawn with intercept V_{batt} on the voltage axis and $\frac{V_{batt}}{R}$ on the current axis where R is the circuit resistance. Intersection of the load line with the voltage-current curves gives points at which an arc can exist. The stable operating point is the point of greater current and lower voltage. This can be explained by noting that if the arc is at the point of large voltage and smaller current, there is more voltage than is needed to maintain a stable arc. The arc will thus heat up, lowering the arc resistance, and the current will increase until the second operating point is reached [15].

If the gap length is slowly increased, the stable operating point moves along the load line in the direction of decreasing current, and increasing arc voltage. When the load line is tangent to the hyperbolic curve the arc extinction length has been reached and any further increase in gap distance will extinguish the arc. Figure 2.3 shows two load lines intersecting one V-I

characteristic curve of an arc. One load line intersects at two points and has a single stable operating point. The second is tangent to the V-I curve and is at the extinction point. For this load line, if the gap length is increased any further, the arc will extinguish because the V-I curve for the larger gap length will no longer intersect the load line.

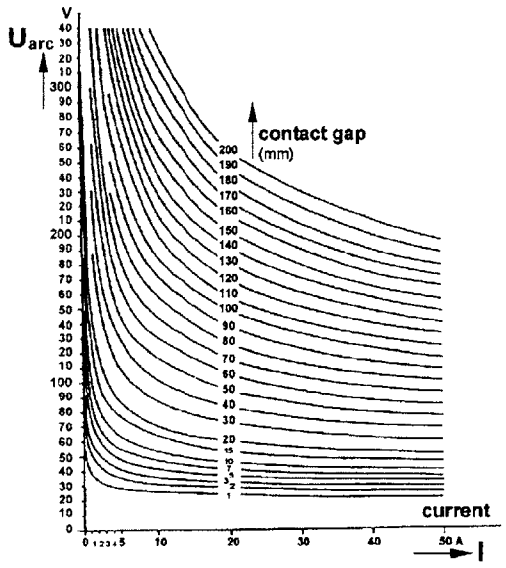

Figure 2.2: Voltage-current characteristics of arcs as a function of gap length for copper electrodes [15]

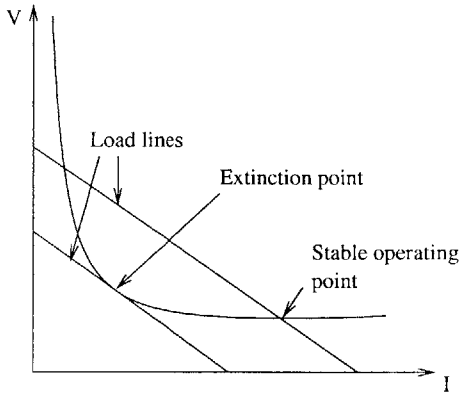

Figure 2.3: Stable operating points and extinction point for different load lines on one V-I characteristic curve of a stable arc

Chapter 3

Detection Methods

It would be desirable to be able to detect an arc event before it occurs. However, such a method does not exist yet. The next approach is to detect that an arc is beginning to occur as reliably and as fast as possible. This thesis work takes the approach of minimizing any possible damage and danger caused by the arc as quickly and as accurately as possible when analyzing detection methods. In this chapter we examine various possible techniques of arc detection for automotive applications.

3.1 Methods

There are a variety of ways to detect arcing once such an event is occurring. Detectors for power distribution feeders have been developed that monitor circuit currents as well as radiated energy in the form of sound, electromagnetic waves, and light during electric arcs. The methods analyzed here have been used either in real applications or in the laboratory.

One important consideration in what method to use for detection is how the arc will be localized. Once the arc is detected, it is necessary to determine the circuit in which the arc is occurring and to turn the current off. For this reason, a method of localization under each detection technique is also analyzed.

3.1.1 Electronic Detection

Electronic detection uses techniques that monitor specific circuit current and voltage changes during an arc event. For real world applications, voltages across the arc may not be a reasonable approach given the uncertainty of the location of the arc fault. Circuit current changes during an arc are therefore a more widely used method of detecting electric arcs. Depending on the system, a variety of approaches can be used.

AC Systems

In AC systems, arc detection can be performed in different ways, all using the fact that the current has positive and negative half cycles. One approach by a group at Texas A&M University was to monitor the change in energy of the current signal [4]. Using the sum of squares of the sampled data they obtained the energy of the signal. Comparing the energy in one cycle to the previous cycle allowed them to characterize the change in energy that an arc produces per AC cycle. This method distinguished steady AC operation from fast transients seen when capacitor banks switch on and off as well as the operation of air switches. Furthermore, filtering the time domain waveform before performing energy calculations using bandpass filters with center frequencies at 180 and 210 Hz yielded vast improvements in the detection of arcing faults. In the filtered waveforms, energy would change by close to a factor of 50 during arcing compared to a factor of 6 in the unfiltered case.

A dynamic threshold was determined as the average energy per cycle and any energy variation over the threshold could take on two possible states, an "event" or an arc fault. If the energy in one current cycle was 25% greater than the previous cycle, the amount of time of that change in energy would be calculated. Further fluctuations in the signal energy by 75% over three cycles would classify as an event. Once again, fluctuations in energy are calculated and if they continue, a fault is said to have occurred. Sensitivity of the detector could be changed by varying the number of cycles over which changes in energy must occur to be classified as events or faults. This algorithm works well because the arcing faults have much longer time durations compared to the time durations of capacitor banks switching on and off. This method would be difficult to implement in the new automotive system given that we must work in a DC system in which we cannot compare current and energy during different cycles. The AC zero crossing of the current can create recurring arcs which create detectable changes in energy while in a DC system recurring arcs will only occur during periodic arcing in which the electrodes make intermittent contact. It is a possible method of detection but not one generally applicable to DC automotive systems.

An improved method used at Texas A&M University was to monitor the content of the harmonics and in-between harmonics of the fundamental line frequency as a function of time [5, 6]. The in-between harmonic frequencies are defined as the frequencies midway between the harmonics. So for a 60 Hz line, some in-between harmonics would be 90, 150, and 210 Hz. The input signal from the monitored 60 Hz line current is filtered by a number of band pass filters whose center frequencies are either the harmonics of the line, or the in-between harmonics. The energy changes per cycle are calculated for various in-between harmonic frequencies. As with their previous work, changes in energy in the filtered signals beyond a specified amount of the dynamic threshold will set the detector to begin calculations to determine whether a fault is occurring. By comparing many odd harmonics and in-between harmonics, ~80% of arc faults are detected. However, as the authors state,

the arcing faults detected were created and controlled and the same detection rate may not apply to real world applications.

The possibilities of using this method in the automotive system are few. We cannot compare the current and energy during different cycles because we are working with a DC system. It may be possible to choose a specified amount of time to monitor but the energy changes would not be the same as in the AC system due to the recurring energy faults caused by the zero crossing of the current. Also, one assumption made is that any transients from switching operations occur in a time on the order of a few cycles or less while arcing will occur over many more cycles. As we will see in Chapter 6, this is not always true of transients in the automotive system.

A different approach to the AC system arc detection problem is to use the asymmetry caused in the waveform by arcing [7]. Two terms are defined, current flicker and half-cycle asymmetry. Current flicker is defined as the difference between the magnitude of the positive current peak from one cycle to the next. This is also done for the negative half cycles. Half-cycle asymmetry is determined by first finding the difference between the peak magnitudes of two successive half cycles. The calculation window moves over by half a cycle, making the previous second cycle the first cycle of the new calculation. The same difference is calculated between half cycles. An overall difference between the two calculations is then determined. These calculations are made based on observations that the fault current magnitude can vary greatly from one cycle to the next and that either the negative or positive half cycle current peak magnitudes are larger. After the calculation of the current flicker and asymmetry, a score is given to any transient based on the values it produces for flicker and asymmetry. Loads such as fluorescent lights, short circuits, and a computer are added to the system and the flicker and asymmetry of the transients they produce are calculated. Flicker and asymmetry are calculated for various arc faults as well and because the flicker and asymmetry are higher in arc faults, a threshold can be determined. An arc welder was used as well and it was determined that the detector could not differentiate an arc fault from the arcing load.

Because the current flicker and asymmetry method relies heavily on how the AC current peaks vary, this method cannot be used for the automotive DC system. Monitoring the variance of the changes of the current in time might be one approach and the possibility of using this method is explored in Chapter 5.

DC Systems

We now shift our focus to DC systems. One possible approach that has been used in the telecommunications industry's 48 V DC system is to monitor the frequency spectrum of

the circuit current. Work performed at Bell Communications has shown that in their 48V system, a threshold of the amplitude of the frequency spectrum can be found to distinguish arcing from normal operation current [11, 12]. Noise current on the DC system was studied and the spectrum of the noise was compared to that of the arc. Noise current was defined as any current that was not DC. It was found that the noise spectrum differed enough from the arc spectrum in amplitude at practically all frequencies. A detector was made that monitored the circuit current and if the amplitude of the calculated spectrum was above a threshold, an arc was considered to be occurring.

This approach looks very promising for the new 42 V DC automotive system. The ability to perform this task in a 48 V system shows that there is a possibility of doing the same in the 42 V system. What may be a difficult task in the automotive system is that the normal operation DC current level varies. Some electrical loads require more current than others, and if they are used in combination, the DC level is different. For this, a dynamic threshold can perhaps be used as in the work by Russell's group. In effect, we would recognize a DC level, ignore it, and only pay attention to the variations which occur around the DC signal.

One particular difficulty with using the method used at Bell Communications, as will be seen in Chapter 6, is that the noise current spectrum in an automotive system is not substantially lower than the arc current spectrum for all cases. In fact, some electrical loads can produce noise transients which are greater in amplitude at some frequencies than in the arcing spectrum.

Another approach for detecting arcs in DC telecommunications systems was taken by a group at Hendry Telephone Products [13]. The arc spectrum is first seen as being fractal in nature. The current is monitored by a current probe and is bandpass filtered at an unspecified frequency. The signal is then passed through a non-linear process which produces an intermodulation of the components of the input spectrum and its output is filtered by a sharp bandpass filter with a center frequency much lower than then initial bandpass filter. The amplitude of the output is determined by the amplitude of the initial input as well as the number of frequency differences produced by the non-linear process meeting the requirement of the center frequency of the second bandpass filter. A detection circuit is then used to determine if the output of the second bandpass filter is constant. Because arcing current is chaotic, the input to the detection circuit must not be constant in order to be considered an arc. Third and fourth bandpass filters are used to determine a "chaos level" and the overall output is checked against a set sensitivity level.

The approach taken by Hendry Telephone Products appears to work well. As we will see in Chapter 5, the spectrum of the arc at ~42 V, and at 48 V as shown by Hendry Telephone Products, contains a continuous range of frequencies and this fact is used in this detection

method by using the non-linear process and sharp bandpass filter. In this research however, we will focus on trying to use simpler methods first before attempting to use more complex method such as this.

Arc Localization

Electronic localization of an arc can be performed in at least two ways. In an automobile, various electrical components are grouped together and protected from over current conditions by a fuse. If the fuse clears, operation of the components protected by that fuse is lost. We can thus incorporate a detector into each of these fused circuits. If any of the detectors determine that an arc is present, the detector's particular circuit is opened to protect the components from major damage.

In the automobile industry, cost is a major factor. Automotive circuits today are protected by far too many fuses to make using a detector in each fused circuit cost effective. We can use only one detector if we place it in the main circuit of the vehicle. Circuit current variations due to an arc will also be seen in the main circuit and determining that an arc is present will not be affected. However, using one detector requires us to develop a method to determine which fuse-protected circuit must be turned off. The arcing circuit can be determined by sampling the current in each fused circuit. In the case of many fused circuits, a method for the order of sampling must also be developed.

3.1.2 Acoustic Detection

When an arc occurs, a sound is emitted by the event. If we can differentiate between other sounds in the system and in the environment of operation, we can detect the arc event. Microphones and transducers can be placed throughout the vehicle to monitor vehicle sound. Noise which may interfere with the arc signature can be characterized and filtered or ignored by other means.

Acoustic emission in AC low voltage distribution switchboards has been characterized and detected using ultrasonic sensors by a group at Schneider Electric Industries [8]. Ultrasonic signals measured during an arc are measured and it can be seen that the time domain waveform has three distinguishing features. The first is a high change in signal energy. It was also seen that the arc signal consisted of a lower but sustained energy in subsequent cycles. This energy was also modulated by the 50 Hz line frequency.

Three tests were performed on the data. The first was a test which compared the energy in k samples of one cycle with a threshold. If the energy of the k samples was greater than the

threshold, a second test would be performed. The second test compared the peak energy of the present cycle with the average energy in the next cycle. Because during arcing, there was a large contrast between the first energy burst and subsequent energy, this allowed the detector to ignore noise such as mechanical shock to the busbar that did not exhibit type of energy behavior. The final test checked for energy modulation. The test gave a positive result if a local maximum between 90 and 110 Hz existed and if that maximum was greater than 50% of a given global maximum. The tests were performed on the rectified 50 Hz signal. This produced 100 Hz time signals and because of this, the test looked for maximums between 90 and 110 Hz.

This particular acoustic detection method would be difficult to implement in automotive systems. Because there is no fundamental frequency in the DC system, we will not see the characteristic energy modulation seen in the above work. In addition, transducers placed on the cars chassis to measure ultrasonic noise would be subject to an enormous amount of mechanical vibration signals from engine and road noise and vibration. Just the operation of the vehicle in different road conditions and at different speeds would change the characteristics of the vibrations. This would make it extremely difficult to detect an arc using this method.

One difficulty that can arise in acoustic detection is how to differentiate between direct and reflected sound due to their arrival time differences at acoustic inputs. One solution is to use a pressure zone microphone (PZM) in which a microphone combined with a boundary plate are used to create an input in which the direct and reflected sound add in phase as was done at the University of Saskatchewan [9]. The microphone used had a sensitivity of -74dB and a frequency response from 20 to 18000 Hz. The sound at the microphone shows a sharp peak when an arc begins, followed by exponential decay. Higher frequency content rides on top of the signal. Pattern recognition techniques using neural-networks were used to create a stored pattern of an arc's sound time domain shape.

Success was shown with this method of acoustic detection. However, this acoustic detection method was one of three different methods used in parallel with two other methods in order to obtain high reliability. Combined with electromagnetic and infrared detection, the overall detector was reliable. In combination, a false trip from one detector would not necessarily mean a false trip from the combination of detectors. Using three detection methods increases cost and we would like to avoid that for the automotive system. If the acoustic detection method alone is prone to false alarms then it may not be the most adequate means of arc detection in automotive applications. Another issue in acoustic detection is that the combined directivity of the microphones would have to cover every part of the car. Because the microphones are not omnidirectional, this can quickly become a difficult problem to solve in the complex frame of a vehicle.

Locating the arc can be achieved using the fact that sound radiated by the arc will arrive at the microphones at different times [9]. This is illustrated in Figure 3.1. Using arrival time

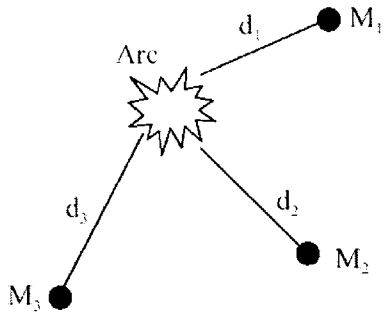

Figure 3.1: Acoustic arc localization using microphones

differences of the arc emitted sound at microphones M_1, M_2, and M_3, distances d_1, d_2, and d_3 can be calculated and a location of the arc determined. For example, we know that the distance travelled to each microphone is $d_n = vt_n$ where t_n is the time it takes the arc sound to reach the nth microphone. By Equation 3.1, where n and m are integers representing the number of the microphone, we can find the difference between the distances travelled between any of the microphones and find the distances to the arc for each microphone. The more microphones used in the localization calculation, the more accurate the result would be.

$$v(t_n - t_m) = d_n - d_m \tag{3.1}$$

Although we would be able to find where on the car the arc was occurring, this would not necessarily tell us which circuit was arcing. Often in automobile wire harnesses, wires leading to different fused circuits are bundled together. If the acoustic detector were to signal an arc in one of these bundled rows of wire, it would take extremely high accuracy by the localization calculation to determine which particular wire was arcing. Any error could lead to a false alarm in the incorrect circuit, leading to unnecessary loss of operation of electrical components and no protection for the arcing circuit. For this reason, this method of localization is not suited for automotive applications.

3.1.3 Electromagnetic Detection

Electromagnetic radiation can also be used to detect arcing. We can see an example of this when lightning is picked up by AM radios. By determining the electromagnetic radiation of arcing events in the 42 V system, we can use antennas to determine if an arc is occurring.

Previous work has been done in detecting arc faults in power systems by monitoring electromagnetic radiation in the very low frequency (VLF) and very high frequency (VHF) bands [10]. The zero crossing of the current causes arcing to occur twice and for this reason the arcing signal is modulated by the line frequency. Non-linearities in the arc produce frequency components at the line frequency up to the UHF band region. During an earth arc fault condition in which an arc occurs on a transmission tower, the tower can serve as a vertical antenna and the radiation is vertically polarized. Using a 9m vertical monopole antenna placed on top of a University of Bath building in England, the radiation from the arcing was measured. The frequency spectrum of the radiation was found from 0-20 kHz (limited by the 40 kHz sampling rate) and was used to characterize the arc. With this set-up, arcs were reliably detected.

The zero crossing of the current and the modulation of the energy during an arc at the line frequency gives the AC arc fault distinct characteristics. It is unknown whether similar characteristics will exist in DC arcing electromagnetic radiation and if not, then the arc will be difficult to detect unless some other clear characteristics can be found.

Work at the University of Saskatchewan has also shown that electric arcs can be detected by its electromagnetic radiation using a 7cm loop antenna [9]. The loop antenna used was able to measure radiation from arcing up to 15m away. The antenna is connected to a parallel tank circuit tuned to the most predominant frequency measured during arcing. The output of the tank circuit is connected to an amplifier and when an arc occurs, the output of the amplifier grows slowly and falls rapidly, all on the order of 100μs. Pattern recognition of this rise and fall was used to detect that an arc was occurring.

This method of electromagnetic detection was combined with the acoustics method performed by the same group. This yielded a more reliable detector. Measurements of electromagnetic radiation during arcing of the new 42 V system could be taken. However, using pattern recognition in the new automotive system as was performed in the work described might be difficult since the AC line frequency gives clearer characteristics to the arcing signal.

Using electromagnetic radiation to locate an arc on a car may also prove to be difficult. A method similar to the acoustic localization can be attempted but the speed of radiation

may be too fast to allow accurate measurement of the arrival time differences. Localization of arcing faults using arrival times at various stations has been used but the stations were at distances on the order of kilometers, far greater than any distance on a car [10]. For this reason it would be best not to attempt localization using electromagnetic means.

3.1.4 Optical Detection

During an arc, visible light is radiated by the event. To detect an arc event, optical detectors can be placed throughout the car to detect the visible light emitted by the arc. One advantage of this method is the possibility of fast detection times. The speed of propagation of the light as well as speed down optic fiber helps give faster response times.

One possible optical detection method is to run optical fiber along the car which connects to various optical sensors. The ABB Group has developed a product called the Arc Guard System. The system uses optical detectors to monitor the light in the electrical installation. A large increase in light intensity will send light into the detector and down the fiber optic cable. The signal sent to trip the circuit breaker is sent within about 2 ms that the arc is detected. Depending on the type of breaker in the system, total turn off of the arcing circuit occurs in fewer than 50 ms. Up to nine arc detectors can be connected to each arc monitor and one detector is usually placed per closed unit or cell.

Although fast detection times may be possible, cost is an issue. Running optical fiber along the car can be costly and a different solution should be found. Using optical detectors can also be a problem. The complex shape of the car may block the path of the emitted light to some of the sensors. In addition, sensors may not be omnidirectional and will only be able to detect light within a limited observable range.

An interesting alternative could be to use optical wire insulation. By doing this, both regular wire and optical fiber do not have to be installed in the car's wire harness. Instead, conducting wire would have insulation that would function as optical wire. Doing this would minimize the increase in cost of an optical detection method. Using this method, every wire's insulation becomes a detector. Visible light from the arcing wire is propagated by the insulation itself and if the light emitted by the arc is characterized, the arc event can be detected.

Optical insulation can be a feasible method of detection. However, previous work in this area has not been found and further investigation is necessary to determine if the optical fiber can survive arcing conditions. The high temperatures reached during arcing may cause enough damage to the optical insulation to render the fiber useless to the detection process.

Localization would be best achieved by using an electronic localization method. As with electromagnetic detection, the speed of radiation is too fast to allow accurate measurements of arrival time differences at sensors. To locate the arcing circuit, signals from the sensors or from optical insulation would be sent to an electronic unit to determine which circuit was arcing.

3.2 Chosen Method: Electronic Detection

There is no single solution to detecting arcs in the new 42 V automotive system. There are, however, advantages and disadvantages to each method of detection. This research focuses on electrical detection, specifically using Fourier analysis, because of its many advantages over the other possible techniques discussed in the following section.

3.2.1 Electronic Detection Advantages

Developing an electronic detection method seems to be the most promising approach. There has been a lot of successful work done in AC system arc detection as well as some successful work in the telecommunications DC system. This work is encouraging and is a good reason to choose electronic detection over detecting a type of arc radiation.

Another main advantage of electronic detection is its lower cost. Electronic components used to monitor the circuit current will be cheaper than using microphones, antennas, or optical detectors. In the automotive industry, even a small difference in price can be a factor. Perhaps detection by radiation methods seems slightly more elegant but the goal is a reliable arc detector and with low cost being essential, electronic detection is the best option.

Electronic detection is also a simpler approach. Detecting any sort of radiation introduces complexities even at the level of monitoring the system. Radiation reflections and interference which are not a problem when monitoring circuit current make taking measurements and ignoring noise more difficult.

Localization is a simpler approach using electronic techniques. As shown in the previous sections, obtaining a circuit location of the arc is difficult using arrival time differences of radiation at sensors. If only one detector is used, some form of electronic localization would be the best approach to determine which circuit to open. One such approach is suggested in Section 3.2.3.

3.2.2 Detection using Fourier Analysis

This research focuses on detecting arcs by monitoring circuit current and determining the frequency content of the signal. Analysis is performed to try to find an arc "signature" in the frequency domain. Comparisons to normal operation, measured on a 14 V bus vehicle, are made to determine if a sufficient difference exists between the frequency content during arcing and normal operation to use this analysis method in the new 42 V system.

The approach to the analysis will be similar to the work performed at Bell Communications using spectral analysis as described in Section 3.1.1. However, before attempting to look just at amplitude, emphasis is placed on finding an arc signature, or, a specific characteristic in the arc spectrum which we can use to detect an arc. No strong and definitive signature is found and as found in other work, the spectrum of the arc contains substantial content at all frequencies with a somewhat constant roll off as frequencies increase.

The main circuit of the arcing apparatus used for this research is described in Chapter 4. The circuit used in the Bell Communications research for finding arcing current is similar but with a different source voltage. Naturally, normal operation current waveforms are different since we are looking at automotive loads. The Fourier analysis of the normal conditions of the telecommunications and automotive systems will be different as well.

3.2.3 Localization Method

Once an arc is detected, the arcing circuit must be interrupted. Because placing a detector in each fused circuit is not a cost effective approach, a single detector can be placed in the main circuit and a method of current sampling can be used to find the arcing circuit.

After the detector determines that an arc is occurring within the car's electrical system, MOSFETs can be used to sample the current. A MOSFET in each fused circuit can be turned on and off to determine the arc location. Figure 3.2 shows the layout of how the detector and MOSFETs will be in relation to the fused circuits. When an arc is detected, the MOSFETs will be turned off and on one by one. When the detector in the main circuit no longer detects the arc current signature, the MOSFET currently off will remain off, thus interrupting the arcing circuit. The automotive electrical system includes many fused circuits so sampling the current from the first to the last circuit may not be the best approach. An optimal sampling order can be determined once the detector is designed. The criteria for the order of current sampling could be determined in many ways. For example, circuits with components closer to fuel vapors could be checked first since these are more likely to cause a fire or explosion during a stable arc. We might also wish to test circuits with

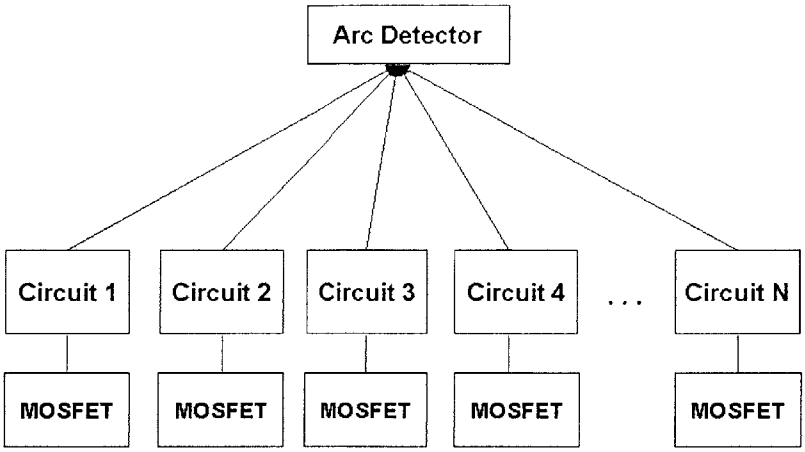

Figure 3.2: Arc detector and MOSFET placement to locate arc

sensitive components and circuits with components necessary to keep the vehicle running first.

The use of a MOSFET provides an additional benefit. Some stable arcing, such as parallel arcing, may cause current to increase above the current rating of the fuse. In this case, the fuse will clear and is adequate protection against the arc. We have two conditions, arcing in which the fuse clears, and arcing in which the current must be sampled in order to determine which circuit to interrupt. With this in mind, we can use the MOSFET to perform two roles, the intended role of aiding in current sampling during an arc, as well as over current protection. If a current threshold is reached, the MOSFET in the circuit can open, providing the same protection as a fuse. We can also save the cost and labor of buying and installing a new fuse since a MOSFET can simply be reset to the "on" state.

Chapter 4

Producing Arcs

In order to analyze current in a circuit during arcing, a reliable method of producing stable arcs is needed. For this reason the experimental setup of the previous MIT experiment was rebuilt [3]. This chapter describes the setup and control of the arcing circuit used for arc current data. Changes to the MIT experiment were made to the measurement technique used and are described in Section 4.3.

4.1 Main Circuit

To create arcs we must have electric contact separation. Figure 4.1 shows the main circuit used to produce arcs. For stable arcing in automotive circuits, V_{batt} is three 12 V batteries

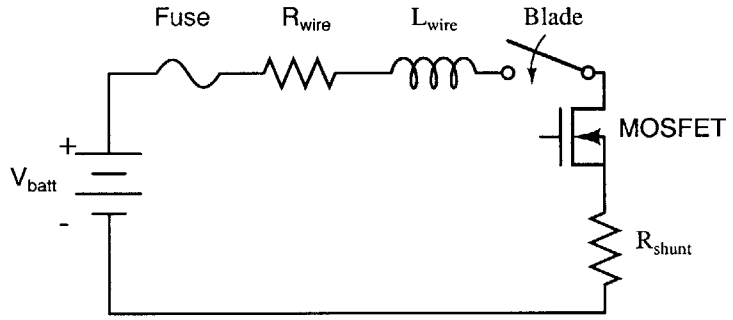

Figure 4.1: Main circuit of arcing apparatus

in series. A fuse is used to simulate worst case conditions in which the fuse may not provide adequate protection for the circuit. This condition can especially be seen in the case of intermittent arcing. In such a case, periodic opening and closing of the circuit creates high peak current but low enough RMS current, defined in Equation 4.1, that does not clear the fuse.

$$I_{rms} = \sqrt{\frac{1}{T}\int_0^T I^2(t)dt} \tag{4.1}$$

Because shorting the car batteries can produce high peak currents, a length of coiled wire of known resistance R_{wire} and inductance L_{wire} is placed in the circuit to limit the peak current. The resistance of this wire is the dominant resistance in the circuit. Values of R_{wire} and L_{wire} can be changed depending on the rating of the fuse being used in the test.

To create either a single arc, or periodic arcing, a DC motor is connected to a steel blade which then opens and closes the main circuit by making contact with a test wire. The test wire typically used is 16 AWG wire with the insulation stripped off of a portion of the wire. When contact is made by the blade, the batteries are short circuited and a DC current flows, limited by R_{wire}. As the blade separates from the test wire, a stable arc forms.

In order to have more control over the circuit current time duration, a MOSFET is placed in the circuit. When the blade makes initial contact with the test wire, the MOSFET is off and no current flows. A DC current time duration can be specified and with the time of blade contact given by the contact detection circuit described in Section 4.2.2, the MOSFET can be turned on at the proper time to give a desired DC current duration as well as a desired arc current duration. With this control over current durations, high currents and long arc durations can be achieved without clearing the fuse.

Measurements of current can be taken by way of the shunt resistor. This resistor introduces a small resistance $R_{shunt} = 230\mu\Omega$ and the current during arcing can be found by measuring the voltage across this shunt. The shunt as well as the rest of the main circuit can be seen in the experimental setup shown in Figure 4.2.

As a matter of convention, we will refer to arcs made on this apparatus as 42 V arcs. However, the three car batteries charge to $\sim$13 V each and during use will slightly discharge. Additionally, we will refer to arcs made using a single, fully charged 12 V battery as 14 V arcs.

4.2 Control Circuitry

If the motor were simply allowed to run freely, stable arcing would occur but the high currents and longer DC current duration would clear the fuse. High energy arcs can still

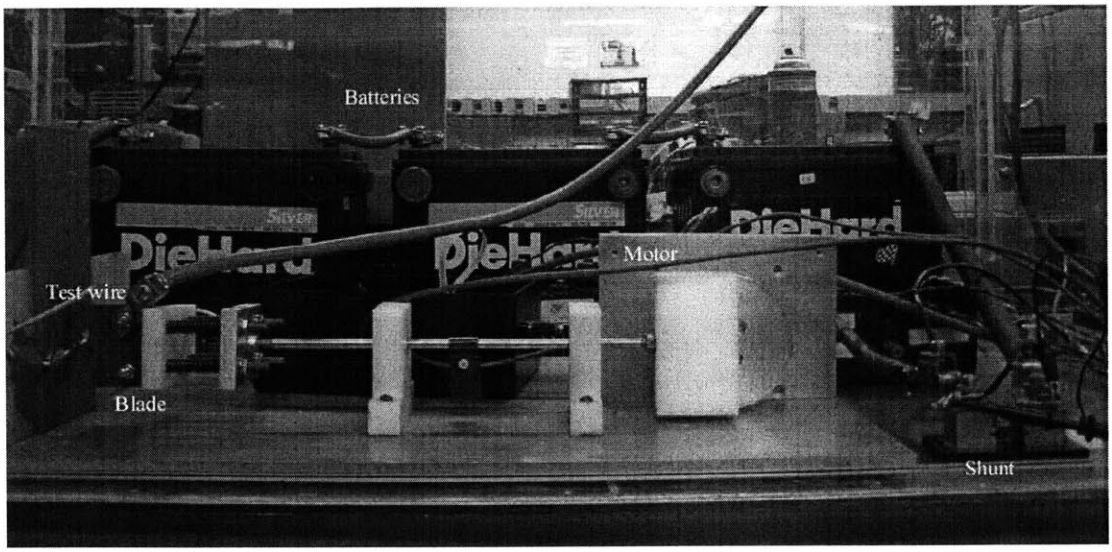

Figure 4.2: Main circuit and chopping blade apparatus to create stable arcs

be produced in a more controlled environment using the various controls for the motor and MOSFET. A block diagram of the complete test system is shown in Figure 4.3 and each control system is described in the following sections. All control circuits are computer controlled using LabView (code in Appendix A).

4.2.1 Motor Control

The purpose of controlling motor speed is to be able to control how many contacts are made within a given period of time. The DC motor is connected to a +12 V supply. The circuit shown in Figure 4.4 is used to send a PWM signal to the input of the motor. By using this circuit, we have a range of speeds from stationary to the speed of maximum motor voltage of +12 V DC directly connected to the motor. The duty ratio of the PWM signal is specified by the user and is typically operated in the range of 0.1 to 0.3, giving typical contact rates of 1 to 2 contacts per second.

The output from the computer drives the input pin 2 on the IR2125 MOSFET driver chip which drives the IR540 MOSFET. A low signal into the IR2125 turns the MOSFET off. Motor current continues to flow due to motor inductance and the motor input is connected to ground through the 40CPQ080 diode. A high signal turns the IR540 on and the motor input is pulled up to + 12 V. The other components of the circuit control the driver chip and limit the gate current as shown in the IR2125 specification sheet.

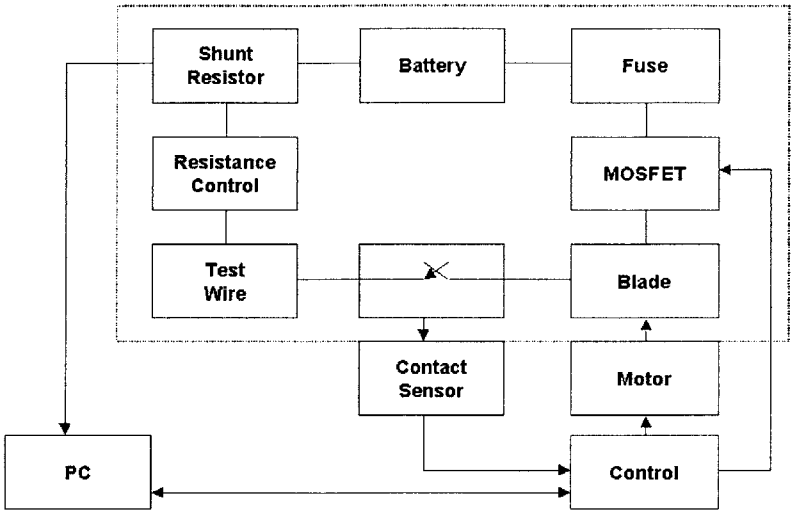

Figure 4.3: Block diagram of complete test apparatus

4.2.2 Contact Detection

The MOSFET in the main circuit is used to allow only a user-specified amount of time of current flow, typically over the range of 50 to 100ms. To do this, we must know the time duration of the blade and test wire contact. This is accomplished by using a comparator circuit shown in Figure 4.5. A connection from the blade of the main circuit is made with V_{in} of the contact detection circuit. If the main circuit is open, the positive input to the comparator is low and the output of the circuit is low. If the blade contacts the test wire, the battery voltage is applied at V_{in} and the circuit output is high. The threshold is set to a level to ensure that any noise does not set the output to high. The 1μF capacitor in

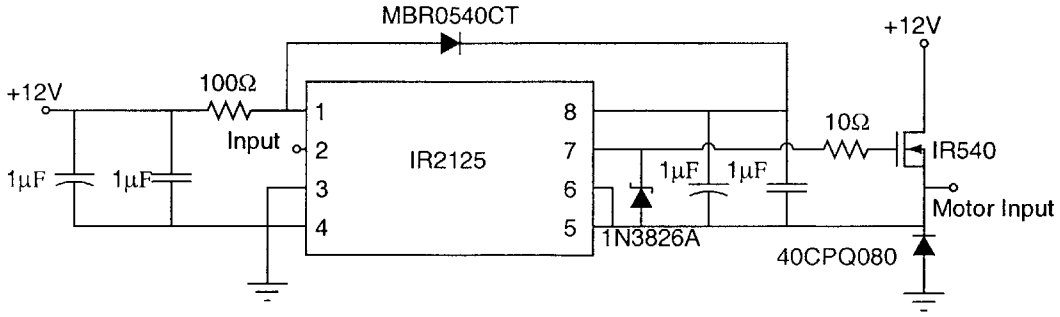

Figure 4.4: Motor control circuit

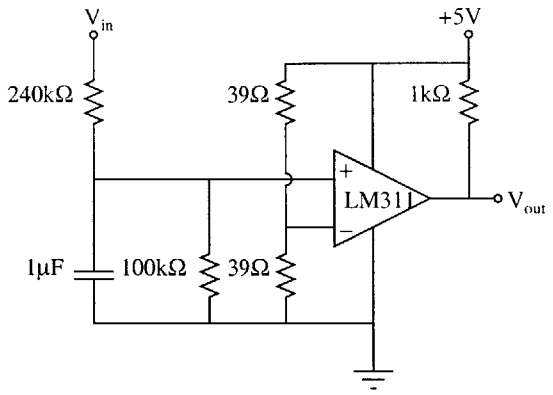

Figure 4.5: Contact detection circuit

Figure 4.5 also helps to reduce susceptibility to noise spikes.

Using a data acquisition board, the output of the comparator circuit is read by LabView and a timer begins when contact is made. When the comparator output becomes low again the timer stops and the time of contact is known. Given a desired time of current duration, LabView can wait for the difference of the contact time and the current duration before turning the MOSFET on. This gives the desired DC current duration.

4.2.3 MOSFET Control

The MOSFET in the main circuit enables us to control how long current flows in the main circuit. By using the MOSFET, we can have a desired current duration regardless of how long the steel blade makes contact with the test wire. The MOSFET used is a PowerFET that is able to handle peak currents of 690A and has an on resistance of $1.8m\Omega$. The PowerFET must be able to handle high peak currents because the shorting of a 36 V car battery source can produce very high currents. Also, a low on resistance is needed so that R_{wire} of the limiting current wire remains the dominant resistance.

The MOSFET control circuit is shown in Figure 4.6. The high or low input at pin 2 of the MIC4422 chip produces a high or low output respectively at pins 6 and 7. The input to the MIC4422 is given by the computer. For most of the test the input to the MIC4422 is low, keeping the MOSFET off. When LabView determines it is time to switch the current on, it sends a high signal to the MOSFET control circuit to turn the MOSFET on.

Another advantage of having a MOSFET in the main circuit is that we can control both

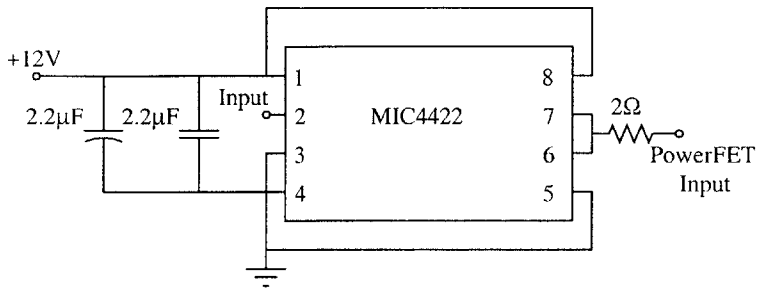

Figure 4.6: MOSFET control circuit

the DC current duration and the arc current duration as well. If an arc duration time is specified, the MOSFET can be left on for the DC current duration plus the arc duration time. In most cases we allow the MOSFET to stay on and allow the distance between the contacts to extinguish the arc. However, if we would like to extinguish the arc after a certain amount of time, perhaps to decrease RMS current, we have the ability to do so.

4.2.4 Noise reduction

The addition of various control circuits adds noise to the main circuit which is picked up in the measurements of the voltage across the shunt resistor. The 100 Hz PWM frequency used in the motor drive shows up in voltage measurements as 100 Hz frequency spikes. Noise from other experiments being performed in the lab are also sources of noise.

The first step taken to minimize noise was the use of batteries instead of power supplies. In the case of a 5 V source, voltage regulators were used with a 12 V battery. The use of batteries eliminated any noise which may have entered the system as a result of power supply noise and line noise.

In order to eliminate the 100 Hz noise produced by the motor control and to fully isolate the main circuit, an optoisolator circuit was used to optically isolate the main circuit from other components. All inputs and outputs to and from the computer were made via a data acquisition board (DAQ). Each input to the DAQ and output from the DAQ were therefore connected to an optoisolator circuit. This fully isolated the main circuit from any other components and allowed cleaner measurement signals at the shunt resistor. The isolator circuit is shown in Figure 4.7. The components in the rectangle are the 6N137 optoisolator chip that was used.

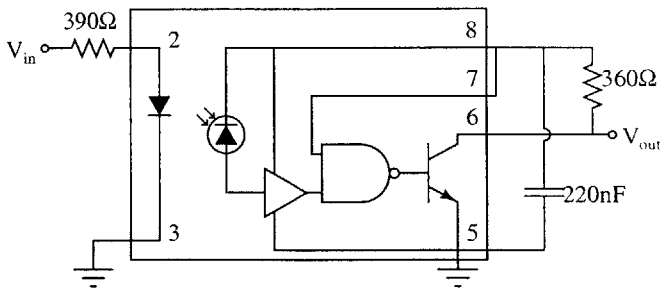

Figure 4.7: 6N137 optoisolator circuit

4.3 Measurement Techniques

Once data of the arcing current is taken, various signal processing needs to be performed. For this reason, clean measurements with minimal noise and high resolution are needed. This section describes the waveforms seen with the test setup as well as improvements made to obtain high resolution measurements.

4.3.1 Current Waveforms

Figure 4.8 shows a typical current waveform using the test setup described in Sections 4.1 and 4.2. When the steel blade makes contact with the test wire, LabView keeps the MOSFET off for a period of time to give the desired DC current duration. When the MOSFET turns on, the blade is still in contact with the test wire and the current steps up. A slight drop in DC current is seen and is due to the increasing resistance of the current limiting wire as it heats up.

When the blade begins to pull back, contact is lost with the test wire and current drops. However, a stable arc is created and the current does not fall to zero. As the blade continues to pull away the arc current decreases and arc voltage increases. When the blade is at a distance at which a stable arc can no longer exist, the current finally drops to zero.

Notice that the peak current in this particular example is about 70A, more than twice the magnitude of the 30A fuse rating used in the test run. The fuse does not clear because of the short time duration of the current pulse and the wire sustains substantial damage. Figure 4.9 shows the damage caused to one test wire after 4 periodic arcs.

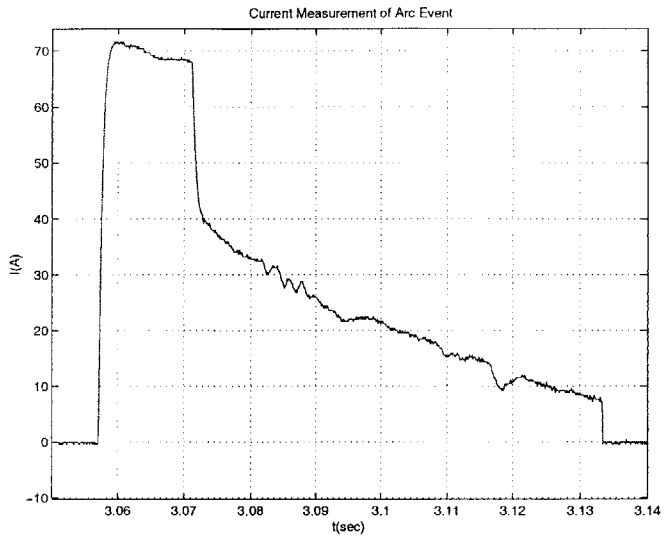

Figure 4.8: Current waveform measured from arcing apparatus

4.3.2 Oscilloscope

Initial measurements were made on an oscilloscope. Figure 4.10 shows a circuit current measurement taken using the scope. We can see from Figure 4.10(b), a close up of a portion of the data in Figure 4.10(a), that there is a large bit error. Fluctuations of the current during arcing are dominated by low resolution data steps. The maximum resolution that could be achieved with oscilloscopes available in the lab was 8 bits. If the full 8 bits of resolution were extended over a 100A range (typical of currents in this test setup), data steps of about 400mA would seen. During arcing, the current fluctuates roughly between 2 and 3A. Using 8 bit resolution can therefore create enough bit error to affect what we see in the frequency spectrum of the arcing current. For this reason, a different method of measurement with higher resolution was needed.

4.3.3 Data Acquisition Board

The method used to measure arc current with high resolution was to use a National Instruments BNC-2120 data acquisition board (DAQ) that has analog inputs. The maximum input rating is ± 10V. The analog to digital card used by the computer was a National Instruments E series 6035-E card, capable of sampling rates up to 200 kHz and having a maximum resolution of 16 bits. Figure 4.11 shows a circuit current waveform measured

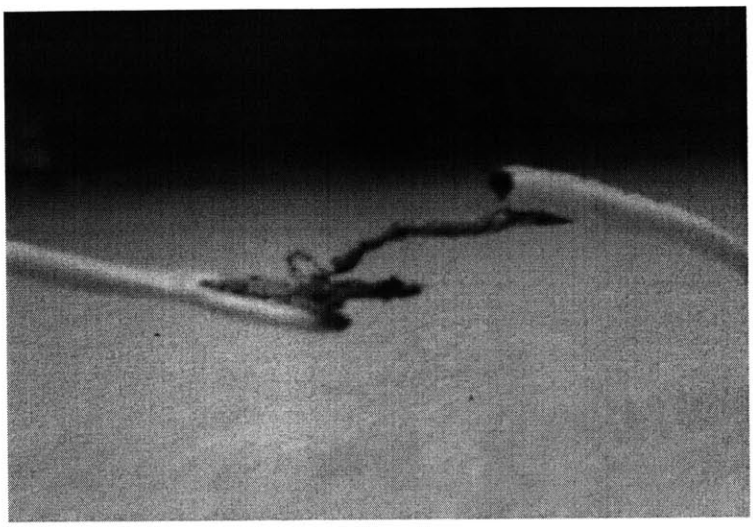

Figure 4.9: Damage caused to wire from periodic arcing

using the DAQ.

Method of triggering, sampling rate, and number of data points are specified by the user in LabView (code in Appendix A). The range values of the input voltage to the DAQ are specified in LabView and the computer sets the 16 bit resolution range over the specified range of input voltages. One limitation is that the 6035 analog to digital card always sets a voltage range symmetric around zero. Therefore, if our voltage ranges from 0 to 50mV, we must specify -50 to 50mV for the DAQ. Because we use only half of the range we lose one bit. Because of this, measurements used in this research are at 15 bit resolution and at a 200kHz sampling rate. Over a 100A range, 15 bit resolution gives ~3mA steps, a factor of ~100 improvement than using the oscilloscope.

Because control of the test apparatus as well as measurements are all being made from the DAQ, there is a software conflict when using LabView. Both virtual instruments (VI) used to control the experiment and measure the voltage across the shunt use a sub VI which cannot be used by two programs at the same time. We can solve this problem by noting that the data retrieval VI uses the sub VI once at the beginning during initialization, and at the end of the program before saving the data to a file. If we release the use of the sub VI as shown in the code in Appendix A, we can force the two VI's into a sequential use of the sub VI and we are then able to run both test control and measurement VI's simultaneously.

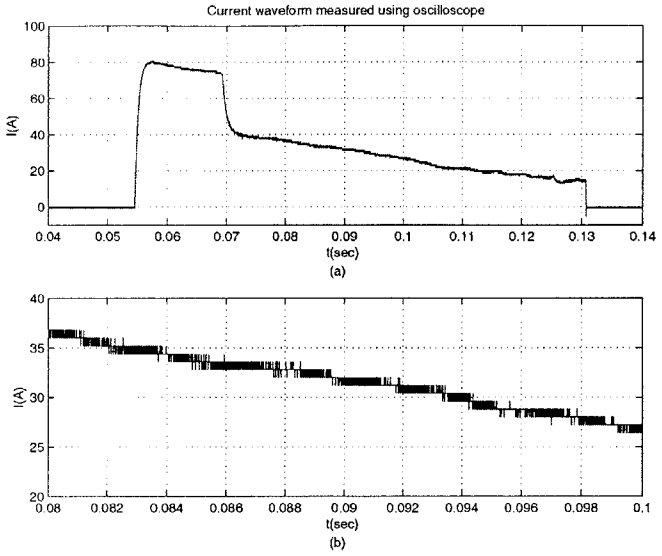

Figure 4.10: Current measured using oscilloscope (a) full test event (b) zoomed in when arc is on to show 8 bit, ~400mA sampling step in amplitude at 200 kHz sampling rate

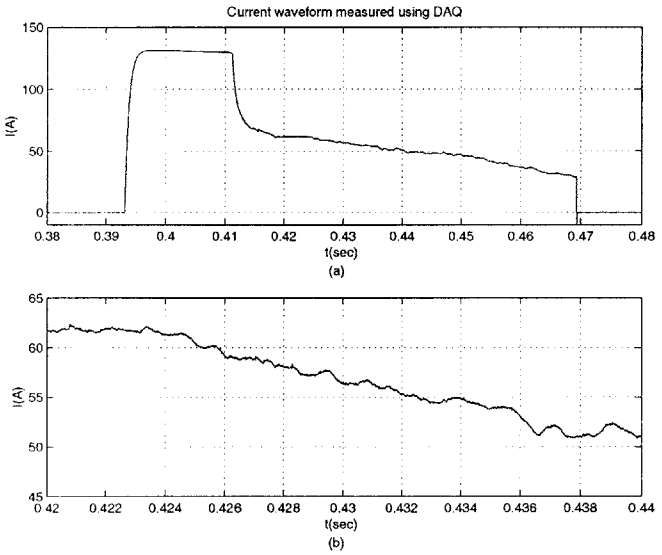

Figure 4.11: Current measured using DAQ showing 15 bit sampling (~3mA steps) (a) full test event (b) zoomed in when arc is on

4.4 Stationary Arcs

The apparatus used to produce drawn arcs was slightly altered to try to produce stable stationary arcs. A mechanical stop was placed behind the steel blade so that when the conductors separated the blade assembly would stop, forcing the the blade to stop with a gap on the order of a millimeter between the electrodes. The current to the motor was turned off once the mechanical stop was reached. The goal was to see how the arc current would behave at a single gap distance.

We do not believe the test set-up available was accurate enough at producing stable stationary arcs. This is because when the mechanical stop was reached, the motor did not immediately turn off. Instead, there was a delay on the order of milliseconds in which the motor remains on because of a short time delay in which LabView determines it is time to stop the PWM signal of the motor. This caused the steel blade to twist slightly. The motor used in this set-up could not be controlled accurately enough and it is suggested in Chapter 8 that a position servo would be useful to have more control ove the position of the blade in order to produce stationary arcs.

Chapter 5

Stable Arc Data Analysis

Once we obtain high resolution data of current during arcing events we can begin to look for an arc signature. This chapter describes the steps taken in the analysis of the data. A method for modelling the time domain circuit current waveform is described first and the use of the model is shown in Section 5.2. Following the description of the model, the frequency and time domain analysis of the arcing current data is presented.

5.1 Arc Event Modelling

Before we begin to take transforms of the data, we must first have a base waveform for comparison to insure that our transform methods are accurate. In our analysis, we wish to ignore the effects the experimental operating condition has on the frequency spectrum since real world conditions may not be exactly the same as the experimental set-up. For example, the steel blade begins to pull away from the test wire at a speed of about 20 cm/s. In a real world scenario, the electrodes may separate at a slower or faster speed so the effects of the pulling back of the motor on the spectrum must be ignored.

We must also ignore the low frequency current transient due to the motor making contact with a test wire and then pulling away. This waveform is specific to our test and will not be seen in real applications. We must therefore ignore the DC current step and focus our attention only on the small variations in current that occur during arcing.

For these reasons a model is developed to represent the base waveform. The Fourier transform of the model can be calculated analytically and then compared to the transforms of events which have small current transients due to arcing.

5.1.1 Linear Model

Looking at the circuit current waveform in Figure 4.8 we notice some major waveform components including the DC current and the falling current during arcing. There is also the small overshoot in current that occurs when the DC current step begins. We can model these components as a square pulse and line functions shifted vertically and horizontally into place. The model of the DC current step is shown in Figure 5.1. The Fourier transform

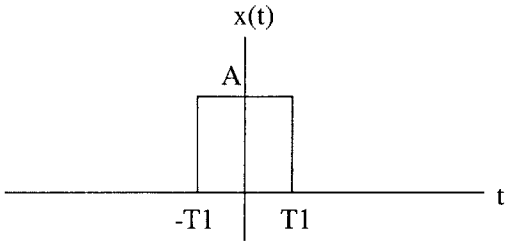

Figure 5.1: Square pulse to model DC current

of this square pulse of height A and width $2T_1$ is given by

$$X_{square}(j\omega) = \frac{2A \sin \omega T_1}{\omega} \tag{5.1}$$

The small overshoot in current as well as the falling of the current during arcing can be modelled as a line centered at zero with slope B/T_2 and width $2T_2$ as shown in Figure 5.2. Calculating the Fourier transform of this line gives us

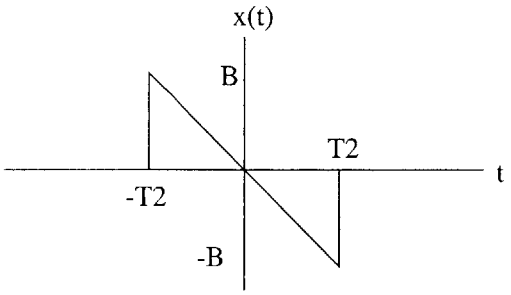

Figure 5.2: Line from $-T_2$ to T_2 to model current falls

$$X_{line}(j\omega) = \frac{B}{T_2}\left[\frac{2T_2}{j\omega}\cos(\omega T_2) - \frac{2}{j\omega^2}\sin(\omega T_2)\right] \tag{5.2}$$

The overshoot of current and decreasing arc current are modelled by shifting this line into the correct position with appropriate amplitude B and time duration T_2. Vertical shifts are accomplished by adding a square pulse in the time domain which adds a sinc $(\sin(x)/x)$ function in the frequency domain. For horizontal shifts in the time domain, we can recall that a signal shifted in time, $x(t - t_o)$, has a transform of the form $e^{-j\omega t_o}X(j\omega)$. The full linear model of one arc event as produced by the test set-up used is modelled in Figure 5.3. Definitions of the constants are given in Table 5.1.

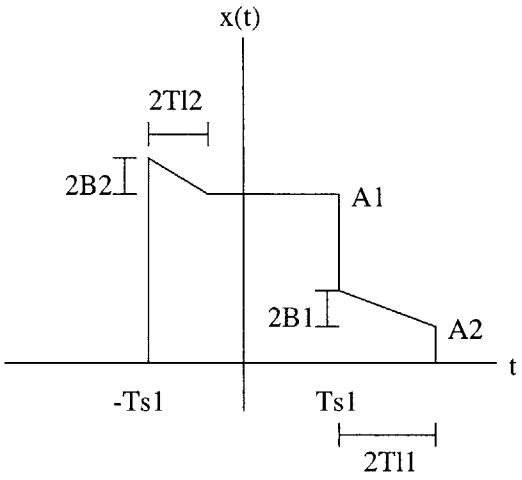

Figure 5.3: Model of arc event

To find the Fourier transform of the model, we take the transforms of each square pulse and ramp lines and add them together with appropriate time delays. The DC current is just a square pulse and its transform is found to be

$$X_{DCcurrent}(j\omega) = \frac{2A_1\sin(\omega T_{s1})}{\omega} \tag{5.3}$$

Table 5.1: Arc Model Constant Definitions

Constant	Definition
$2T_{l1}$	width of arc
$2T_{l2}$	width of overshoot
$2T_{s1}$	width of DC current duration
A_1	height of DC current
A_2	arc termination height
$2B_1$	height of arc
$2B_2$	height of overshoot

The overshoot and arc lines must be shifted into position before finding the transform. Square pulses are added to accomplish the vertical shift. Equations 5.4 and 5.5 are the Fourier transforms of the square pulses used to shift the arc line and overshoot line respectively.

$$X_{SquareArcShift}(j\omega) = \frac{2(A_2 + B_1)\sin(\omega T_{l1})}{\omega} \tag{5.4}$$

$$X_{SquareCurrentShift}(j\omega) = \frac{2B_2\sin(\omega T_{l2})}{\omega} \tag{5.5}$$

The transform of the arc will be the transform of the line through zero, vertically shifted by a square pulse with transform $X_{SquareArcShift}$ and horizontally shifted by $T_{l1} + T_{s1}$. We obtain the full transform of the arc portion as

$$X_{arc}(j\omega) = \left(\frac{B_1}{T_{l1}}\left[\frac{2T_{l1}}{j\omega}\cos(\omega T_{l1}) - \frac{2}{j\omega^2}\sin(\omega T_{l1})\right] + \frac{2(A_2 + B_1)\sin\omega T_{l1}}{\omega}\right)e^{-j\omega(T_{l1}+T_{s1})} \tag{5.6}$$

The same can be done for the DC current overshoot to obtain

$$X_{overshoot}(j\omega) = \left(\frac{B_2}{T_{l2}} \left[\frac{2T_{l2}}{j\omega} \cos(\omega T_{l2}) - \frac{2}{j\omega^2} \sin(\omega T_{l2}) \right] + \frac{2B_2 \sin \omega T_{l2}}{\omega} \right) e^{j\omega(T_{l2} - T_{s1})} \quad (5.7)$$

The total Fourier transform of the arc event model from Figure 5.3 is shown in Equation 5.8 and is the sum of the DC current, the arc model, and the overshoot model transforms.

$$X_{ArcEvent}(j\omega) = X_{DCcurrent}(j\omega) + X_{arc}(j\omega) + X_{overshoot}(j\omega) \quad (5.8)$$

We can choose some constants from measured data shown in Table 5.2 in order to get an idea of what the Fourier transforms of the arc event models will look like. Plotting the

Table 5.2: Arc Model Constant Values

Constant	Value
$2T_{l1}$	122 ms
$2T_{l2}$	8 ms
$2T_{s1}$	16 ms
A_1	68 A
A_2	7 A
$2B_1$	33 A
$2B_2$	3 A

transform gives the frequency spectrum shown in Figure 5.4. We notice that the transform is dominated by the square pulse which translates to a sinc function in the frequency domain with the negative slope lines producing milder effects.

5.1.2 Polynomial Model

When looking more closely at just the arcing current portion of the time waveform, we need to use a more accurate model. A better

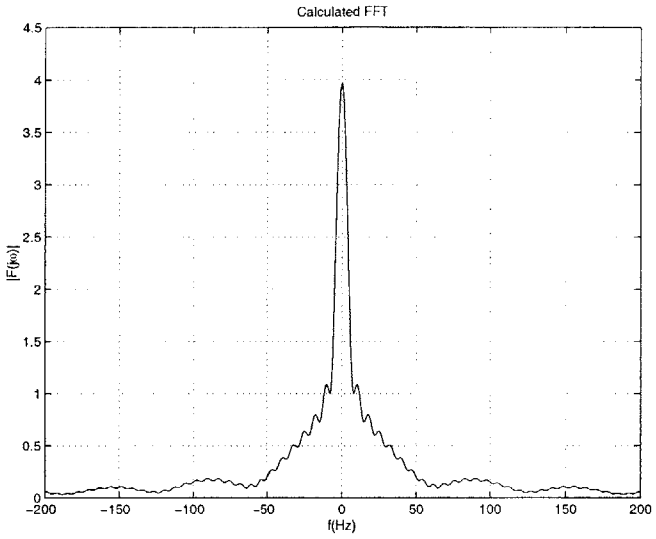

Figure 5.4: Calculated FFT magnitude of one arc model

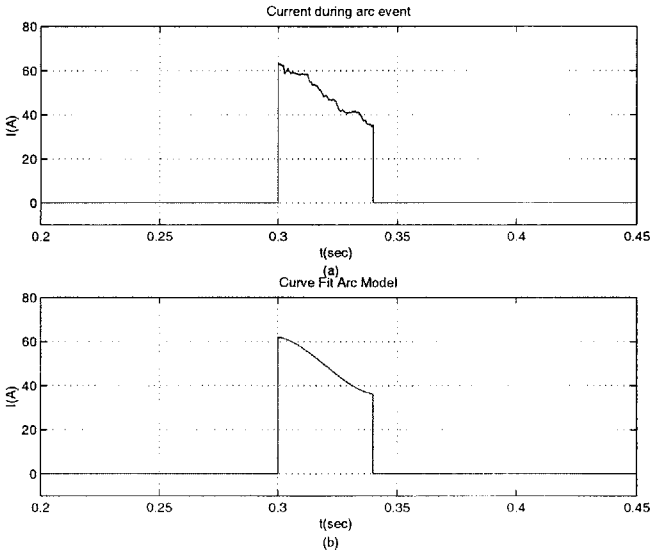

Figure 5.5: Current (a) measured during arcing current and (b) the 3rd order approximating polynomial model

fit model helps when we wish to eliminate the DC component of the current and only focus on the higher frequency transient as described in Section 5.2.4.

One way to obtain a better fit model is to fit a polynomial curve for the arcing current portion of the time waveform. After obtaining measurements of arcing current, MATLAB can be used to obtain polynomial fits of any order to the arcing current points as shown in Appendix B. Figure 5.5 shows an arc event with the DC step up in current removed and its third order approximating polynomial model. We can see that the polynomial fit better characterizes the slow current variations during arcing. We can thus subtract this model from the measured waveform to obtain a transient which consists mainly of higher frequency variations of arcing current.

5.2 Fourier Analysis

The following sections present data analysis that was performed. Fourier analysis using the full arc event and the linear model is first described and subsequent sections present changes and improvements made to analysis procedures. The full code written to perform the analysis is given in Appendix B.

5.2.1 Full Arc Event

We begin by looking at the frequency spectrum of the full arc event and comparing

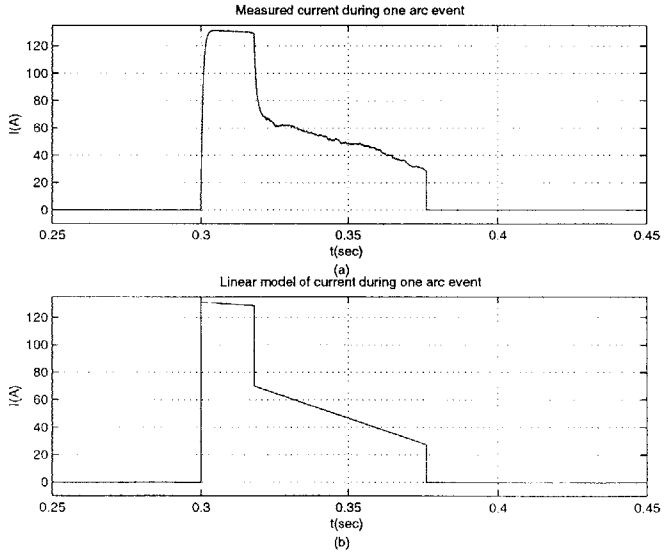

Figure 5.6: Current (a) measured during a full arc event and (b) its approximating linear model

it to the spectrum of its linear model. The goal of the comparison is to find differences that occur in the spectrum of the model due to higher frequency variations during arcing current. Figure 5.6 shows one measured arc event and its corresponding linear model.

Taking the Fourier transform of each gives us the frequency spectrums shown in Figure 5.7. Both the transform of the measured event as well as the model appear to be dominated by low frequency content due to the step up in current. This step up in current produces a sinc function seen in both transforms. We notice some differences in the transforms beginning to appear near 500Hz as shown in Figures 5.7(b) and (d).

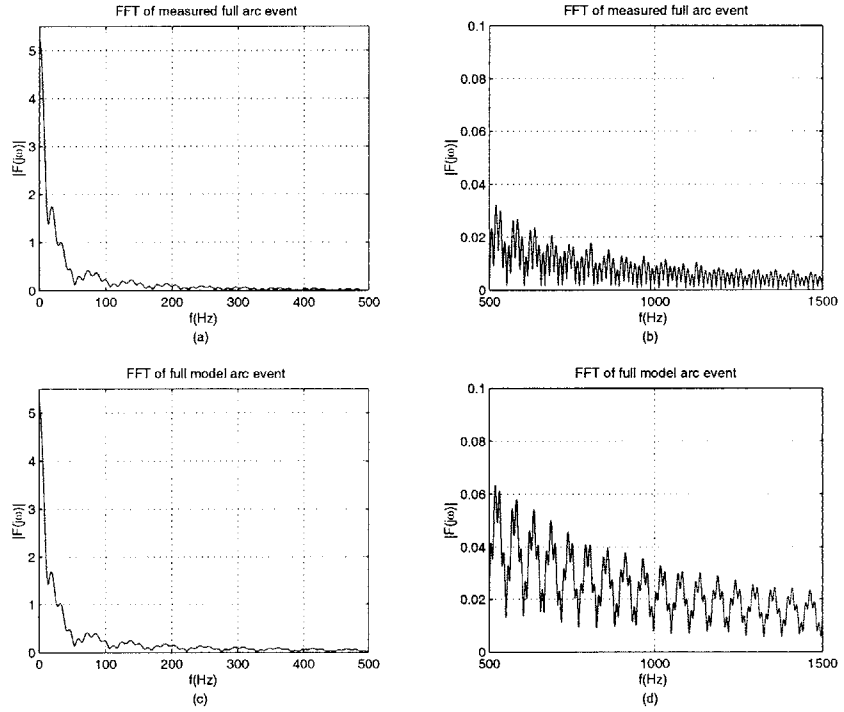

Figure 5.7: FFT magnitude of (a)&(b)current measured during a full arc event and (c)&(d) of its linear model for the waveform in Figure ??

We can also look at the phase of the FFT of the full arc event from Figure 5.6 shown in Figure 5.8.

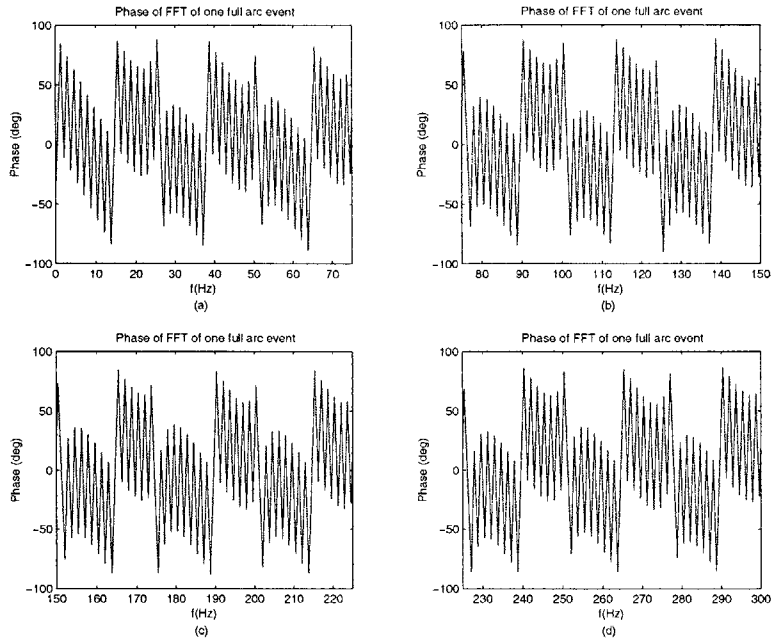

Figure 5.8: Phase of the full measured arc event in Figure 5.6 from zero to 300 Hz

Because of the random behavior of the current during arcing, the phase of the FFT varies quickly and in a periodic manner. The phase of other arc events exhibit the same behavior but have different shapes of variation. For this reason, we will limit ourselves to analyzing the magnitude of the FFT.

If we are to find an arc signature in the frequency domain, we would hope to see the same small variations in the magnitude of the transform of the real data from Figure 5.7 in all measured waveforms. A second arc event is shown in Figure 5.9 and their transforms are shown in Figure 5.10. Figures 5.10 (b) and (d) show higher frequency components of the second arc event transforms.

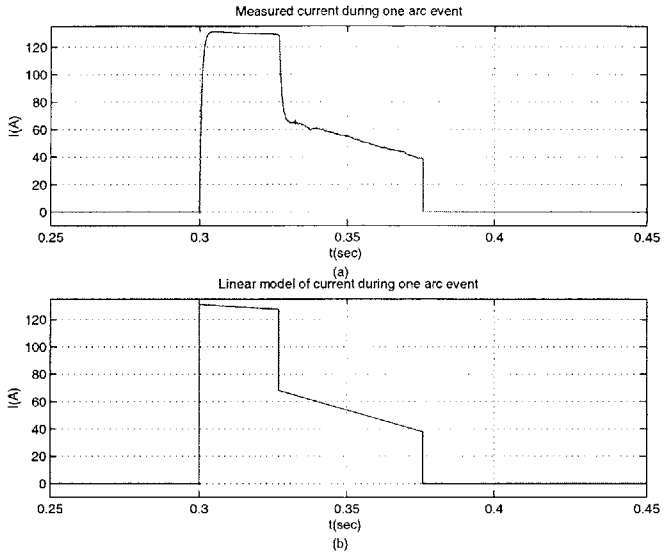

Figure 5.9: Current (a)measured during a second full arc event and (b)its approximating linear model

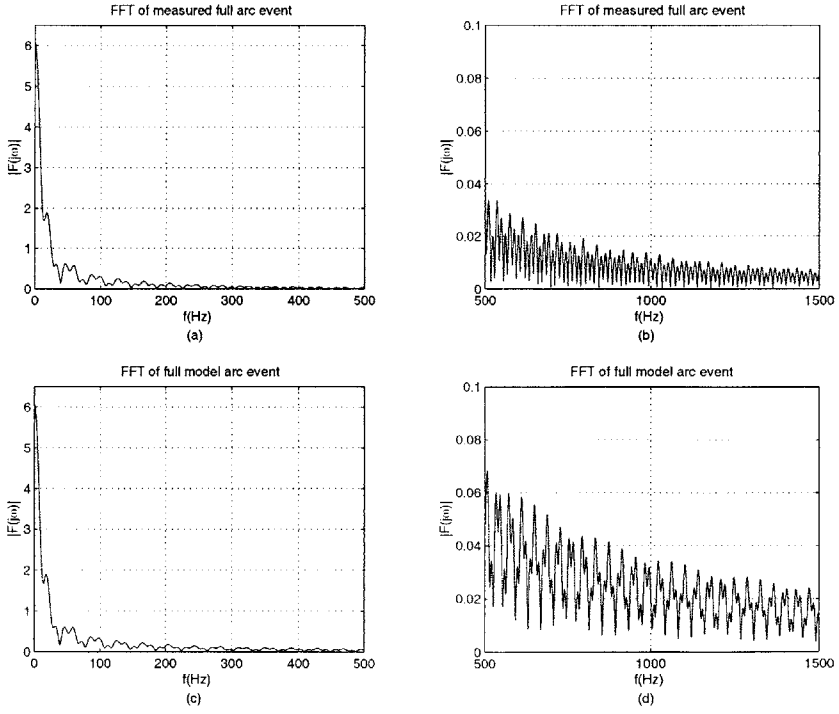

Figure 5.10: FFT magnitude of (a)&(b) current measured during a second full arc event and (c)&(d) of its linear model for the waveform in Figure 5.9

Once again the sinc function has the dominant amplitude with some variations seen in the real data transform. However, the variations between nominally the same arc events appear to be slightly different and do not take exactly the same shape nor do they appear at the same frequencies. From this analysis we deduce that the transform of the DC current step masks what the transform due to only the arc looks like. The next step is to eliminate the DC current component of the time waveform.

5.2.2 DC Current Removed

If we remove the DC current in the time waveform, we are left with just the decreasing current during the stable arc. This will still have a sinc shape in the frequency domain because of the height of the current and the decreasing current but perhaps the effect is not as prominent. When we ignore the DC current we obtain the waveform shown in Figure 5.11 (a). The initial step up in current has been removed and only the decreasing arcing

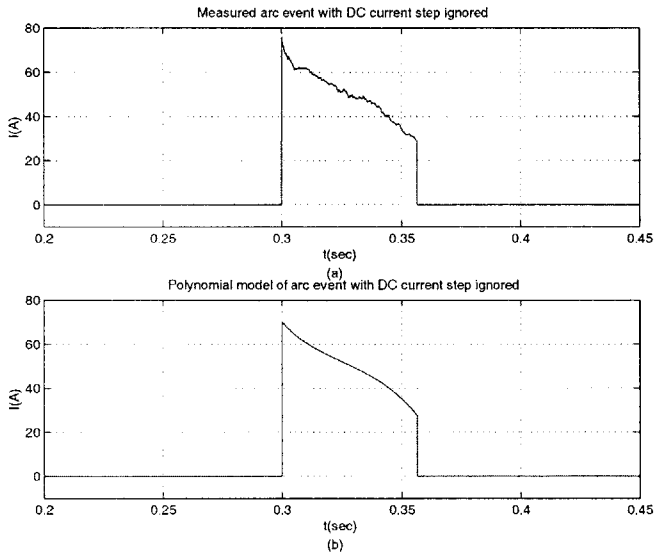

Figure 5.11: (a) An arc event with DC current step removed and (b) its approximating polynomial model

current remains. The model of the event then becomes a model of only the arcing current shown in Figure 5.11 (b). The Fourier transforms of the new event and model are shown in Figure 5.12.

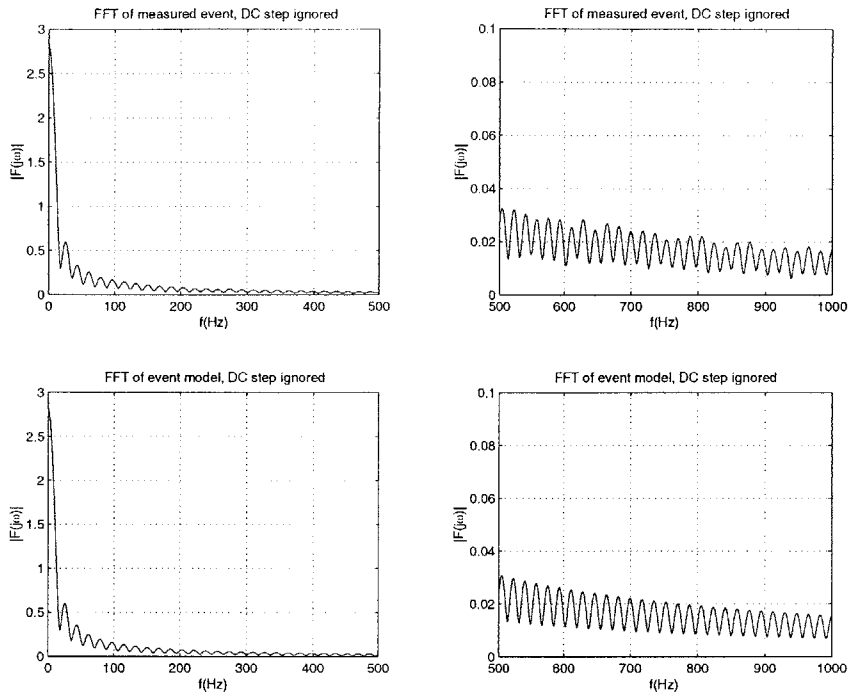

Figure 5.12: FFT of (a)-(b) one arc event with DC current step removed and (c)-(d)FFT of its polynomial model

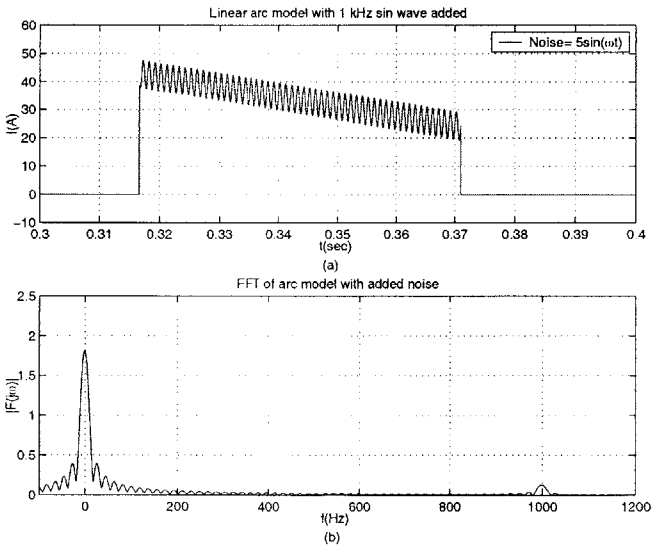

Figure 5.13: (a) Linear arc model with 10 A peak to peak noise added and (b) its FFT

Once again the stepped height of the current produces a sinc function which dominates the lower frequency components of the spectrum. We do see variations again in the higher frequency components in the measured current from the model as in Figures 5.12(b) and (d) but it is still difficult to determine a definitive signature of the arc.

Differences in the transform can be seen at higher frequencies but they are not large enough to form the basis for finding an arc signature. We must find a method for looking only at the faster transients that occur during the slow falling arc current. Also, variations in one arc event may be too random to obtain a clear signature. We will thus take a look at the average over a number of events and try to observe an arc signature. Before studying the higher frequency variations, a brief description of how the magnitude of the falling current affects the overall transform is given.

5.2.3 Effect of Average Arcing Current Magnitude on the FFT

This section will explore how small variations in current affect the Fourier transform of an arc event. For simplicity we will neglect the DC step in current and focus only on the decreasing current and current variations that occur during arcing.

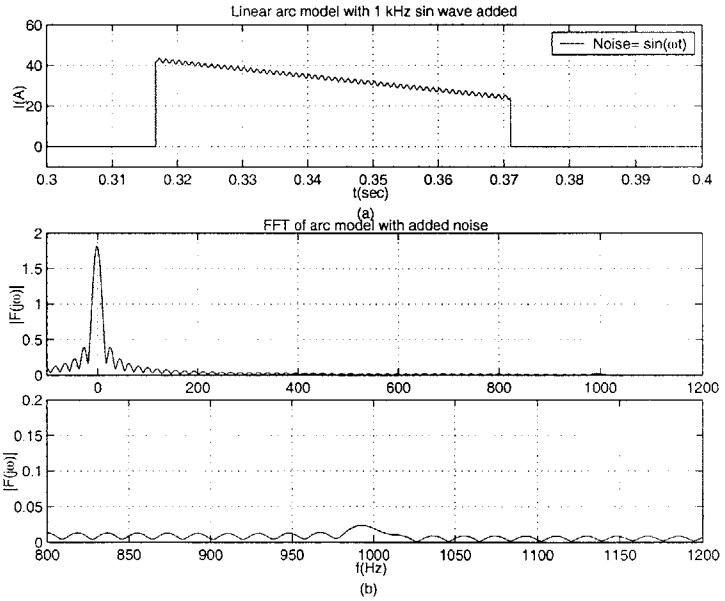

Figure 5.14: (a) Linear arc model with 2 A peak to peak noise added and (b) its FFT

We need to determine the effects of noise during the linear fall of the model on the FFT.

The noise that will be added will be a continuous sine wave at a single frequency. We know the Fourier transform of a sine wave is a pair of impulses at the plus and minus frequency of the sine wave and what we expect to see is an increase in the amplitude of the overall transform at the frequency of the noise. Figure 5.13(a) shows the linear model with a 1kHz sine wave added as noise.

The noise is of a large magnitude and such variations in current are not the norm during arcing but looking at Figure 5.13(b) we can see that the spike at 1kHz is an order of magnitude less than the DC current contribution to the transform. Decreasing the amplitude by a factor of 5 decreases the amplitude of the spike at 1kHz as shown in Figure 5.14, as expected.

Decreasing the amplitude of the noise even further makes the spike in the frequency domain negligibly small. Figure 5.15 demonstrates that there is content at 1kHz due to the sinusoidal noise but it is not clear that it is an impulse due to a sine wave.

After this analysis it is clear that in order to examine the frequency content of the current variations during arcing current we must not just ignore the DC current, but the average magnitude of current during arcing as well since this average DC current value introduces a dominant sinc function in the frequency domain.

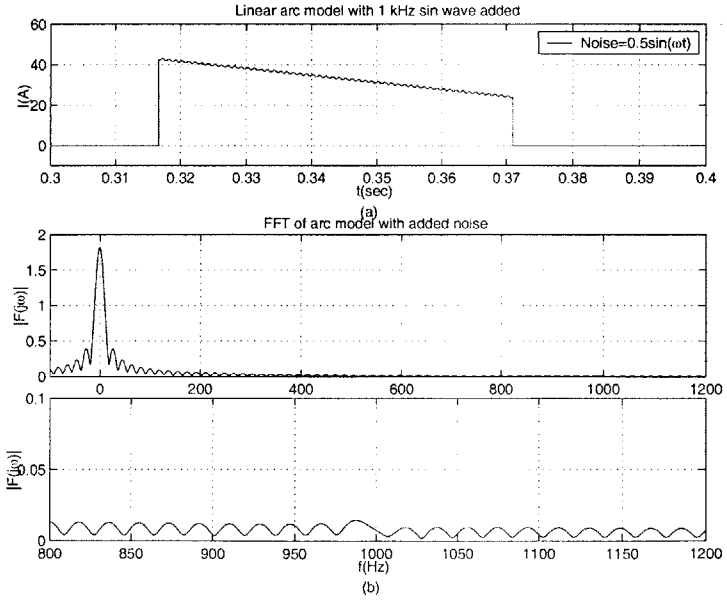

Figure 5.15: (a) Linear arc model with 1 A peak to peak noise added and (b) its FFT

5.2.4 Zero Centered Arc Transients

As shown in the previous section, it is difficult to see what the actual frequency content of the arc transient is due to the dominance of the content introduced by the current magnitude. Using our polynomial model however, we can take each arc event and subtract out its corresponding polynomial fit. This gives us an arcing transient approximately centered around zero and with no DC component.

As mentioned in Section 5.2.2, one arc event may not be sufficient to find an arc signature. An average of the transforms over a number of events can help reveal the average characteristics of the arcing transients. To make any differences in power in the frequency domain more apparent, we will use the periodogram, defined in Equation 5.9 where N is the number of points in the transform, to observe the power density distribution of the time waveform in the frequency domain.

$$P = \frac{1}{N}|X_N(j\omega)|^2 \tag{5.9}$$

We know that $|X_N(j\omega)|^2$ is the energy distribution in frequency of the corresponding time signal $x_N(t)$ and dividing by N gives us the power spectral density estimate of the time domain signal. Averaging the periodograms over more than one event gives us the expression in Equation 5.10.

$$P_{avg} = \frac{1}{M}\sum_{i=1}^{M}\frac{1}{N}|X_{Ni}(j\omega)|^2 \tag{5.10}$$

where N is the number of data points of the transform and M is the total number of transforms to average over. Using the average of the periodograms will give us a better understanding of what the power distribution is in the frequency domain due to general properties of the arcing current.

Figure 5.16 shows one arc event and its third order polynomial model. Subtracting the model from its measured waveform we obtain the zero centered transient of Figure 5.17. We now have a transient in the time domain that we can analyze. Figures 5.18 and 5.19 show all 10 zero centered arc transients used for the averaging analysis.

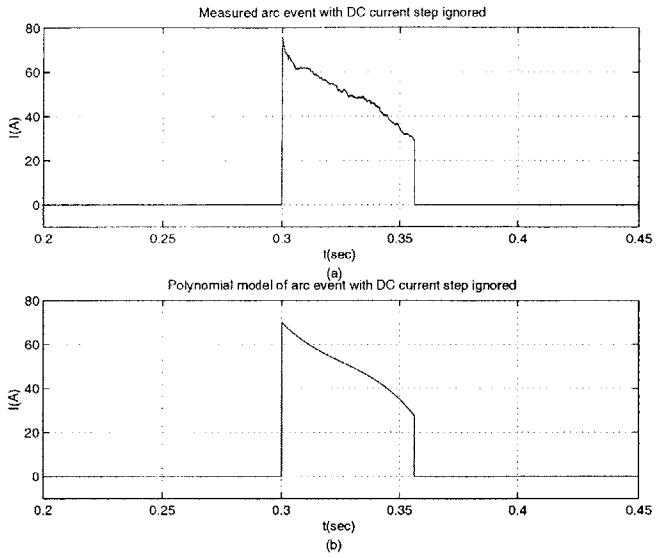

Figure 5.16: (a) One arc event and (b) its 3rd order polynomial model

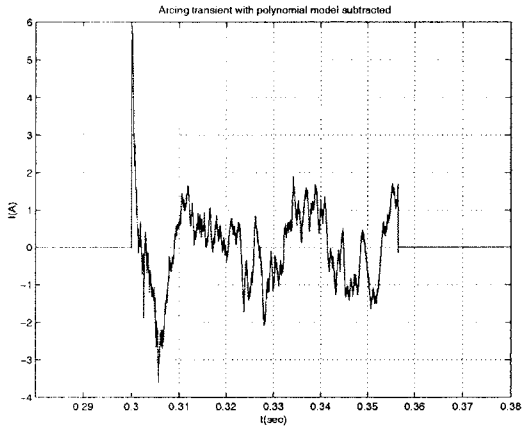

Figure 5.17: Arc event from Figure 5.16 (a) with its polynomial model subtracted out

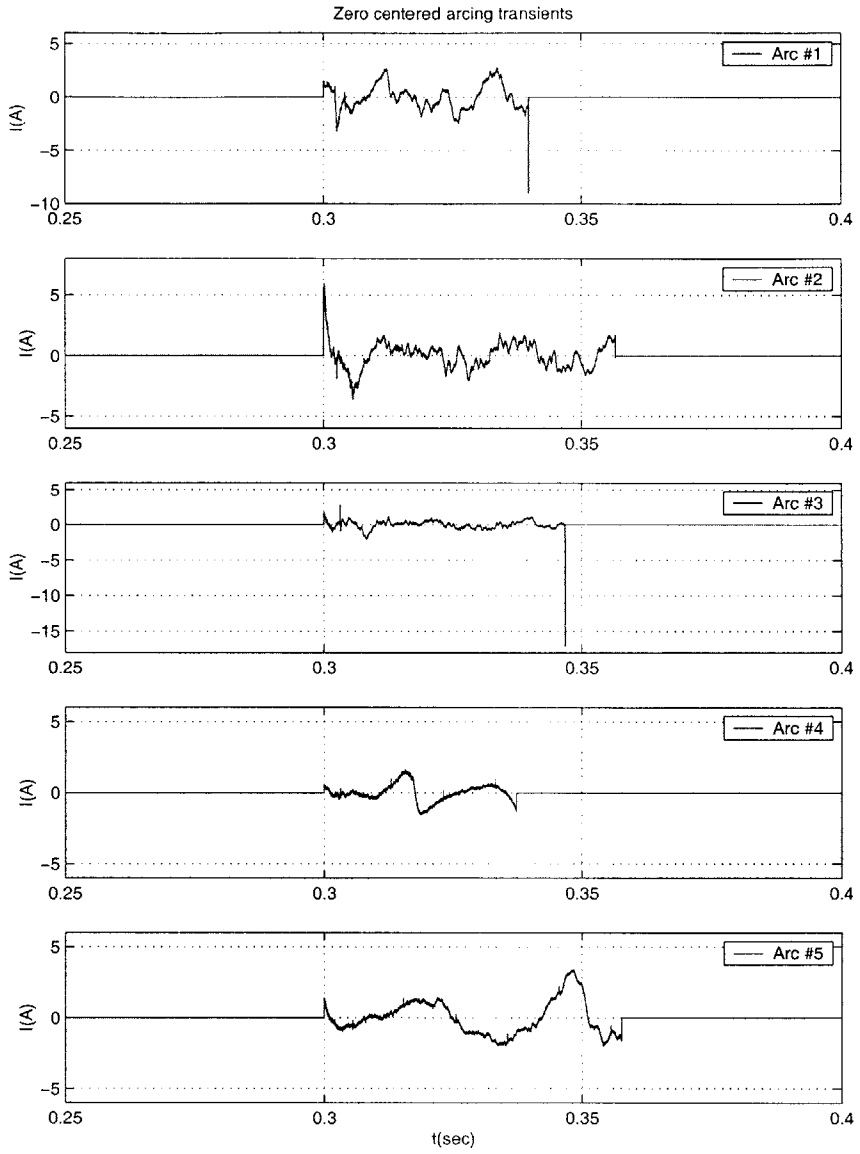

Figure 5.18: Zero centered arc transients 1 through 5 used in the average periodogram analysis

Obtaining the periodogram we see that just as expected there is no longer any DC component in the frequency domain as shown in Figure 5.20(a). The periodograms for the ten individual periodograms are shown in Appendix C.

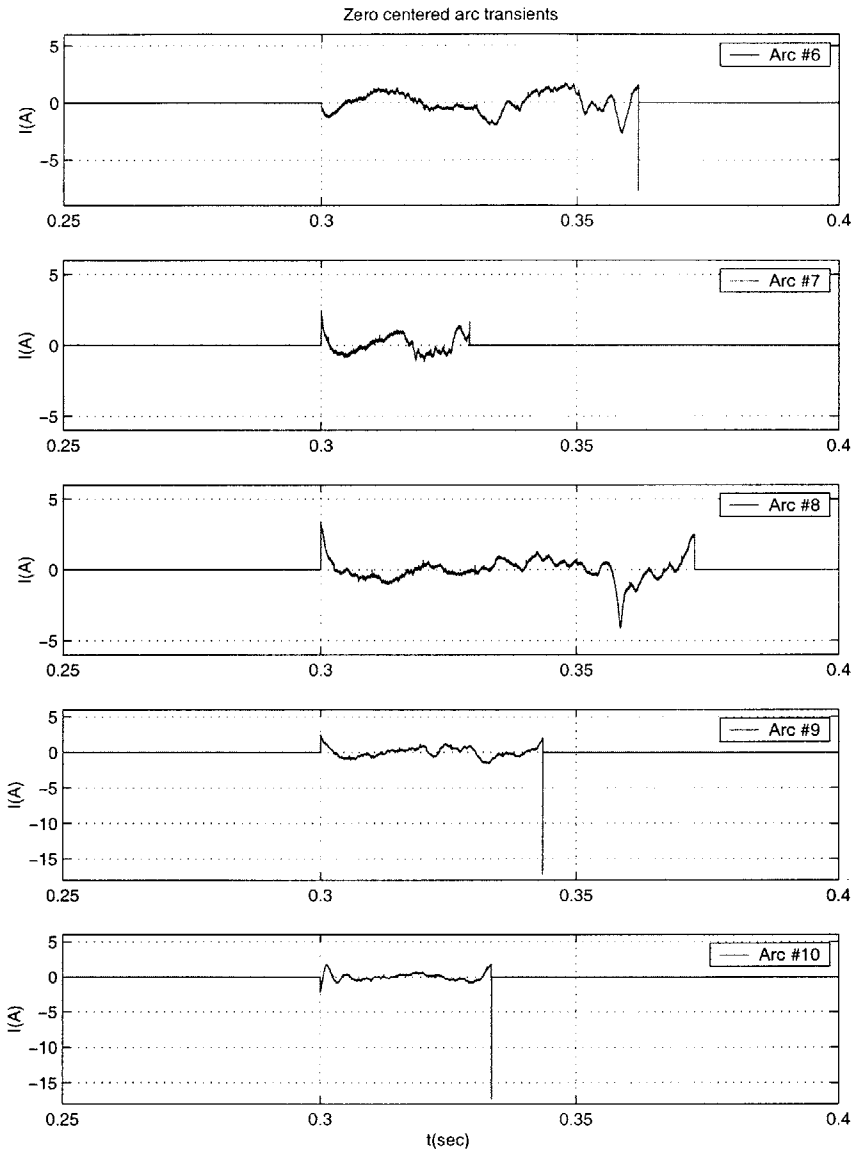

Figure 5.19: Zero centered arc transients 6 through 10 used in the average periodogram analysis

Performing the above computations on 10 arc events and averaging the periodograms according to Equation 5.10 we obtain the average periodogram in Figure 5.21.

We first notice a peaking in the vicinity of 40 Hz. For the rest of the average periodogram we do not see any specific signatures. In fact, the spectrum simply seems to fall off as 1/f with no arc signature uniquely defined up to 10 kHz. Above 10 kHz the amplitude of the

spectrum reaches the amplitude of the spectrum of the noise caused by the measurement equipment. The analysis of the frequency domain began with the thought that there might be an arc signature which would allow us to easily distinguish electric arcing from any other transient.

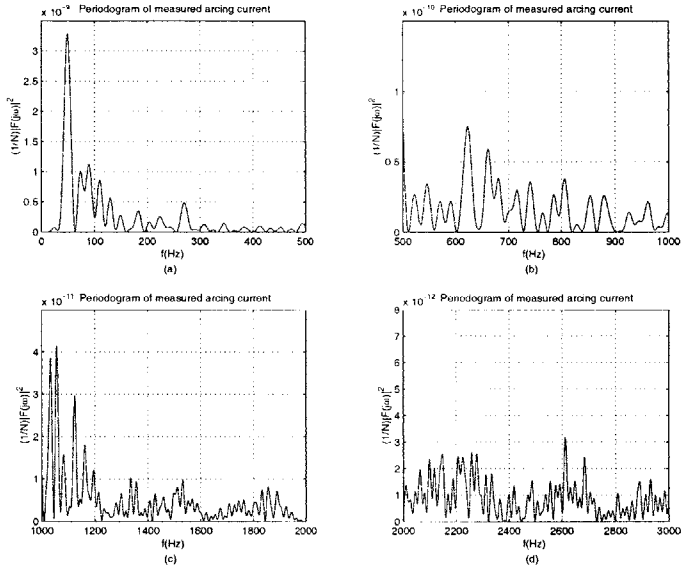

Figure 5.20: Periodogram of one arc event transient

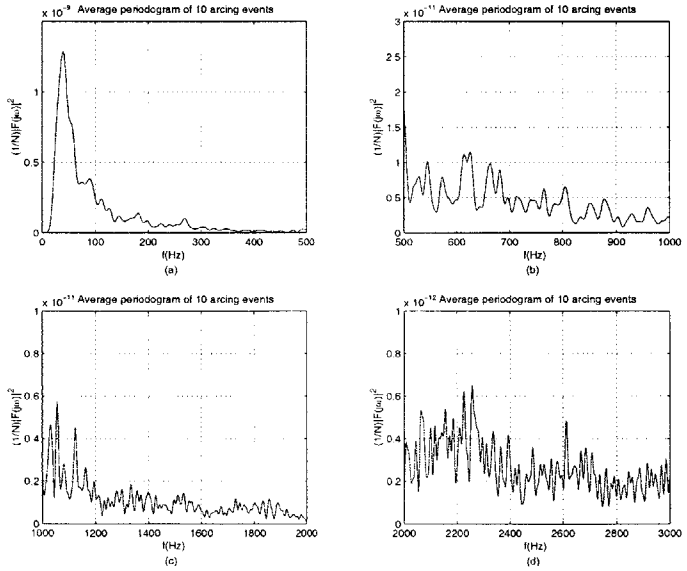

Figure 5.21: Average of 10 arc event periodograms

As we can see from Figure 5.21, this is not the case. Aside from a peak at 40 Hz, which we will discuss further in Section 5.2.6, there is no definite arc spectrum shape which we can use to design a filter to adequately detect arc transients.

We next look at using just the amplitude of the spectrum to detect arcs. If the arcing spectrum amplitude is substantially higher than during normal operation current then this can be used as a detection method. The next section discusses the arc spectrum compared to variations seen during DC current and Chapter 6 describes measurements taken from a real car to determine if this new amplitude comparison method is feasible.

5.2.5 Comparison to DC current

In Section 5.2.4 we found that the arc spectrum does not contain defining characteristics which can be used to detect an arc. We now look at how the amplitude of the arcing transient spectrum compares to the spectrum of the small transients seen during DC current. This section will consider the DC current that flows when the blade and test wire are in contact as normal operation. Chapter 6 will consider more complex transients as can occur during operation of electrical loads such as lights, power door locks, or power windows.

In order to compare small transients, the average DC value during normal operation is subtracted out. We will thus have two zero centered transients, the arc and the normal operation transients, that we can compare. Figure 5.22 shows the arcing and normal operation transients.

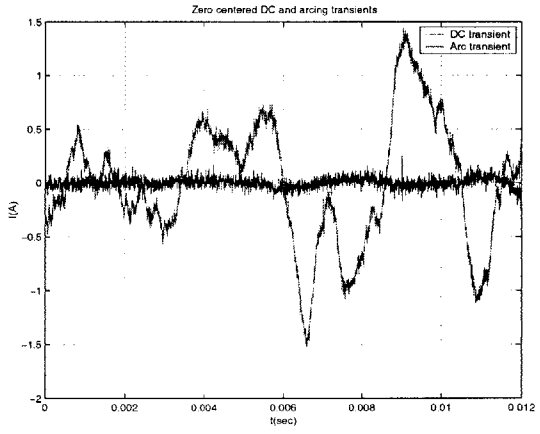

Figure 5.22: Zero centered DC current and arcing transients

The variations in the time domain of the normal operation transients are small compared to the arc transients. If normal operation were a pure DC signal, the transients would be zero and the frequency spectrum during normal operation would also be zero.

Using the process previously described, the periodogram of each signal is found and is shown in Figure 5.23. There is a large difference between amplitudes of the spectrums of the two transients. We can see that if the normal operation of a system is a steady DC current and the electric load transients are small in amplitude in the time domain compared to the arcing transients we can use the difference in amplitude of the periodograms to identify arcing. Also, if normal load transients have known frequency characteristics, as in the PWM signals sent to the headlights, these can be distinguished from arcing transients.

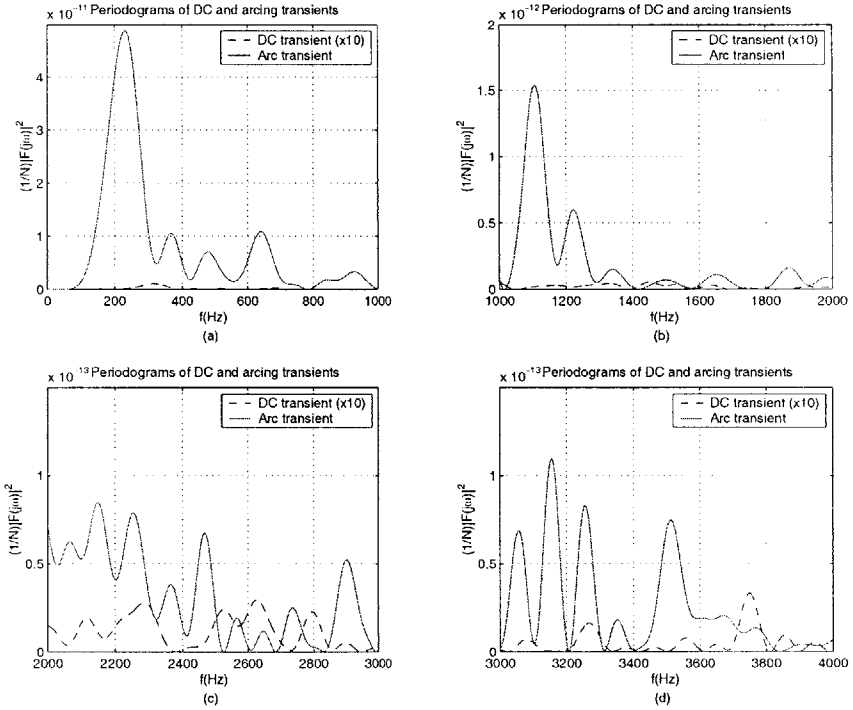

Figure 5.23: Periodograms of DC and arcing transients over the frequency range of zero to 4 kHz. The DC transient periodogram is multiplied by 10 to be viewable on the same scale as the arc transient periodogram

Notice that the normal operation examined in this section was basically a steady DC signal whose transform is nearly zero at all frequencies except the zero frequency. One problem that can occur in the automotive case is that a variety of noisy transients occur. Normal operation in a car will include some arcing from the alternator commutation, noise from various motors, and other noisy transients which may not be easily characterized. Previous

work in arc detection has used just the amplitude of the frequency spectrum of the arc in 48V DC telecommunications systems [11, 12]. However, transients in the automotive system can sometimes reach an amplitude at specific frequency ranges in the frequency domain comparable to the amplitude during arcing as will be shown in Chapter 6.

5.2.6 Effect of Motor Speed on Arc Periodogram

In Section 5.2.4 it was shown that there was a peak near 40 Hz in the spectrum of arcing transients. We wish to determine if this peak at 40 Hz is representative of arc characteristics and exists in different arcing situations. One way to vary the arc in the time domain is to change the speed of the motor. Here we double the speed of the motor so the blade makes 2 contacts per second by doubling the duty cycle of the PWM signal being sent to the motor. Each arc is now drawn twice as fast. Figure 5.24 shows the time domain waveform of the measured arc event when the motor speed is doubled.

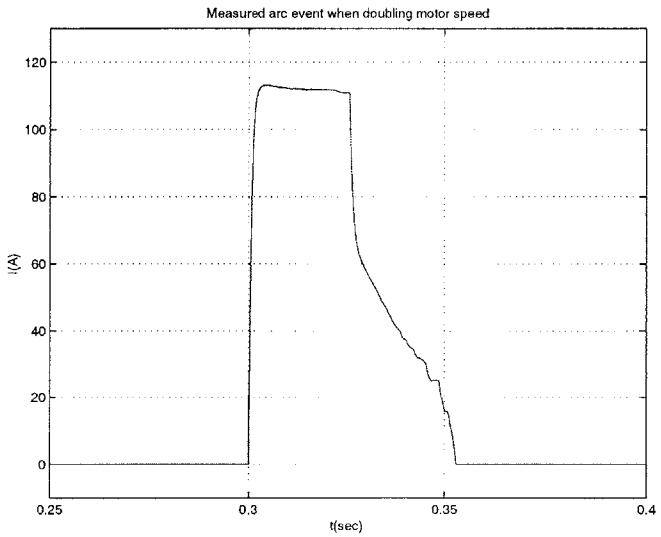

Figure 5.24: Full arc event with the chopping motor at twice the speed (2 contacts/second)

The current falls faster due to the blade pulling away at a greater speed. Using the model shown in Figure 5.25(b) for the arc event in Figure 5.25(a) we can create a zero centered transient.

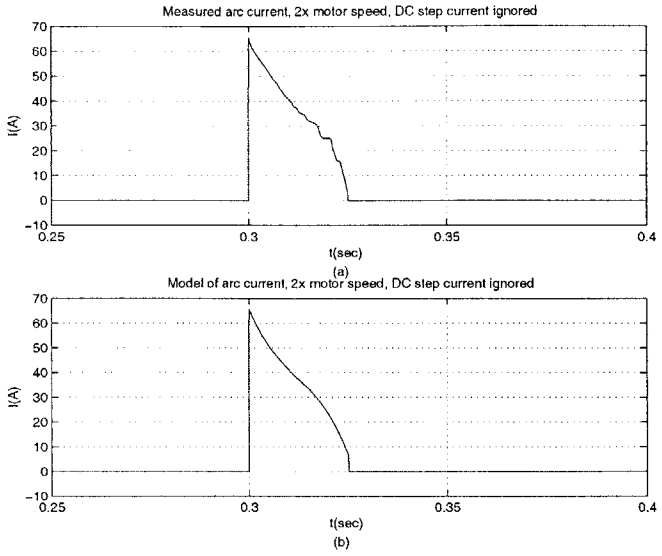

Figure 5.25: Waveform of (a) measured arc from Figure 5.24 with DC step ignored and (b) its model with the motor at twice the speed (2 contacts/second)

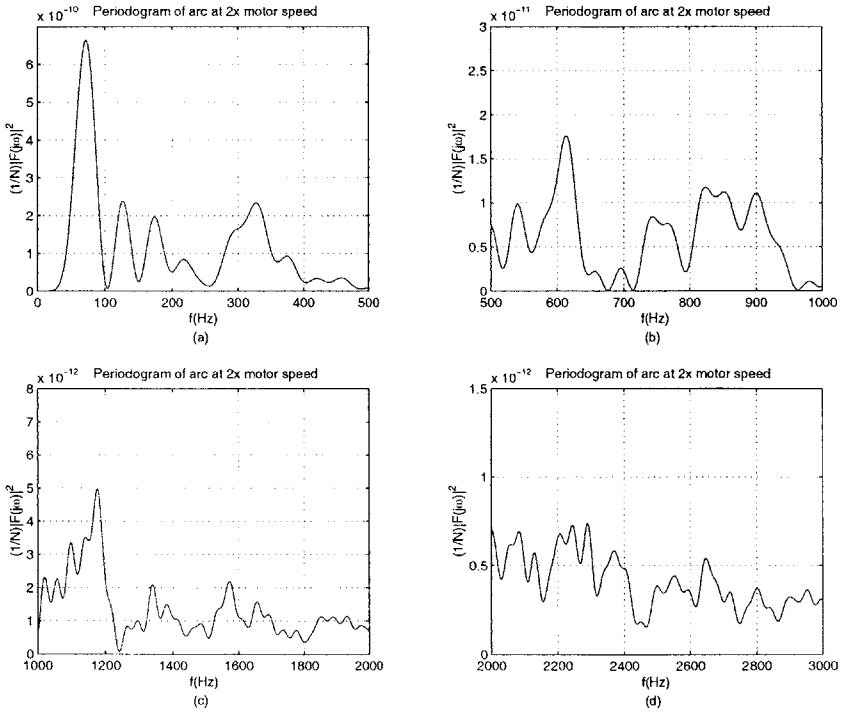

Figure 5.26: Periodogram of one arc transient with the motor operated at twice the speed from zero to 3 kHz

The periodogram of the new arcing transient is shown in Figure 5.26. We can see that the doubling of motor speed has caused the peak near 40 Hz to move closer to 80 Hz. This peak is therefore an effect of the speed at which the arc is drawn and not a characteristic of the arc itself. At higher frequencies however, the spectrum is similar to those seen before. We see the same change in the periodogram in the average over 10 arc events as seen in Figure 5.27.

The low frequencies of the spectrum are thus greatly affected by the details of the experimental setup used in this research and cannot be used to design a detector for all arcing conditions.

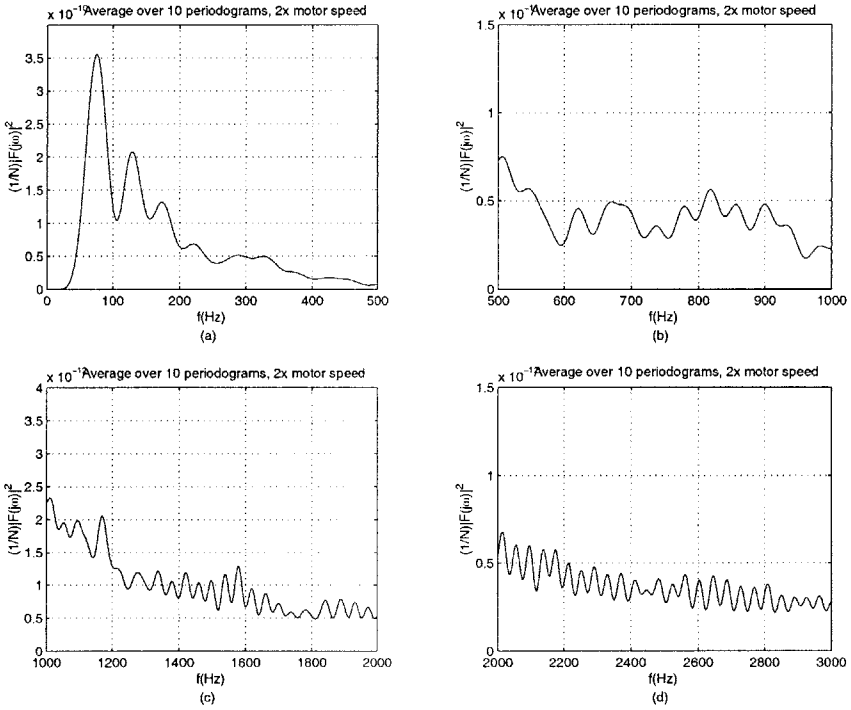

Figure 5.27: Average periodogram over 10 arc events with the motor at twice the speed

5.2.7 Sine Windowing to Improve Periodogram

In Section 5.2.4 we created zero centered arc transients by subtracting a polynomial fit model from the measured data. Because of slight errors at the ends of the data, there are larger peaks that occur at the edges of the waveform. In order to reduce the effects of the edges due to the subtraction we can multiply the time domain waveform by a sine window. This window will begin at the first data point at zero and rise sinusoidally for a quarter

cycle until it reaches an amplitude of 1. When the next edge of data is close, the window decreases sinusoidally for a quarter cycle until it reaches the final transient data point with a magnitude of zero. The width of each of the quarter cycles of the sinusoidal ends of the window are 5% of the total number of data points of the arcing transient. Therefore, if an arc transient is 10,000 points, the sine quarter cycles will affect 1,000 of the points, 500 at each end of the data.

Figure 5.28 shows how the time domain data is affected by the windowing. We can see that the edges of the waveform are reduced in magnitude and the high peaks seen at the end points of the data are now eliminated. We are left with data which better represents the arcing transient. The average periodogram over 10 arc events of the new arcing transients is shown in Figure 5.29. We notice that the peaks on the edges of the data created by the error between the model and the measured waveforms affect the amplitude of the periodograms. The overall shape of the spectrum remains basically the same. What we have accomplished by windowing the data is a more accurate representation of the spectrum as well as help to obtain more accurate analysis in the the time domain as shown in Section 5.3.

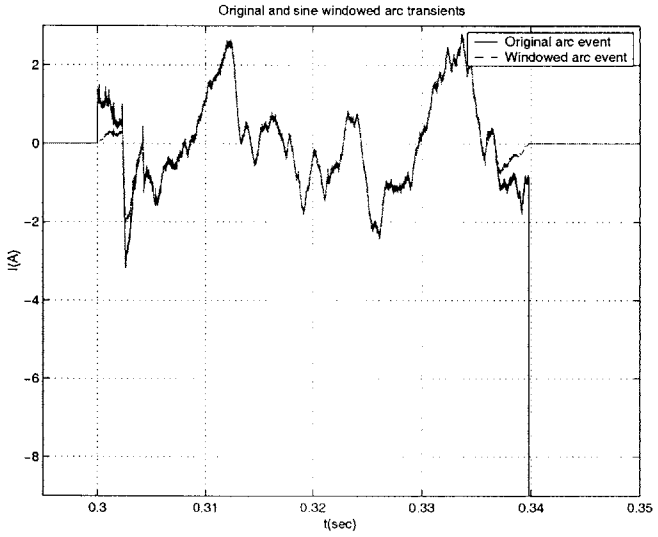

Figure 5.28: Effect of sinusoidal windowing on arc transient data of Figure 5.18 arc #1

5.3 Time Domain Analysis

Most of the analysis so far has been in the frequency domain. We can also look at the variations in time during arcing transients. The variations of the current in time are fairly

random but we can find the variance of the transient using the zero centered arc signals shown in Section 5.2.4. The variance can be calculated using Equation 5.11

$$E[(x-\mu)^2] \approx \frac{1}{N}\sum_{i=1}^{N}(x_i-\mu)^2 = \sigma^2 \tag{5.11}$$

where μ is the mean of the data, x_i is the ith data point, N is the number of data points, and σ^2 is the variance. This approximation for the variance is valid for large N by the law of large numbers. Also, in the zero centered transients, μ is much smaller than the variations in data so we can assume that $\mu \approx 0$.

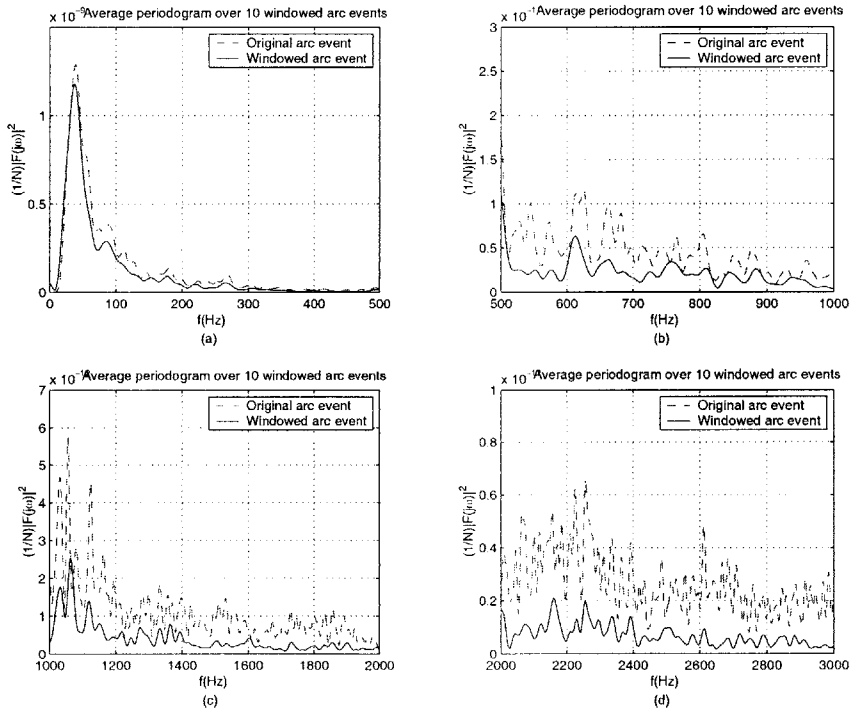

Figure 5.29: Average over 10 periodograms of windowed arc transients

The variances of the 10 arc transients used to find the average periodogram were found and are shown in Table 5.3. We can see that the variances of the transients are not very similar. The randomness of each arc event creates ranging variances. Although the variance is not always the same, we now have an idea of how the current varies and we can compare these variances to those during normal current operation. The first steps of this analysis

are described in Chapter 6.

One problem that arises in detecting the arc in the time domain is the range of operation modes of the automotive electrical system. As will be shown in Chapter 6, the current during normal operation varies, from noisy transients to structured PWM signals. A combination of these currents can also occur if more than one load is operating at one time. In previous arc detection work for DC systems using comparisons between arcing and normal operation, the electrical system was steady with transients such as capacitor bank disconnection riding on top of the signal. This steady normal operation signal does not always exist during vehicle operation and it is for this reason that determining a normal operation circuit current is difficult compared to a system such as the 48V DC telecommunications system described in Section 3.1.1.

Steps in current as well as large and noisy transients make it difficult to monitor the changes in energy of the current. For example, a change from parking lights to high beams creates a large step in current. If a real time detector were to compare the change of the sum of the squares of the sampled current to that of a typical arc event, they could be comparable and this would make discrimination difficult.

Table 5.3: Variances of 10 Arc Events: Motor Speed at 1 contact/second

Event #	σ^2
1	1.399
2	1.192
3	0.302
4	0.3798
5	1.494
6	0.807
7	1.334
8	0.648
9	0.522
10	0.385

Chapter 6

Electric Loads on a Mercury 14V Bus

We now know what the spectrum of the arc is such that there are no measurable distinguishing characteristics. We may however, still be able to compare the spectrum of the arc to the spectrum of normal operation current. This chapter examines what current during real load operation looks like. For circuit current measurements, a 1997 Mercury Sable donated to the MIT/Industry Automotive Consortium was used. This particular car does not have a power train nor interior trim but includes a complete wire harness including all electrical loads. The ignition was bypassed as shown in Appendix D in order to place the electrical system into the off, accessory, and start positions. All current measurements were taken using a current probe on the wire connected to the positive battery terminal.

6.1 Current During Loads

6.1.1 Ignition Off Mode

First we can examine the time domain waveforms during operation of various electrical loads. In the off mode, the electric door locks, CD changer, parking lights, and the seat tilt mechanism are operational. Figure 6.1 shows the time domain waveforms of these circuit currents.

We can begin to see the difficulty in recognizing arcing transients from the normal mode operation current. Figure 6.1(a) shows the current during power door lock operation. We can see a step up in current as the actuator unlocks or locks the doors as well as a large noisy transient on top of the step. The parking light waveform shown in Figure 6.1(b) has a more definitive structure. The PWM signal sent to the headlights is easier to recognize than the transients that occur in other components. The CD changer current waveform shown in Figure 6.1(c) is once again a transient which can be difficult to characterize and the seat tilt, which is run by a motor, is a somewhat structured transient as seen in Figure 6.1(d). As we will see, signals which have some sort of structure to them will be easier to recognize in the frequency domain compared to the arcing spectrum.

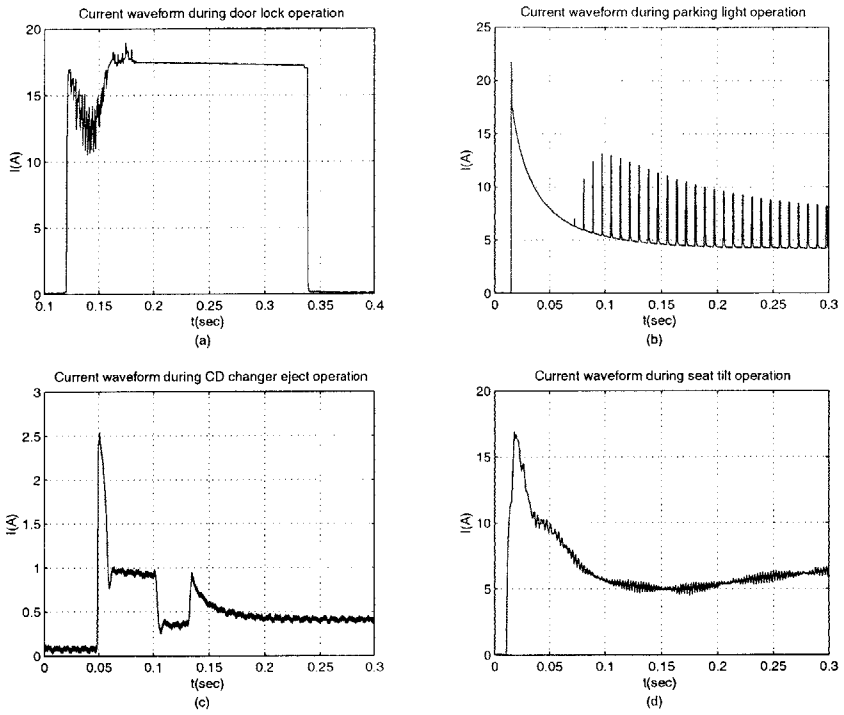

Figure 6.1: Current during turn-on operation of (a) door locks (b) parking lights (c) CD changer (d) seat tilt

6.1.2 Ignition Accessory Mode

Turning the ignition to accessory mode enables the power windows, sunroof, and the windshield wipers. Figure 6.2 shows the circuit current waveforms during the operation of these electrical loads. The three electrical loads shown are produced by motors. This gives noisy current transients during operation of the components. We must once again notice that these waveforms are measured when only one component is operating at any given time. If the window and sunroof were being operated simultaneously we would see a combination of the transients.

6.1.3 Ignition Start Mode

The final mode of operation is the start mode. During the start mode, the radiator cooling fan is started and the dashboard lights go on or blink. In a regular car, this is the mode of the electrical system during start up of the engine. Figure 6.3 shows the circuit current

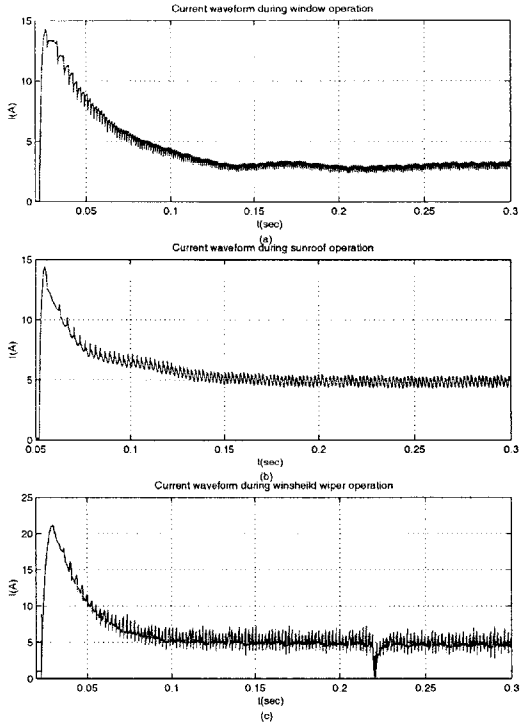

Figure 6.2: Current during turn-on operation of (a) windows (b) sunroof (c) windshield wipers

during this start mode.

We must note that although we are in the start mode, Figure 6.3 does not represent the true engine start waveform. This is because the dominant start-up load, the starter motor, was not available to include in the test.

Again we see that after the step up, the current is not steady. There are variations that occur and seem to increase in frequency until the current reaches a steady state DC level. Once the level is reached, the frequency of the variations becomes somewhat constant as can be seen in other components such as the head lights and windshield wipers.

6.2 Fourier Analysis of Load Currents

The next step in analyzing vehicle electric load currents is to find each of the component's frequency spectrum. By doing this, we can determine if the shape or amplitude of the arc

spectrum, or both, can be used to differentiate between normal and arcing currents.

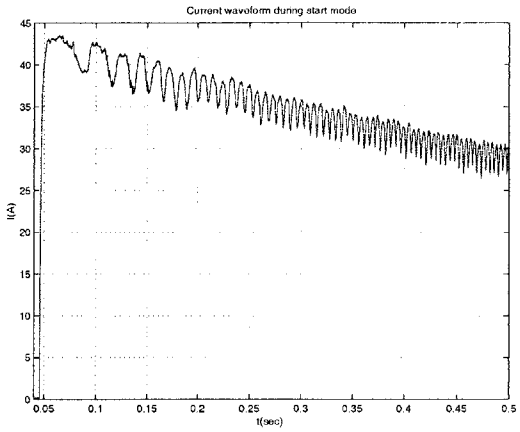

Figure 6.3: Turn-on current waveform during ignition start mode of radiator fan and dashboard lights

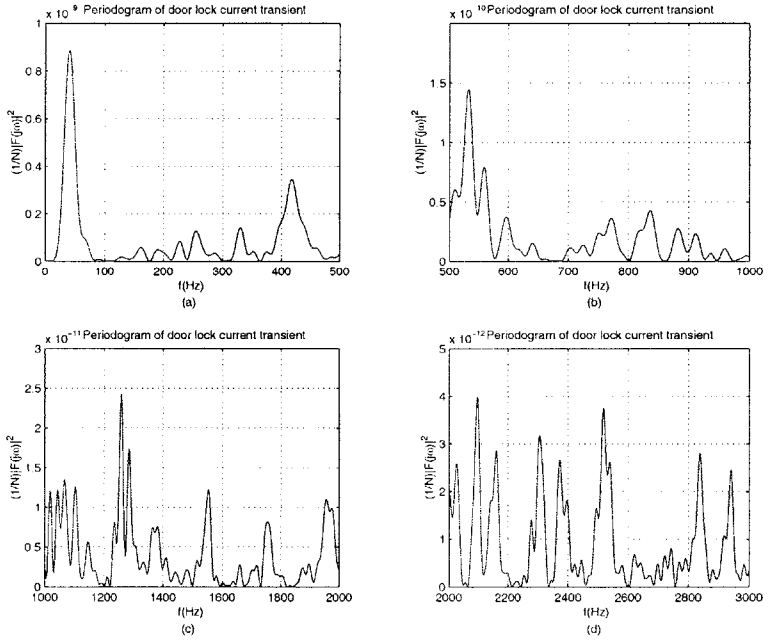

Figure 6.4: Periodogram of measured door lock transient from Figure 6.1(a) over the frequency range of zero to 3 kHz

6.2.1 Ignition Off Mode

We first look at the components which can be used in the ignition off mode. The periodogram of each waveform is found by selecting a portion of the transient and creating a zero centered waveform by model subtraction as was done in Chapter 5 for the arcing current.

Figure 6.4 shows the periodogram of the door lock transient. We can see peaking at various frequencies and there is no definitive structure as was the case with the arcing spectrum. Comparing the door lock spectrum with the average arcing spectrum we can see that although the spectrums have different shapes, their magnitudes are of the same order. It will therefore be difficult to differentiate between the arcing spectrum and the door lock spectrum by using only spectrum amplitudes. If the shape of the spectrum of the locks can be fully characterized we can use the shape of the spectrum to differentiate between arcing current but because of the complexity of the shape of the door lock spectrum this is an unlikely solution.

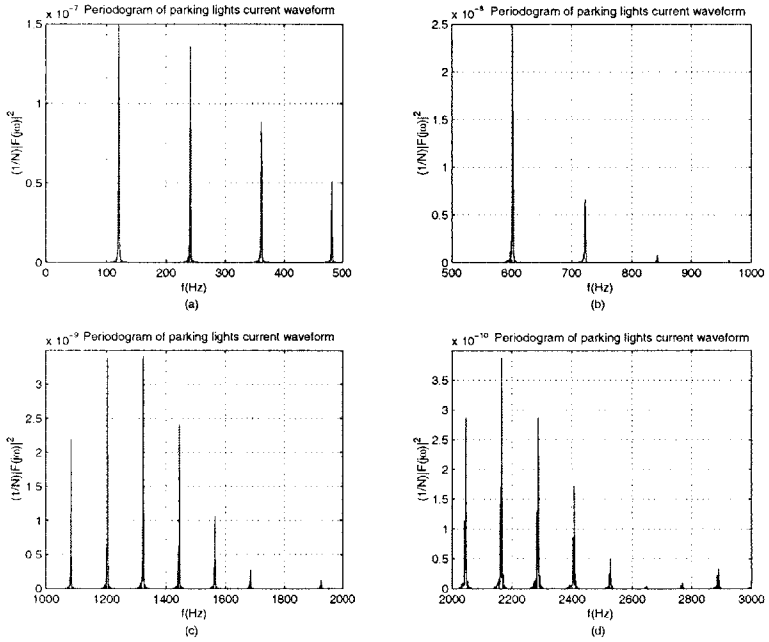

Figure 6.5: Periodogram of measured parking lights transient from Figure 6.1(b) over the frequency range of zero to 3 kHz

We saw in the previous section that the parking and headlights had an easily recognizable structure. Figure 6.5 shows the periodogram of the parking lights waveform.

As we expected from the time domain PWM waveform, the spectrum shows a peak at the fundamental frequency of the PWM signal at approximately 120 Hz as well as its harmonics. We notice that the amplitude of the peaks of the fundamental as well as the first few harmonics are greater than the amplitude of the arcing spectrum. There is an easily recognizable spectrum however, and we can use this to our advantage and design the detector to ignore the spectrum of the parking and headlights.

Next we look at the spectrum during the CD changer eject operation. Figure 6.6 shows the periodogram of the CD changer current waveform.

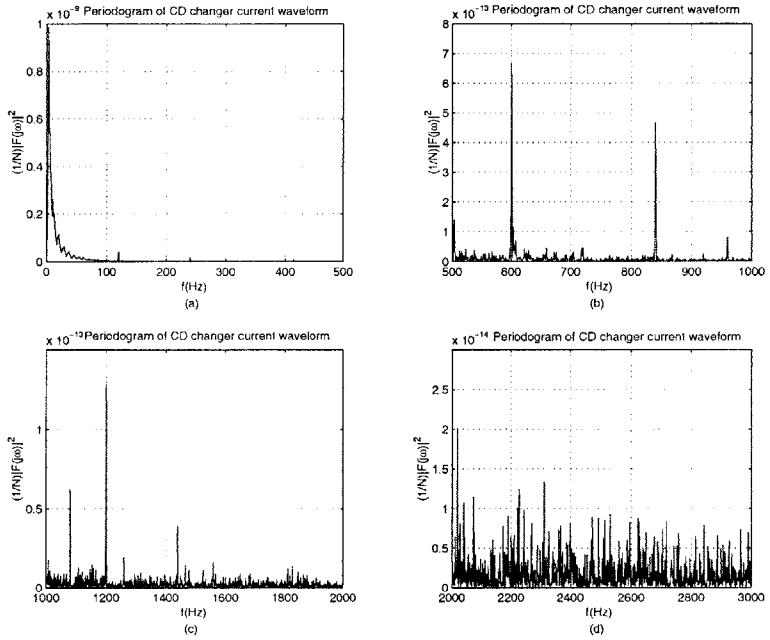

Figure 6.6: Periodogram of measured CD changer waveform from Figure 6.1(c) over the frequency range of zero to 3 kHz

We can see some peaks and what looks like random variations at the higher frequencies. Although this spectrum is not as recognizable as the headlights, the amplitude of the spectrum is about two orders of magnitude less than that of the arcing spectrum. This could easily be used to differentiate arcing spectrum from the waveform during CD changer operation. However, if the CD changer is operated while other electrical loads are operating, the amplitude of the overall spectrum can quickly become of the same order of the arc transient spectrum.

The seat tilt mechanism is a motor driven component that produces a noisy transient. The

spectrum of this waveform is shown in Figure 6.7.

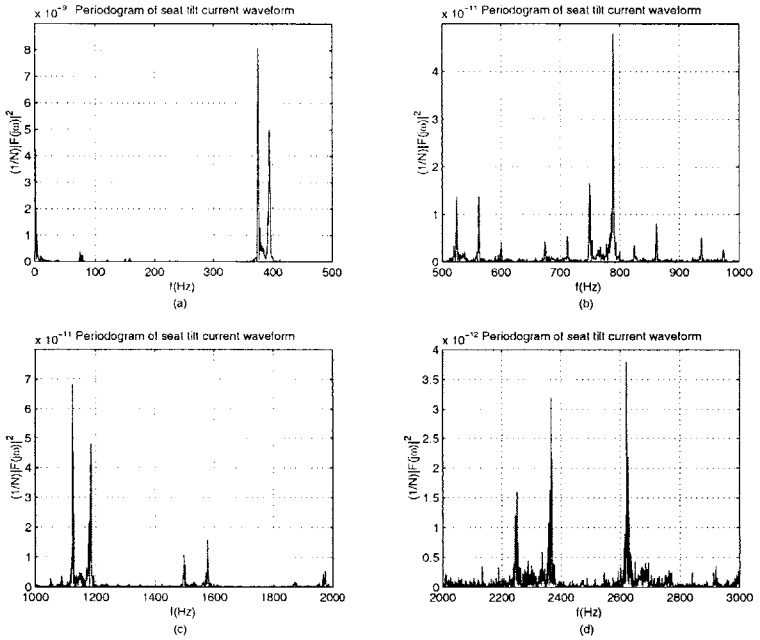

Figure 6.7: Periodogram of measured seat tilt waveform from Figure 6.1(d) over the frequency range of zero to 3 kHz

The oscillations of the current appear as peaks beginning at around 380 Hz. These peaks dominate the spectrum and like the PWM signal of the headlights, this spectrum shape can is recognizable and can be characterized.

6.2.2 Ignition Accessory Mode

In the accessory mode we are able to run three more loads. The first is the power windows. Figure 6.8 shows the periodogram of the current waveform produced by the motor that moves the windows. We can see that the majority of the energy is distributed between about 500 and 650 Hz. We also see peaks and smaller content at other higher frequencies.

If we compare this spectrum to the average arcing spectrum we can see that the shapes are different and it may be possible to distinguish between the two. The amplitudes are of the same order however, and having a threshold amplitude to distinguish the spectrums would not work.

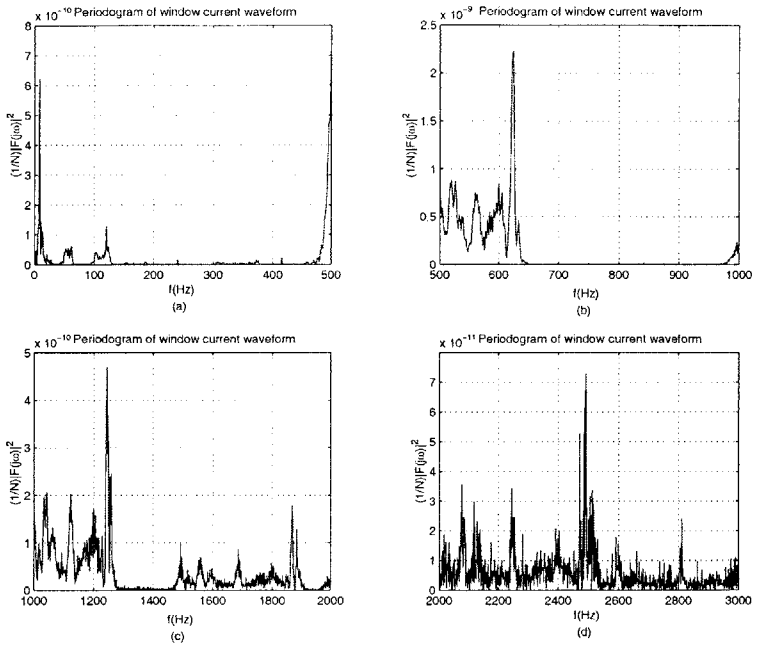

Figure 6.8: Periodogram of measured power window waveform from Figure 6.2(a) over the frequency range of zero to 3 kHz

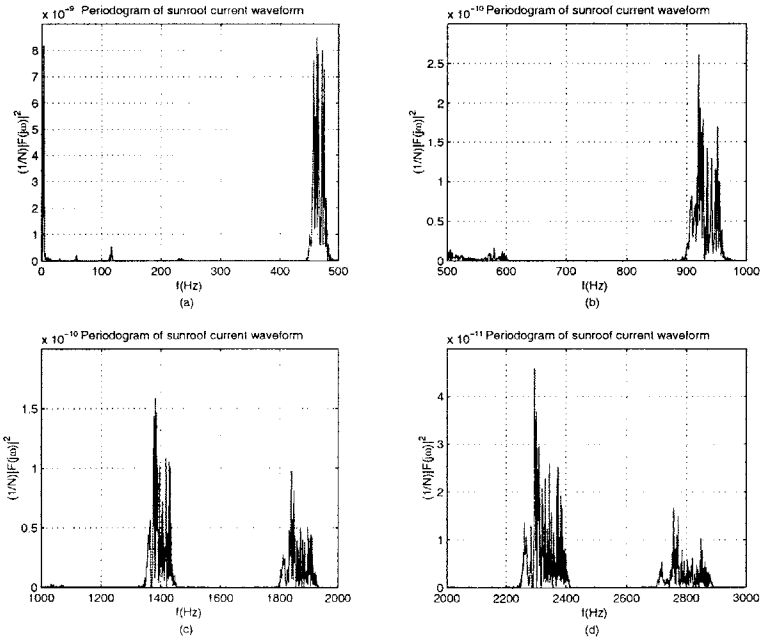

Figure 6.9: Periodogram of measured sunroof waveform from Figure 6.2(b) over the frequency range of zero to 3 kHz

The sunroof gave a similar low frequency variation in the time domain but its higher frequency oscillations produced by its own motor were different. As can be seen in Figure 6.9, the spectrum peaks are slightly more defined than in the window spectrum.

The amplitudes of the peaks are great than the amplitude of the arc spectrum at the frequencies at which they occur. The rest of the spectrum is of the same order. We would thus have a difficult time using the amplitude of the arc spectrum as an arc event determining factor against such a load. As with some of the other loads, the peaks and shape of the sunroof spectrum could make this type of load easier to recognize and ignore under road operation.

The windshield wipers produce a slightly more complex spectrum as can be seen in Figure 6.10. We can see a large number of peaks, of which many are of a greater amplitude than

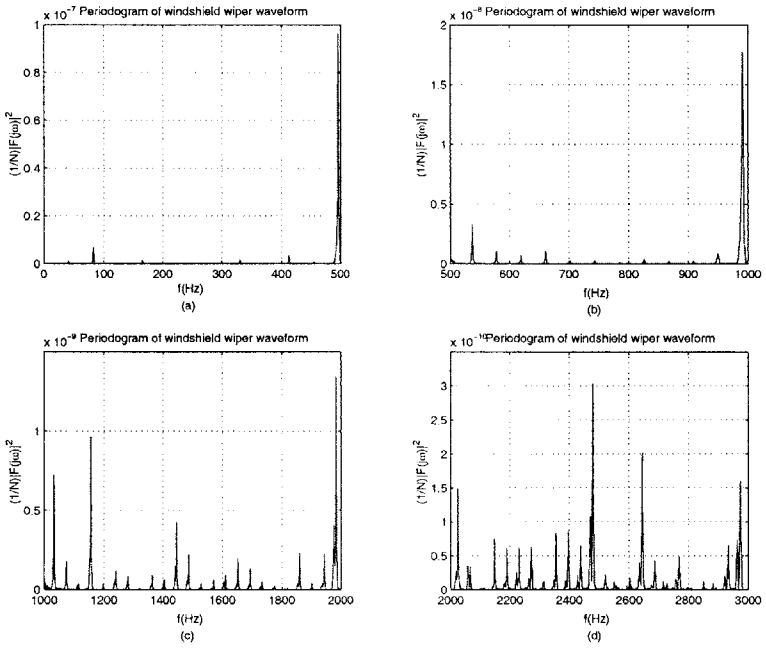

Figure 6.10: Periodogram of measured windshield wipers waveform from Figure 6.2(c) over the frequency range of zero to 3 kHz

the average arcing spectrum at the same frequency. The large number of peaks would make this a more difficult waveform to characterize and ignore. We can see how the complexity of some of the spectrums of the electrical loads in the automotive system make it difficult to detect arcs using frequency analysis.

6.2.3 Ignition Start Mode

The final waveform measured on the vehicle was the start mode. As stated before, this mode is how the electrical system behaves when you turn the key in the ignition to the engine start position. Figure 6.11 shows the spectrum of the current waveform during this mode. The reader is reminded some components such as the alternator are not included in this spectrum. As with previous spectrums, the transients in the time domain are large enough

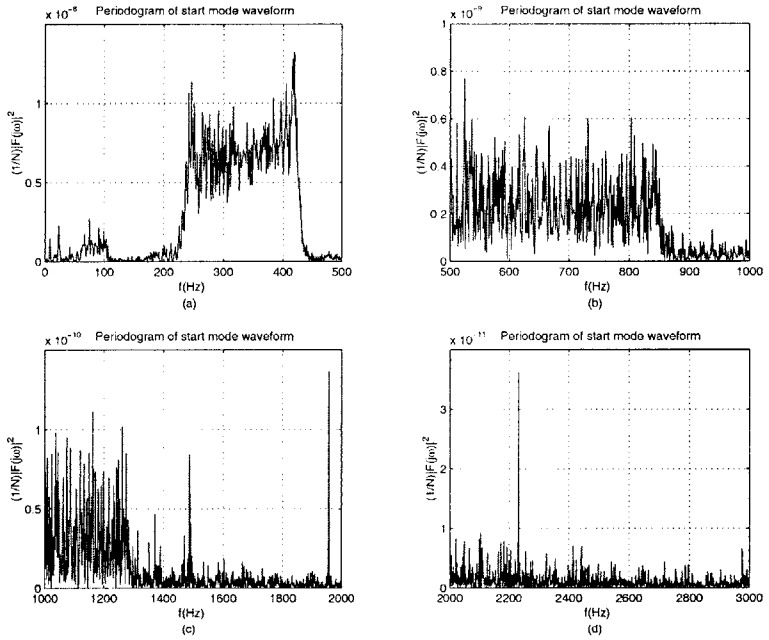

Figure 6.11: Periodogram of measured ignition start waveform from Figure 6.3 over the frequency range of zero to 3 kHz

that the amplitude in the frequency domain is of the same order of the arcing spectrum.

Unlike the other electric loads, the start mode contains electrical components which are always on as long as the vehicle is on. For example, the radiator cooling fan will be operating on and off continuously and the alternator runs at all times. During the time when the car is on, we will thus see a frequency domain picture similar to that seen in Figure 6.11 as opposed to just a transient as we would see with turn-on loads such as door locks, with transients on the order of hundreds of milliseconds. So for the automotive system, normal operation is not a steady DC current with transients due to loads. Instead, normal operation current is a varying value dependent on which loads are operating at any given time. A different combination of loads operating gives a different frequency spectrum,

making arc detection by frequency analysis a more difficult task.

Chapter 7

Arcing on a Mercury 14V bus

We now know what the circuit current looks like in the time and frequency domain of drawn arcs at the new 42 V bus voltage. We also know what load current looks like during normal operation in a 14 V system. Although arcing at 14 V will not be stable, it is still interesting to measure the circuit current during a 14 V arc. At the new 42 V voltage, electric loads will create higher amplitude transients similar to those seen in Chapter 6. In this chapter we will analyze the arcing current and the circuit current in the main circuit of the vehicle during a parallel arc.

7.1 Experimental Setup

In order to create controlled periodic arcs, the positive battery terminal of the Mercury Sable used in the Chapter 6 measurements is shorted to ground via a switching current through a $250m\Omega$ 5 Watt resistor used to limit the current. The controlled switch is made by the same mechanical apparatus used to create periodic 42 V arcs. However, the test wire is connected to the positive battery terminal and the blade is grounded by connecting the blade to the vehicle frame. A 30A fuse is also placed in series with the resistor and the car battery for protection. Figure 7.1 shows the setup placed in the engine compartment of the Mercury Sable. The speed of the motor is controlled by a 100Ω potentiometer connected to its 12 V supply battery. For user protection in case of battery or component explosion due to battery shorting, a plexiglas cover is placed over the entire engine compartment and the motor is turned on by a switch placed about 2 feet from the car. When the switch is closed, the motor moves back and forth and upon each separation with the test wire, a 14V arc is produced.

Measurements of the arcing current when no loads are on are taken by a current probe on the wire connecting the $250m\Omega$ resistor to ground. For obtaining current transients when electrical loads are operating and parallel arcs are produced the current is measured on the wire connecting the positive battery terminal to the fuse box.

Figure 7.1: Experimental setup for creating 14 V parallel arcs in the engine compartment of the Mercury Sable

7.2 Arc Current

Running the motor at a speed comparable to the set-up described in Chapter 4 we can create unstable 14 V arcs. Figure 7.2 shows the current waveform obtained during one of these unstable arcs. The current begins at zero and when the wire makes contact with the wire there is essentially a shorting of the battery with only the $250m\Omega$ resistor and the impedance of the vehicle's frame as resistance. When the blade separates from the test wire, a small transient is seen as a spark is produced. Notice that the transient occurs quickly and the current falls almost immediately to zero. The current is high enough to sustain a stable arc but the voltage across the electrodes is too low to sustain a stable long column and for this reason the current falls to zero.

Because we wish to monitor the current flowing through the main circuit (flowing through the battery), it is instructive to look at what happens to the current when arcing occurs. We must however, keep in mind that the parallel arcs created while electrical loads are operating are unstable 14 V arcs and will not have exactly the same characteristics as stable 42 V arcs.

The electric loads used for the test are the car headlights. The PWM signal of the headlights

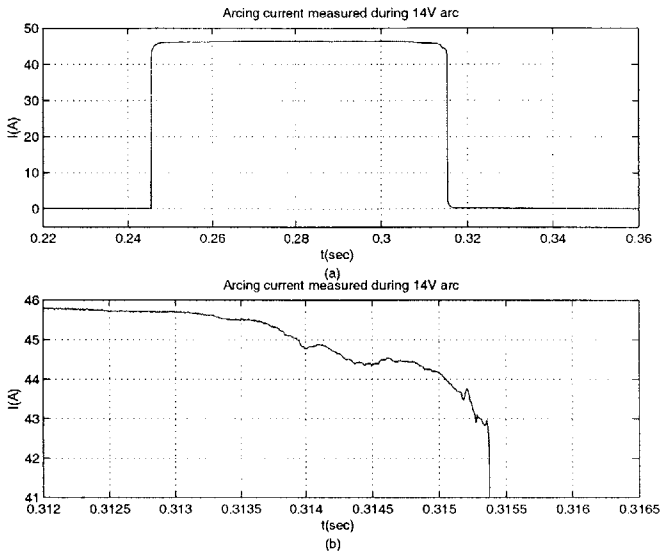

Figure 7.2: (a) Current waveform during one 14 V arc event (b) zoomed in near 14 V arc and current turn off

will be easy to recognize and we can thus recognize the arcing transient more easily. Figure 7.3 shows the transient caused by creating a parallel arc while the headlights are on. We can see the normal PWM current followed by a drop in current as the chopper motor shorts the battery through the $250m\Omega$ resistor. There is then a sharp rise in current as the unstable arc occurs and then it returns to normal as the arc self-extinguishes. We would expect that a 42 V arc would create a longer transient because of its stability. As can be seen in Figures 7.2 and 7.3, the time duration of the unstable 14 V arc is on the order of 2ms while the duration of the 42 V arcs produced using the same apparatus have a duration of ~50ms.

7.3 Fourier Analysis

As we can see in Figure 7.2, it is difficult to determine exactly where the 14 V arc begins because there is no defining current drop as is the case in the stable 42 V arcs. In this section, we will therefore limit ourselves to comparing the normal operation of the headlights with that of the arcing operation.

Figure 7.4 shows the periodograms of the current waveform during normal and parallel arcing operation of the headlights.

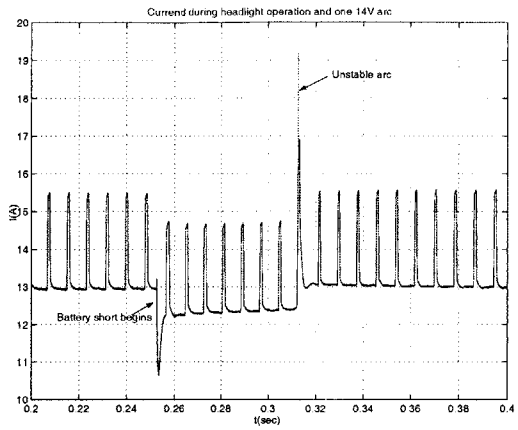

Figure 7.3: Current measured during headlight operation and one parallel arc event

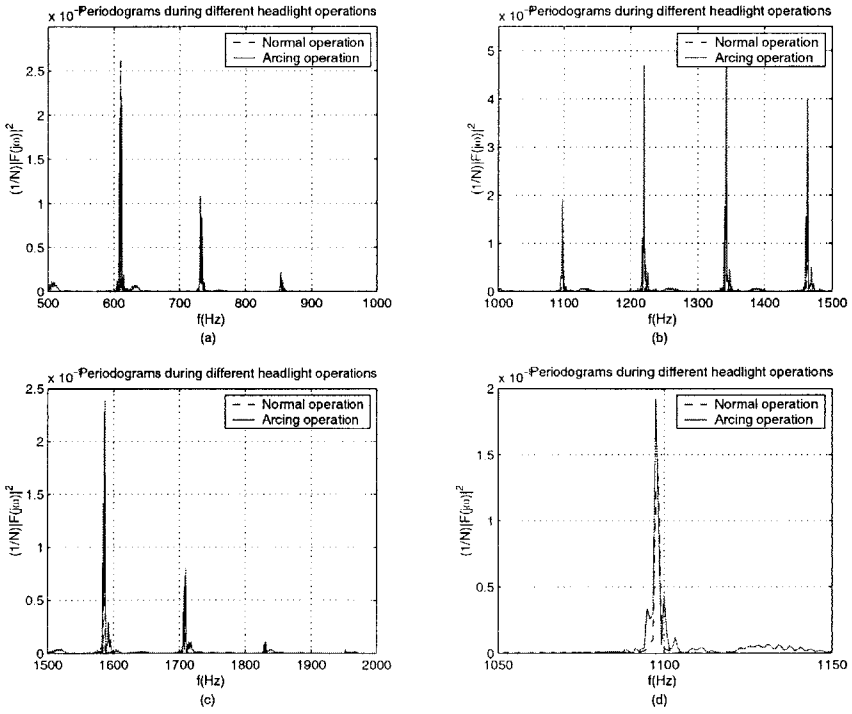

Figure 7.4: Periodogram of headlight operation and one arc event of Figure 7.3 showing little different between normal and arcing operation

The peaks seen are the same as those shown in Chapter 6 for the headlights and occur at the PWM frequency and its harmonics. We can see from Figure 7.4(a), (b), and (c) that the

peaks during the shorting of the battery and arcing waveform are at the same frequencies as during normal operation. Figure 7.4(d) is a closer look at one of the peaks at 1100 Hz. The peak in the periodogram in which the 14 V arc occurs is slightly wider and of the same magnitude as the normal operation periodogram. In addition, we see some extra content due to the arc at the frequencies just above the peak frequencies not seen during normal operation.

We can conclude that arcing, even in the unstable 14 V arc case, indeed contains some additional frequency content. However, in this 14 V case, the differences are insufficient to accurately differentiate between the two cases. We expect that in 42 V arcs, the frequency content and random variations in time of the arc are similar and just occur for a longer period of time because of the arc's stability. If a 42 V source is used, the arc would be stable and the large step up transient in current seen in Figure 7.3 would include more arcing current variations. We would see a greater magnitude in the frequency domain at the frequencies the arc produces, but insufficient differences in magnitude to be able to detect the arc using frequency analysis.

Chapter 8

Conclusions

In this work we have qualitatively evaluated the feasibility of different detection methods for use in the new 42 V automotive system. Electronic detection was determined to be the best approach because of its previous success in the 48 V DC telecommunications system as well as its lower cost. In particular, Fourier analysis of arcing waveforms in the time domain was chosen for investigation of frequency domain amplitude and signature.

The MIT arcing apparatus used in earlier research was then rebuilt to create stable drawn 42 V arcs [3]. Improvements were made to the measurement techniques used in order to obtain high resolution data of the arcing current. The arcing current of the 42 V arcs was analyzed in the frequency and time domains and it was found that this method of analysis for the use of detection may not be of accurate enough for detection of electric arcs in 42 V automotive systems because the arcing is not sufficiently repetitive from arc to arc and the frequency spectra of the arcs were not significantly different from normal automotive electric loads.

8.1 Evaluation of the use of Fourier Analysis

After careful analysis of the spectrum of the arcing current we found that arcing current does not exhibit a sufficiently large and distinct arcing signature. The frequency spectrum of arcing current shows broadband characteristics with no significant or distinguishing characteristics that can be used for simple detection of all arcs.

With no signature in the spectrum of the arc, we attempt to use differences in amplitude of the spectrums of the arcing current and normal operation current as was done in previous work for telecommunications applications [11, 12]. A Mercury Sable is used to measure the current during normal electrical load operation and the frequency spectrum is compared to that of measured arcing currents at 14 and 42 V. Unlike in the 48 V telecommunications work, we do not see the same difference in amplitudes of the spectrums. Some loads produce recognizable shapes, such as loads using PWM signals, but the amplitudes are of the same order as the spectrum of the arcing current.

The electric loads are then operated and a parallel 14 V arc is created during load operation. The spectra during 14 V arcing and during normal operation are compared and once again the differences in the spectra are negligible. We believe that a 42 V arc would create greater differences but at this point not sufficient enough to be able to differentiate the arc from normal operation.

From this work it is concluded that because of the wide variety of electric loads which cause similar amplitudes in the frequency spectrum, using Fourier analysis to detect arcs in automotive systems is not yet the most effective method. In the next section we discuss future work and possible routes for a better method of detection and discrimination.

8.2 Suggestions for Future Work

It was shown that the speed of the test chopper motor affects the lower frequency components of the measured spectrum of the arc. The analysis of stationary stable arcs could eliminate this dependence on motor speed. The present apparatus was altered in an attempt to produce stationary stable arcs. However, the lack of accurate control of the motor position makes this difficult since we wish to pull the motor back and stop it millimeters away from the test wire. Replacing the DC motor with a position servo would give accurate control of the steel blade position and it would be informative to know how stationary and drawn arcs differ in the lower frequency range of the spectrum.

Since Fourier analysis did not yield any simple answers to the arc detection and identification problem, it may be useful to explore more complex methods of electronic detection. A detection method similar to the detection scheme performed by Hendry Telephone Products is a possibility [13]. This method can account for the broadband nature of the arcing spectrum using the intermodulation process and clever methods of successive bandpass filtering considers the randomness of the time domain arc current waveform. Although a more complex system, it may be necessary to develop such a method to detect and identify arcs in automotive systems due to the large number of transients that can occur on the vehicle under normal operation of electrical loads that might be mistaken for electric arcs.

Finally, trend analysis could be performed on the spectra of automotive electrical loads. It was seen that the spectra of some loads exhibited significant structure when the loads were operated using a PWM signal. If each of the electrical loads is fully characterized in the frequency domain, a list of what the spectrum of circuit current looks like under all normal operating conditions can be used to identify arcing and normal operation. In addition, a PWM signal could be used with all electric loads, making them easily differentiable from

each other and from arcing current.

Appendix A

LabView Test Control and Measurement Code

A.1 Virtual Instrument Front Panel and Diagram to Control Chopper Motor Test Apparatus

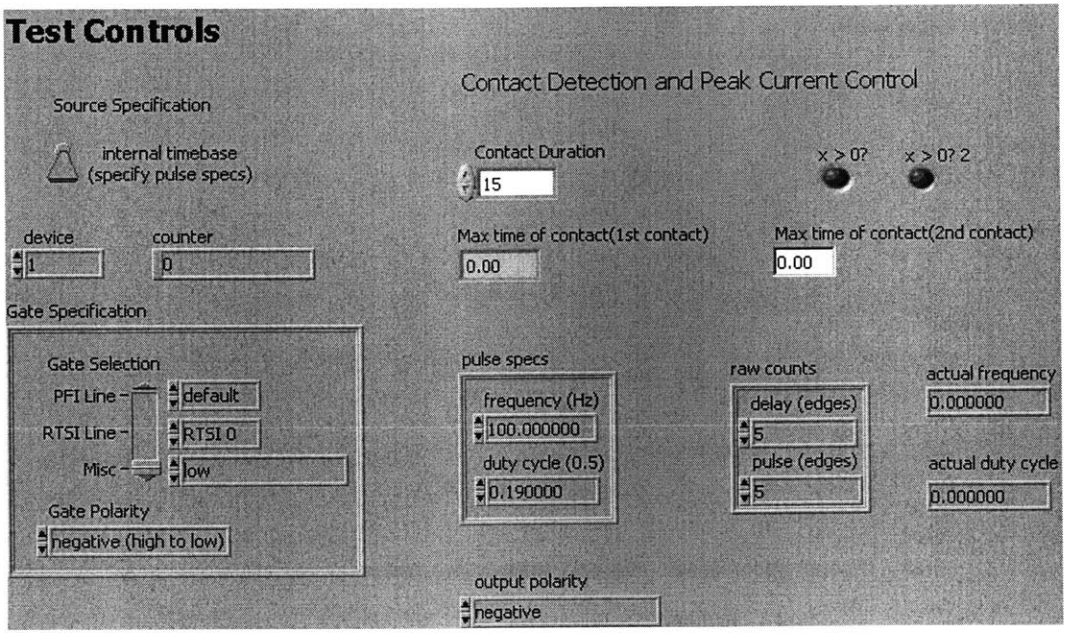

Table A.1: Operating Range and values used in tests for variables on test controls VI

User Input	Operating Range	Value Used
Contact Duration	0-40ms	15ms
Frequency(PWM)	100 Hz	100 Hz
Duty Cycle(PWM)	0.1-0.3	0.19
Output Polarity	+/-	Negative

This VI is used to control all circuit components of the test. A contact duration is specified by the user and is the time in milliseconds that the MOSFET will be turned on. The max time of contact windows are indicators that tell the user the time durations of the first and second contacts with the test wire. The pulse specifications of the motor PWM signal (frequency and duty ratio) are specified by the user to control the speed of the chopper motor. The remaining front panel displays are controls for the timing of the motor and for our specific application do not need to be changed from the default values. The following is the LabView diagram of the test controls VI.

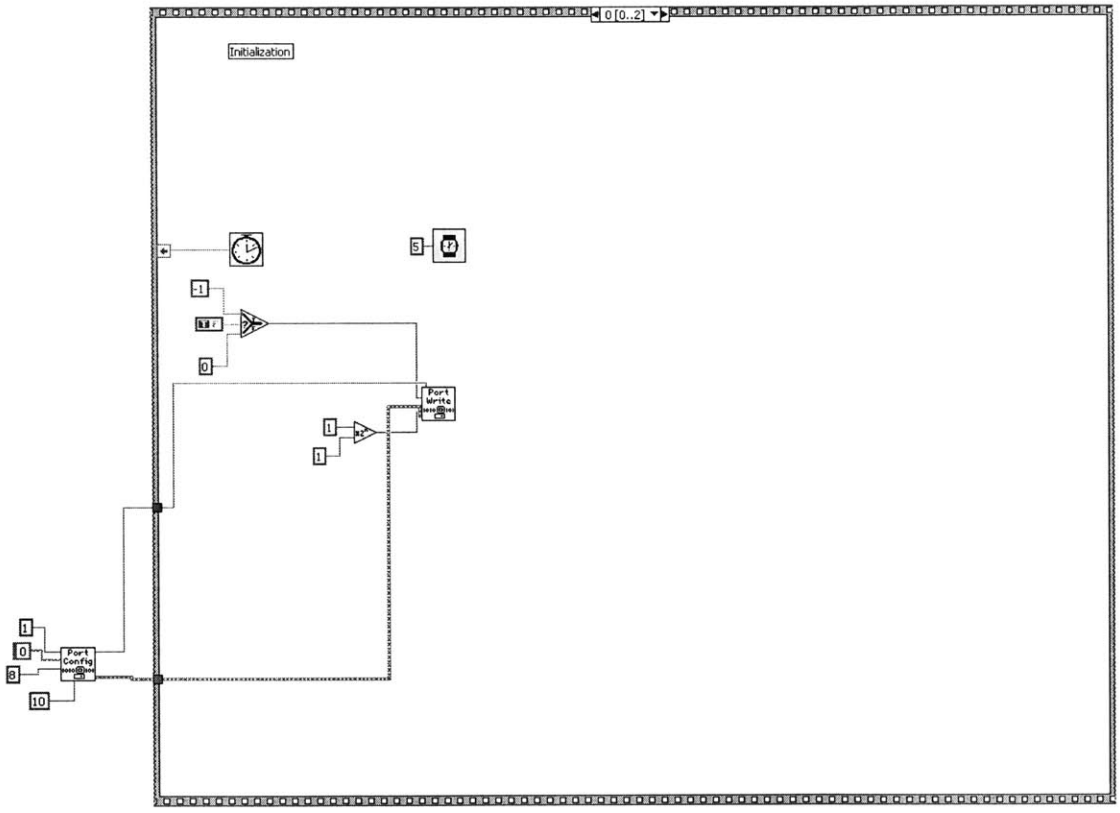

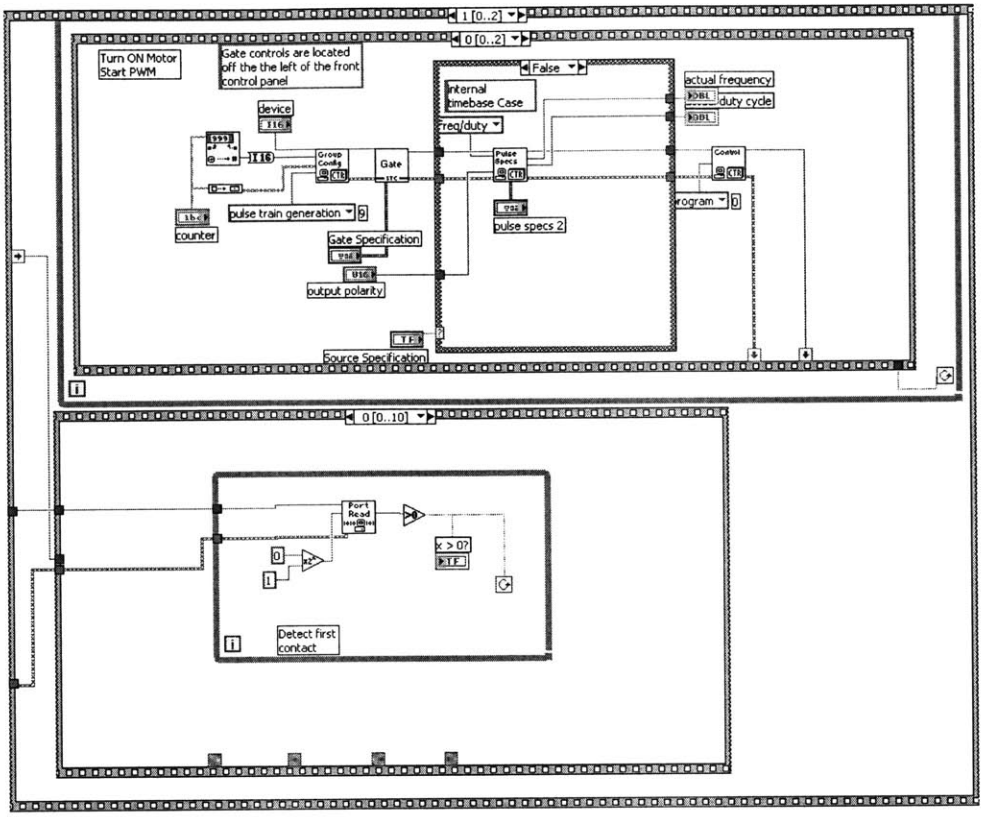
1 [0..2]
0 [0..2]
Turn ON Motor
Start PWM
Gate controls are located
off the the left of the front
control panel
False
internal
timebase Case
freq/duty
actual frequency
duty cycle
device
Group
Config
Gate
Pulse
Specs
Control
program
counter
pulse train generation
Gate Specification
pulse specs 2
output polarity
Source Specification
0 [0..10]
Port
Read
x > 0?
Detect first
contact

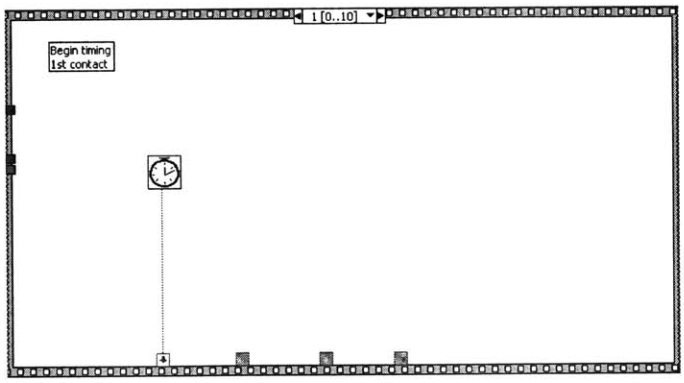
1 [0..10]
Begin timing
1st contact

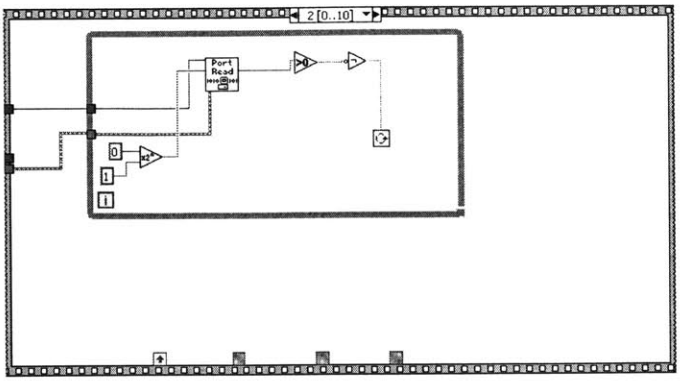
2 [0..10]
Port Read
0
1
1

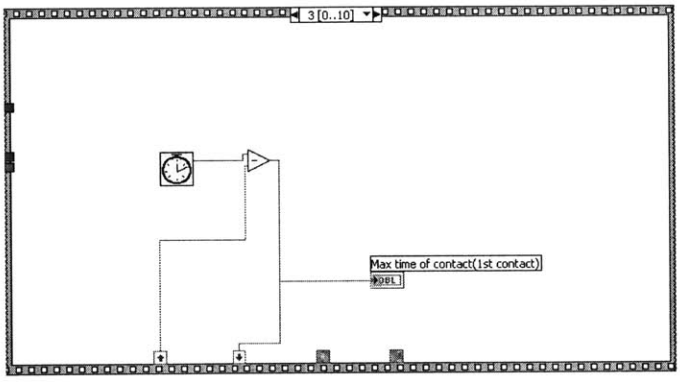
3 [0..10]
Max time of contact(1st contact)
DBL

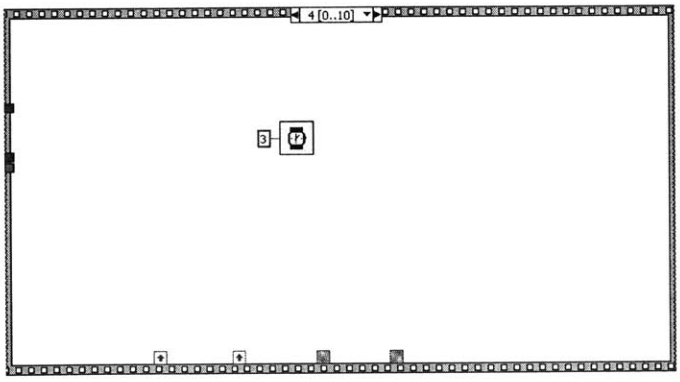
4 [0..10]
3

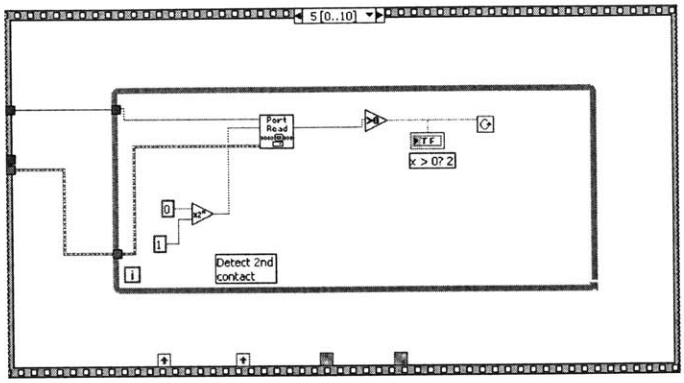
5 [0..10]
Port Read
TF
x > 0? 2
0
1
i
Detect 2nd contact

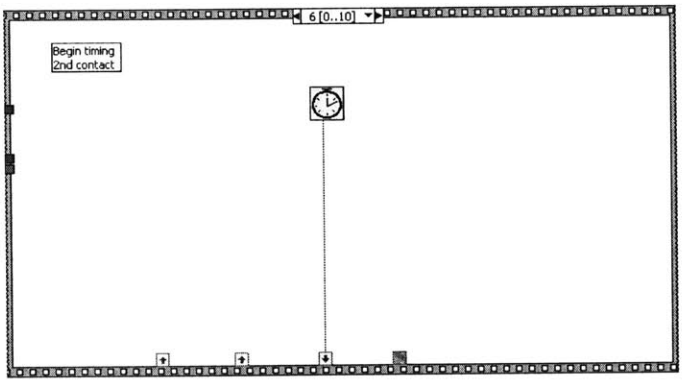
6 [0..10]
Begin timing 2nd contact

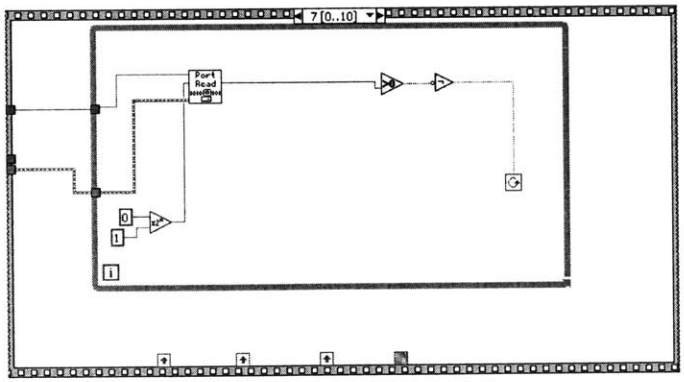
7 [0..10]
Port Read
0
1
i

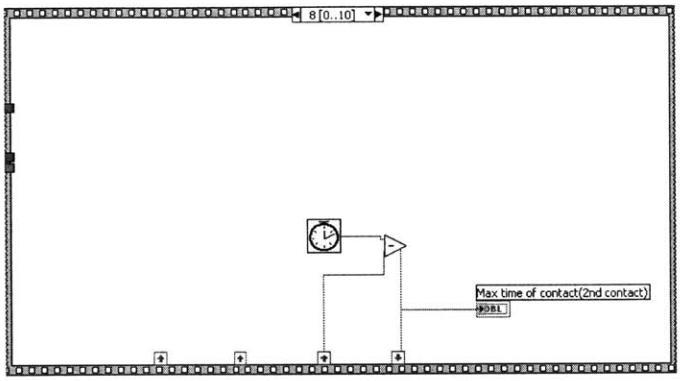
8 [0..10]
Max time of contact(2nd contact)
DBL

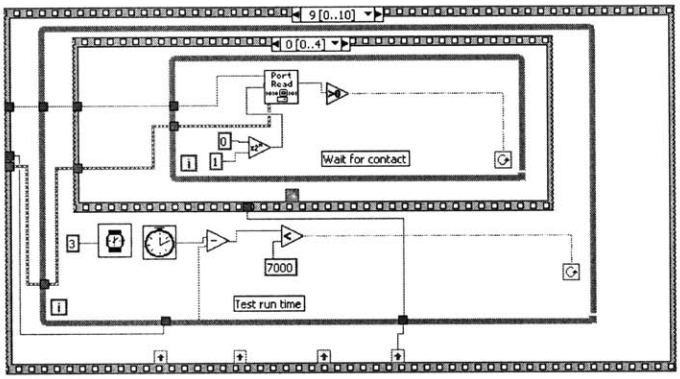
9 [0..10]
0 [0..4]
Port Read
Wait for contact
7000
Test run time

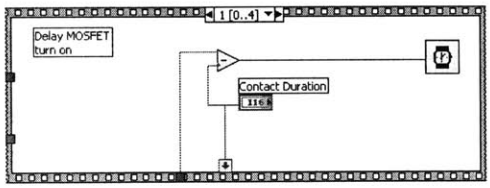
1 [0..4]
Delay MOSFET turn on
Contact Duration

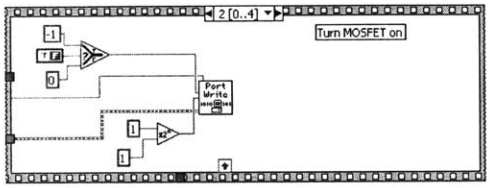
2 [0..4]
Turn MOSFET on
Port Write

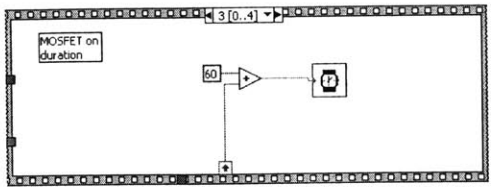
3 [0..4]
MOSFET on duration
60

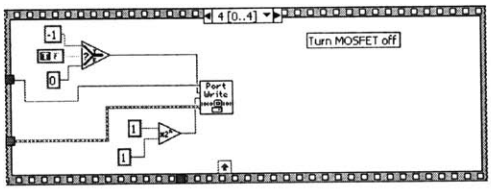
4 [0..4]
Turn MOSFET off
-1
0
1
1
Port Write

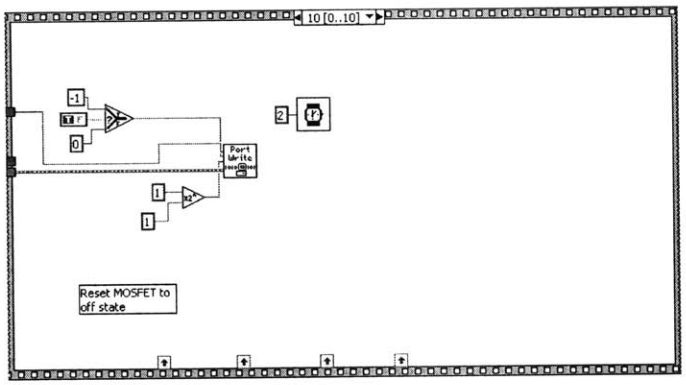
10 [0..10]
2
-1
0
1
1
Port Write
Reset MOSFET to off state

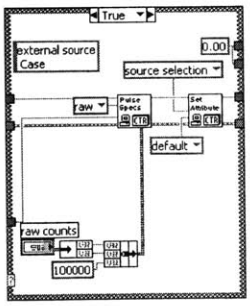
True
external source Case
0.00
source selection
raw
default
raw counts
100000

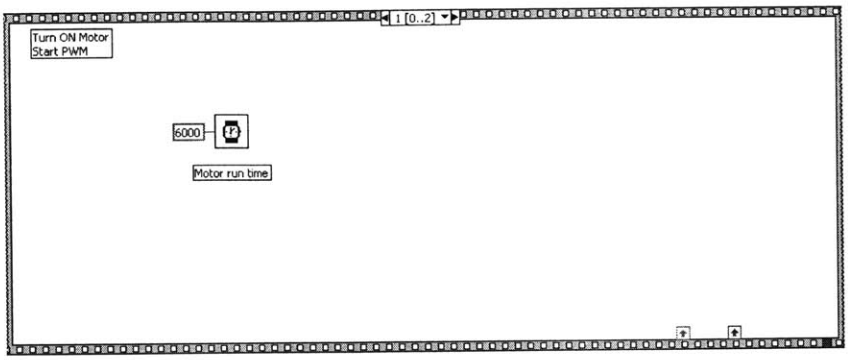
1 [0..2]
Turn ON Motor
Start PWM
6000
Motor run time

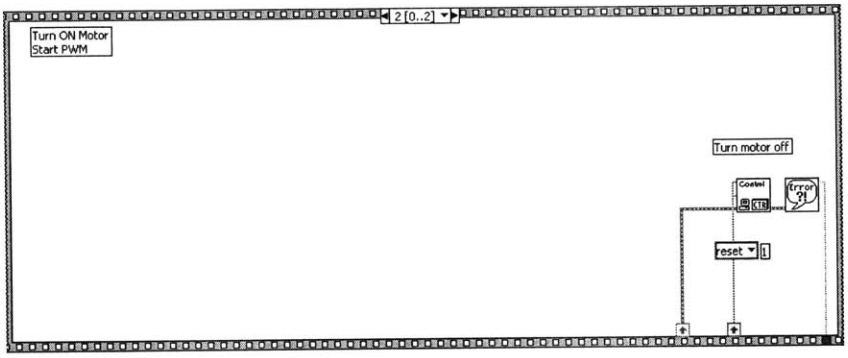
2 [0..2]
Turn ON Motor
Start PWM
Turn motor off
Control
error
reset

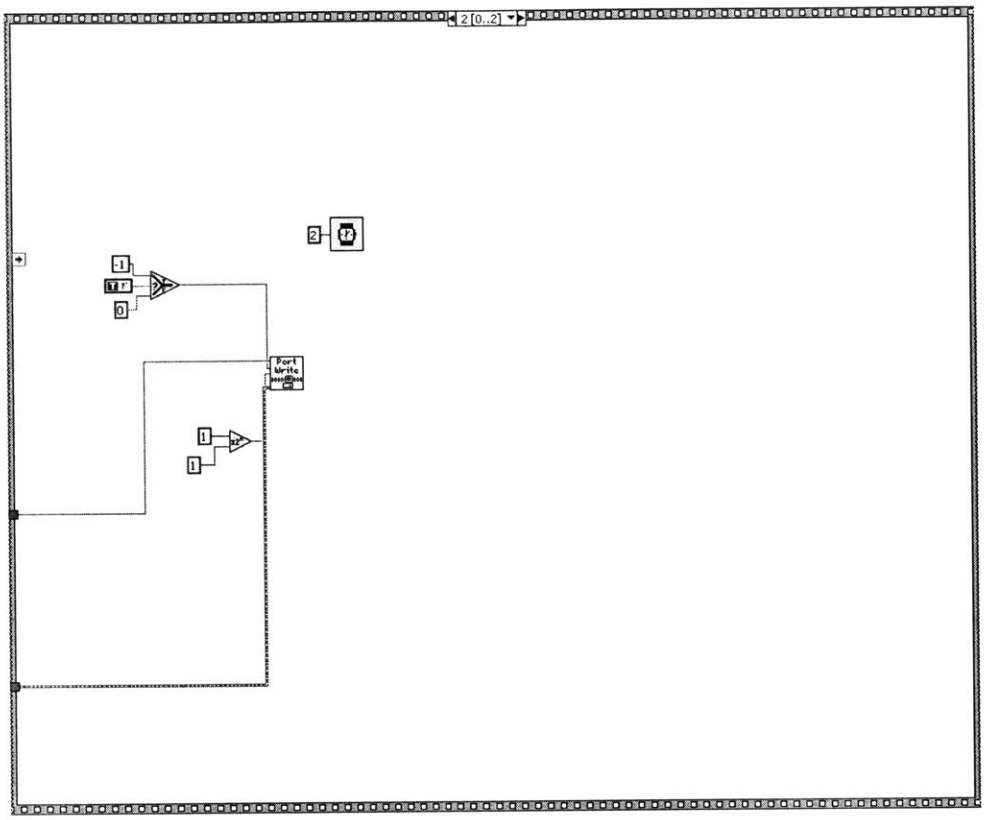
2 [0..2]
2
-1
0
Port Write
1
1

A.2 Virtual Instrument Front Panel to Measure Arcing Current

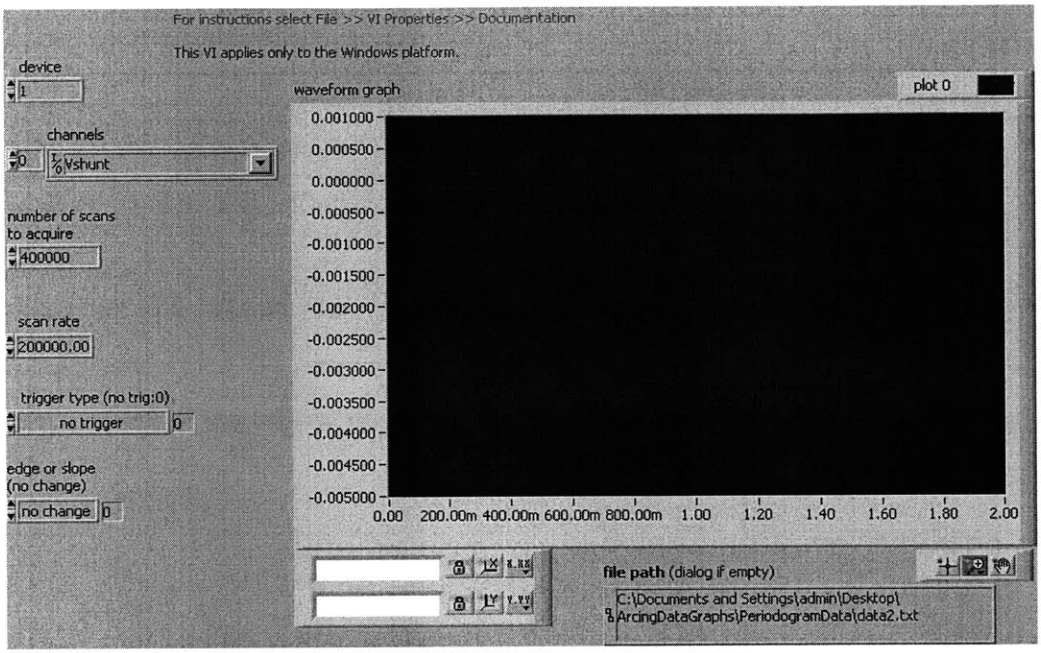

Table A.2: Values used in tests for variables on measurement controls VI

User Input	Value Used
Number of scans	400000
Scan rate	200000
Trigger type	no trigger

This VI obtains the arcing current waveform data. Analog channel measurements are set-up using Measurement and Automation Explorer and the channel is specified in the channel selection box of the VI front panel. In this case, a channel Vshunt was set-up to measure voltage across the shunt resistor. The number of data points to obtain is set in the number of scans box and the sampling rate is specified in the scan rate box. Sampling at 200 kHz and obtaining 400,000 points gave data measurements of 2 seconds in length. Triggering can be set in the trigger type box but because the test controls VI and measurements VI ran at the same time, no trigger was needed. Finally, the filename to which the data will be written is specified in the file bath box.

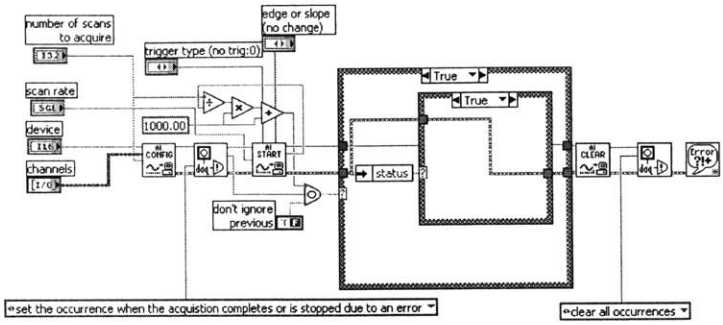
number of scans to acquire
1523
edge or slope (no change)
trigger type (no trig:0)
scan rate
1000.00
device
channels
CONFIG
START
status
True
True
CLEAR
error
don't ignore previous
set the occurrence when the acquistion completes or is stopped due to an error
clear all occurrences

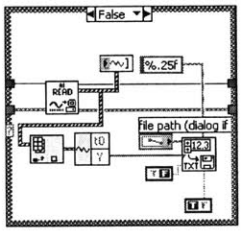
False
%.2f
READ
File path (dialog if
txt

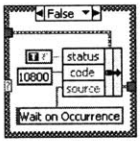
False
status
10800
code
source
Wait on Occurrence

Appendix B

MatLab Analysis Code

B.1 Calculation of the Periodogram of Equations 5.9 and 5.10

```
%%%%%%%%%%%%%%%%%%%%%%%%%%%%%%%%%%%%%%%%%%%%%%%%%%%%%%%%%%%%%%%%%%%%%%%%%%%%
%This code takes M arc data files of length N and creates M files
%with data points of the power spectrum of each of the M arc data
%files.  Power spectrum is |F(jw)|^2  The sum of all the power
%spectrums are averaged.  The result is:
% (1/M)*sum((1/N)*|F_i(jw)|^2)
%%%%%%%%%%%%%%%%%%%%%%%%%%%%%%%%%%%%%%%%%%%%%%%%%%%%%%%%%%%%%%%%%%%%%%%%%%%%

%Constants for time domain of arc event
SampleRate=200000;
NumOfSamples=400000;
delt=1./SampleRate;
TimeMeasured=NumOfSamples.*delt;
t_full=linspace(0,TimeMeasured,NumOfSamples);
Rshunt=(230e-6);

%Select a portion of the arc event data
Vshunt=dlmread('data2.txt','\t');
VshuntOneArc=Vshunt(280000:400000);
ArcCurrentOneArc=VshuntOneArc./Rshunt;
Upper_t_bound=delt*size(ArcCurrentOneArc,1);
t_one=linspace(0,Upper_t_bound,size(ArcCurrentOneArc,1));

%Set non-arc data to zero
NewArcCurrent=ArcCurrentOneArc;
NumPoints=size(ArcCurrentOneArc,1); for i=1:NumPoints
    if i<90320                                  %Eliminate DC current
        NewArcCurrent(i,1)=0;
    elseif abs(ArcCurrentOneArc(i,1))<1.5       %Lower current bound
        NewArcCurrent(i,1)=0;
```

```
            elseif abs(ArcCurrentOneArc(i,1))>50.52 %Upper current bound
        NewArcCurrent(i,1)=0;
    elseif ArcCurrentOneArc(i,1)<-2;
        NewArcCurrent(i,1)=0;
    end
end ArcCurrentOneArc=NewArcCurrent;

%Output the single arc event to a file
%Naming convention for the ith arc event : ArcTimei.txt
FileNameOut='ArcTime10.txt';
fid=fopen(FileNameOut,'w');

for i=1:NumPoints;
    fprintf(fid,'\%12.25f\n',ArcCurrentOneArc(i));
end fclose(fid);

%Creat a "time=zero" point where the all arcs in all data files begin
N=120001;
M=10;
ArcCurrentZeros=zeros(N,1);

for i=1:M
    index=num2str(i);
    FileNameIn=strcat('ArcTime',index,'.txt');
    ArcTimeTemp=load(FileNameIn);
    I=find(ArcTimeTemp);
    LowT=min(I);
    HighT=max(I);
    ArcTimeTemp=ArcTimeTemp(LowT:HighT);
    ArcTimeTemp=[zeros(60000,1);ArcTimeTemp;zeros((60000-(HighT-LowT)),1)];
    FileNameOut=strcat('ArcTimeFixT',index,'.txt');
    fid=fopen(FileNameOut,'w');
    for i=1:N;
        fprintf(fid,'\%12.25f\n',ArcTimeTemp(i));
    end
    fclose(fid);
end

%Subtract each model from its respective arc event
N=120001;
M=10;

for i=1:M
    index=num2str(i);
```

```
    FileInArc=strcat('ArcTimeFixT',index,'.txt');
    FileInModel=strcat('ArcFitModel',index,'.txt');
    ArcTemp=load(FileInArc);
    ModelTemp=load(FileInModel);
    JustArcTemp=ArcTemp-ModelTemp;
    FileNameOut=strcat('ArcTimeJustArc',index,'.txt');
    fid=fopen(FileNameOut,'w');
    for i=1:N;
        fprintf(fid,'\%12.25f\n',JustArcTemp(i));
    end
    fclose(fid);
end

%Constants for periodogram
M=10;                           %Number of arc data files
N=size(ArcCurrentZeros,1);      %Number of data points in time
FFTN=2*N;                       %Number of FFT data points
delt=t_full(2)-t_full(1);       %Sampling period
Ws=2*pi/delt;                   %Sampling frequency(rad/s)
W=Ws*(-FFTN/2:(FFTN/2)-1)/FFTN; %Frequency scale of FFT(rad)
Fscale=W./(2*pi);               %Frequency scale of FFT(Hz)

%Finding the PSD(power spectral density) of the arcs and writing
%the individual PSD's to files.
%Naming convention for the ith PSD:  ArcPoweri.txt

PowerSum=zeros(FFTN,1); for i=1:M;
    index=num2str(i);
    FileNameIn=strcat('ArcTimeJustArc',index,'.txt');      %Input arc data
    ArcDataTemp=load(FileNameIn);
    F=fft(ArcDataTemp,FFTN);
    Fc=fftshift(F)*delt;                                   %FFT of arc data
    Pc=(abs(Fc)).^2;                                       %PSD of arc data
    PowerSum=PowerSum+Pc;                                  %Sum the PSD's
    FileNameOut=strcat('ArcPowerJustArc',index,'.txt');    %Write PSD to file
    fid=fopen(FileNameOut,'w');
    for i=1:FFTN;
        fprintf(fid,'\%12.25f\n',Pc(i));
    end
    fclose(fid);
end

PowerAvg=(1/M)*(1/FFTN)*PowerSum;
FileNameOut='ArcPowerAvg10ArcsJustArc.txt';
```

```
fid=fopen(FileNameOut,'w'); for i=1:FFTN;
    fprintf(fid,'%12.25f\n',PowerAvg(i));
end fclose(fid);
```

B.2 Polynomial Curve Fitting from Section 5.1.2

```
%%%%%%%%%%%%%%%%%%%%%%%%%%%%%%%%%%%%%%%%%%%%%%%%%%%%%%%%%%%%%%%%%%%%%%%%%%%%
%This file includes code to fit a Nth polynomial curve to measured arc data
%Individual data files with one arc event each are loaded and an Nth order
%polynomial is fit to the arc portion.  The arc models are then written to
%text files.
%%%%%%%%%%%%%%%%%%%%%%%%%%%%%%%%%%%%%%%%%%%%%%%%%%%%%%%%%%%%%%%%%%%%%%%%%%%%

M=10;                    %Number of data files to make models of
N=120001;                %Number of data points in files
FFTN=2*N;                %Number of data points to use in FFT
Order=3;                 %Order of polynomial to fit to data
SampleRate=200000;
delt=1./SampleRate;
Upper_t_bound=N*delt;
t_one=linspace(0,Upper_t_bound,N); Ws=2*pi/delt;
W=Ws*(-N/2:(N/2)-1)/N;

FitArcModel=zeros(N,1); for i=1:M;
    index=num2str(i);
    FileNameIn=strcat('ArcTimeFixT',index,'.txt');
    RealDataTemp=load(FileNameIn);
    I=find(RealDataTemp);
    Lowt=min(I);
    Hight=max(I);
    [Parc,S]=polyfit(t_one(Lowt:Hight)',RealDataTemp(Lowt:Hight),Order);
    FitArc=polyval(Parc,t_one(Lowt:Hight));
    NumPoints=size(FitArc,2);
    for i=1:NumPoints
        FitArcModel(Lowt+i-1,1)=FitArc(1,i);
    end
    FileNameOut=strcat('ArcFitModel',index,'.txt');
    fid=fopen(FileNameOut,'w');
    for i=1:N
        fprintf(fid,'%12.25f\n',FitArcModel(i));
    end
    fclose(fid);
    FitArcModel=zeros(N,1);
end

%Find the average periodogram of all models
PowerSum=zeros(FFTN,1);
```

```
for i=1:M;
    index=num2str(i);
    FileNameIn=strcat('ArcFitModel',index,'.txt');  %Input model data
    ArcDataTemp=load(FileNameIn);
    F=fft(ArcDataTemp,FFTN);
    Fc=fftshift(F)*delt;                            %FFT of arc model
    Pc=(abs(Fc)).^2;                                %PSD of arc model
    PowerSum=PowerSum+Pc;                           %Sum the PSD's
    FileNameOut=strcat('ArcModelPower',index,'.txt');   %Write PSD to file
    fid=fopen(FileNameOut,'w');
    for i=1:FFTN;
        fprintf(fid,'%12.25f\n',Pc(i));
    end
    fclose(fid);
end

PowerAvg=(1/M)*(1/FFTN)*PowerSum;
FileNameOut='ArcModelPowerAvg10Arcs.txt';
fid=fopen(FileNameOut,'w'); for i=1:FFTN;
    fprintf(fid,'%12.25f\n',PowerAvg(i));
end fclose(fid);
```

B.3 Sine Windowing of Section 5.2.7

```
%%%%%%%%%%%%%%%%%%%%%%%%%%%%%%%%%%%%%%%%%%%%%%%%%%%%%%%%%%%%%%%%%%%%%%%%%%%%%%%%
%This code windows a time domain arc event of any length
%by multiplying it by a window whose ends are decreasing
%cosine functions and whose center portion is magnitude 1.
%%%%%%%%%%%%%%%%%%%%%%%%%%%%%%%%%%%%%%%%%%%%%%%%%%%%%%%%%%%%%%%%%%%%%%%%%%%%%%%%
SampleRate=200000;
delt=1/SampleRate;
Upper_t_bound=delt*120001;
t_one=linspace(0,Upper_t_bound,size(ArcWaveform,1));
N=size(ArcWaveform,1);
PeriodogramAvg=zeros(FFTN,1);
for i=1:10;
    index=num2str(i);
    FileNameIn=strcat('ArcTimeJustArc',index,'.txt');      %Input arc data
    ArcWaveform=load(FileNameIn);
    I=find(ArcWaveform);
    LowT=min(I);
    HighT=max(I);
    Ncos=round(0.1*size(I,1));
    t_start=LowT*delt;
    t_end=HighT*delt;
    t_cos=Ncos*delt;
    t_cos1=t_start+t_cos;
    t_cos2=t_end-t_cos;
    t_rectpuls=t_cos2-t_cos1;
    LeftCos=zeros(N,1);
    RightCos=zeros(N,1);
    for i=1:N
    if and((i*delt)>=t_start,(i*delt)<=t_cos1)
        LeftCos(i)=(1/sin(t_cos1-t_start))*sin(t_one(i)-t_start);
    elseif and((i*delt)>t_cos2,(i*delt)<=t_end)
        RightCos(i)=(1/cos(t_cos2-(t_end-pi/2)))*cos(t_one(i)-(t_end-pi/2));
    end
    end
    SquarePulse=rectpuls(t_one-(0.5*t_rectpuls+t_cos1),t_rectpuls);
    CosWindow=LeftCos'+SquarePulse+RightCos';
    WindowedArcWaveform=ArcWaveform.*CosWindow';
    FileNameOut=strcat('ArcJustArcWindowed',index,'.txt');
    fid=fopen(FileNameOut,'w');
    for i=1:N;
        fprintf(fid,'%12.25f\n',WindowedArcWaveform(i));
```

```
    end
    fclose(fid);
    FFTwindowed=fftshift(fft(WindowedArcWaveform,FFTN))*delt;
    FFTwindowedP=(1/FFTN)*(abs(FFTwindowed)).^2;
    PeriodogramAvg=PeriodogramAvg+FFTwindowedP;
    FileNameOut=strcat('JustArcPeriodogramWindowed',index,'.txt');
    fid=fopen(FileNameOut,'w');
    for i=1:N;
        fprintf(fid,'%12.25f\n',FFTwindowedP(i));
    end
    fclose(fid);
end
PeriodogramAvg=(1/10)*PeriodogramAvg;
```

B.4 Analysis of Car Circuit Current from Chapters 6 and 7

```
%%%%%%%%%%%%%%%%%%%%%%%%%%%%%%%%%%%%%%%%%%%%%%%%%%%%%%%%%%%%%%%%%%%%%%%%%%%%
%This file performs similar analysis on the car circuit current waveforms
%as is performed in ArcPeriodogram.m
%The frequency spectrums of the electric load transients are shown
%as well as spectrums of 14V arcs
%Normal operation load currents are then compared to load currents during
%14V arcing
%%%%%%%%%%%%%%%%%%%%%%%%%%%%%%%%%%%%%%%%%%%%%%%%%%%%%%%%%%%%%%%%%%%%%%%%%%%%

%Constants
SampleRate=200000;
NumOfSamples=400000;
delt=1./SampleRate;
TimeMeasured=NumOfSamples.*delt;
t_full=linspace(0,TimeMeasured,NumOfSamples);

%Selecting operation modes
CarWaveform=load('Car14VArc1.txt')*500;
NormalOperation=CarWaveform(150000:270000);
Ncar=size(NormalOperation,1);
ShortOperation=CarWaveform(80000:200000);
t_car=linspace(0,size(NormalOperation,1)*delt,size(NormalOperation,1));
Avg_Norm=(1/Ncar)*sum(NormalOperation);
Avg_Arc=(1/Ncar)*sum(ShortOperation);
NormalOperation2=NormalOperation-Avg_Norm;
ShortOperation2=ShortOperation-Avg_Arc;
%Computing the FFT of each waveform

%NcarFFT=2*Ncar;
NcarFFT=FFTN;
FscaleCar=(1/delt)*(-NcarFFT/2:(NcarFFT/2)-1)/NcarFFT;

FFT_Normal=fftshift(fft(NormalOperation2,NcarFFT))*delt;
FFT_Arcing=fftshift(fft(ShortOperation2,NcarFFT))*delt;

Periodogram_Norm=(1/NcarFFT)*(abs(FFT_Normal)).^2;
Periodogram_Arc=(1/Ncar)*(abs(FFT_Arcing)).^2;
```

Appendix C

Arc Spectrum Figures

The following section contains the individual periodograms for the zero centered arcing transients shows in Section 5.2.4. Arcing circuit current was sampled at 200 kHz, giving us a range of zero to 100 kHz in the frequency domain. Above 10 kHz, the frequency content of the noise introduced into the system by the measurement equipment begins to dominate the spectrum. Here we show the frequency range of zero to 5 kHz to illustrate how the spectrum behaves randomly and how it varies from arc to arc. The average periodogram over all 10 zero centered arc transients is shown, followed by the individual periodograms.

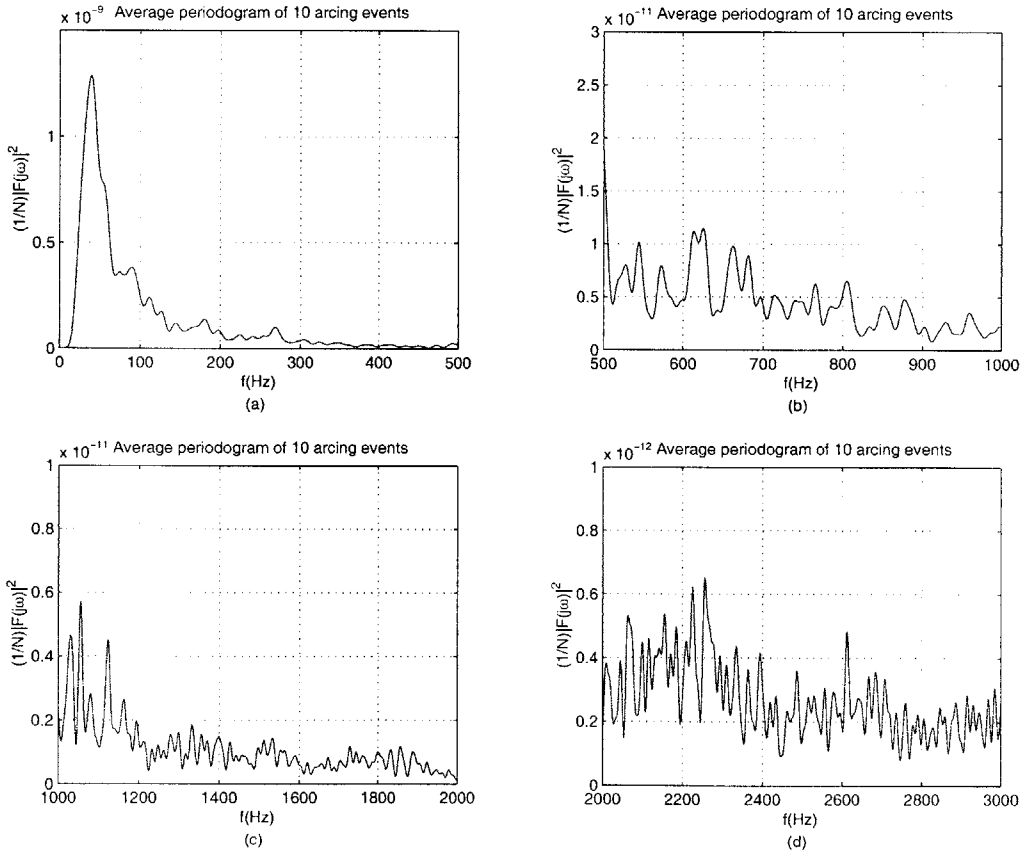

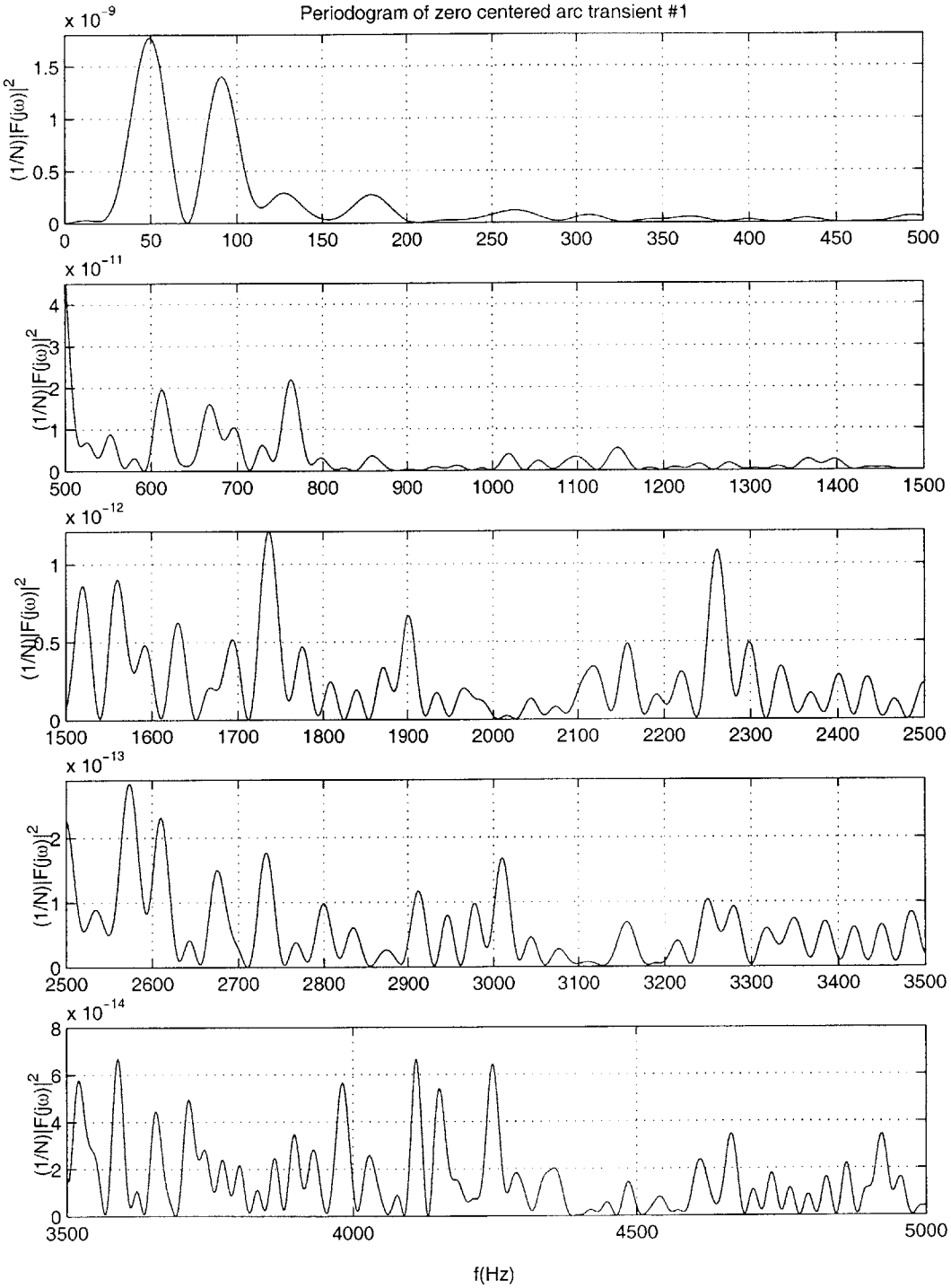
Periodogram of zero centered arc transient #1
x 10^-9
(1/N)|F(jω)|^2
x 10^-11
x 10^-12
x 10^-13
x 10^-14
f(Hz)

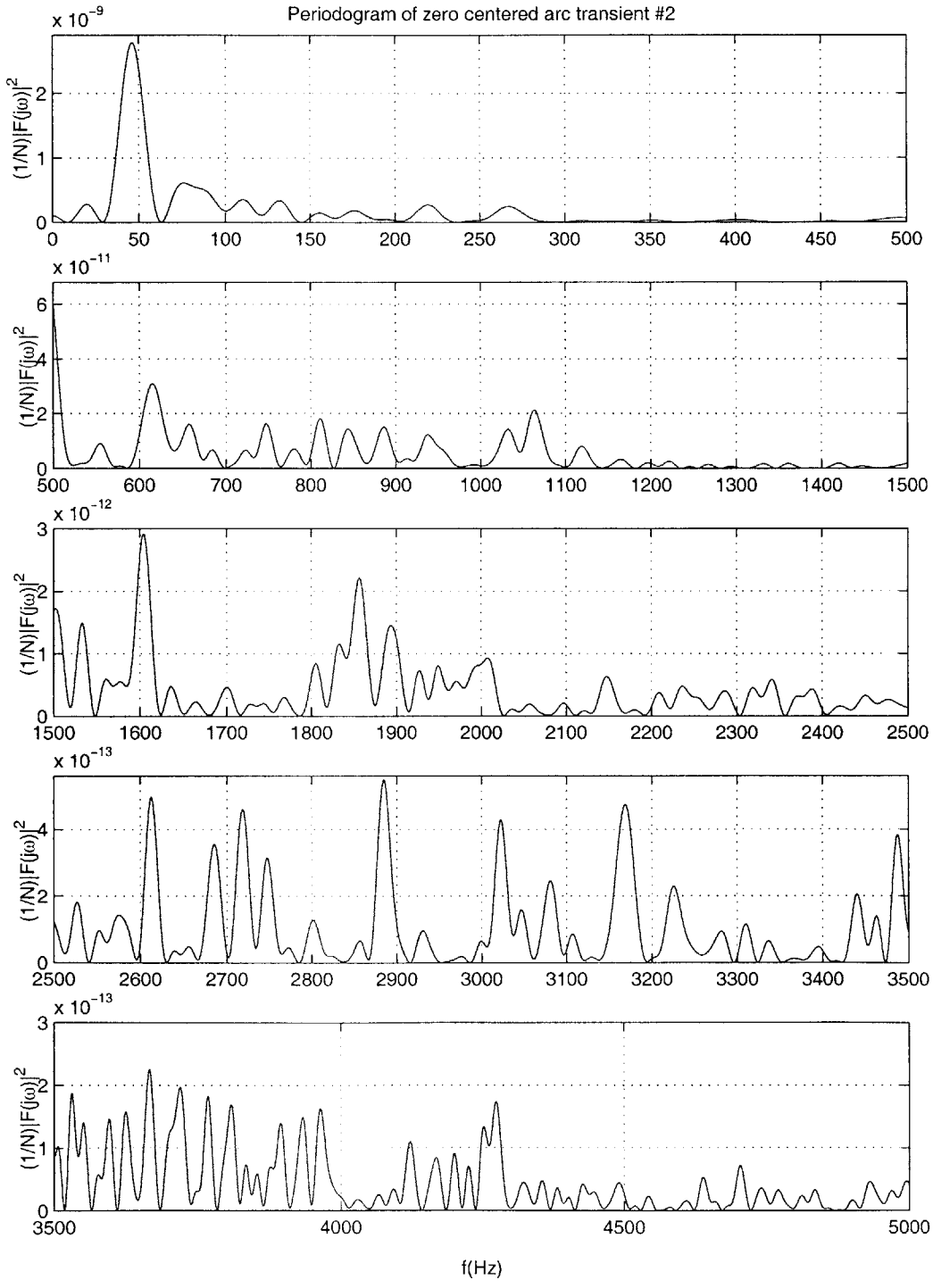
Periodogram of zero centered arc transient #2
x 10^-9
(1/N)|F(jω)|^2
0
50
100
150
200
250
300
350
400
450
500
x 10^-11
(1/N)|F(jω)|^2
500
600
700
800
900
1000
1100
1200
1300
1400
1500
x 10^-12
(1/N)|F(jω)|^2
1500
1600
1700
1800
1900
2000
2100
2200
2300
2400
2500
x 10^-13
(1/N)|F(jω)|^2
2500
2600
2700
2800
2900
3000
3100
3200
3300
3400
3500
x 10^-13
(1/N)|F(jω)|^2
3500
4000
4500
5000
f(Hz)

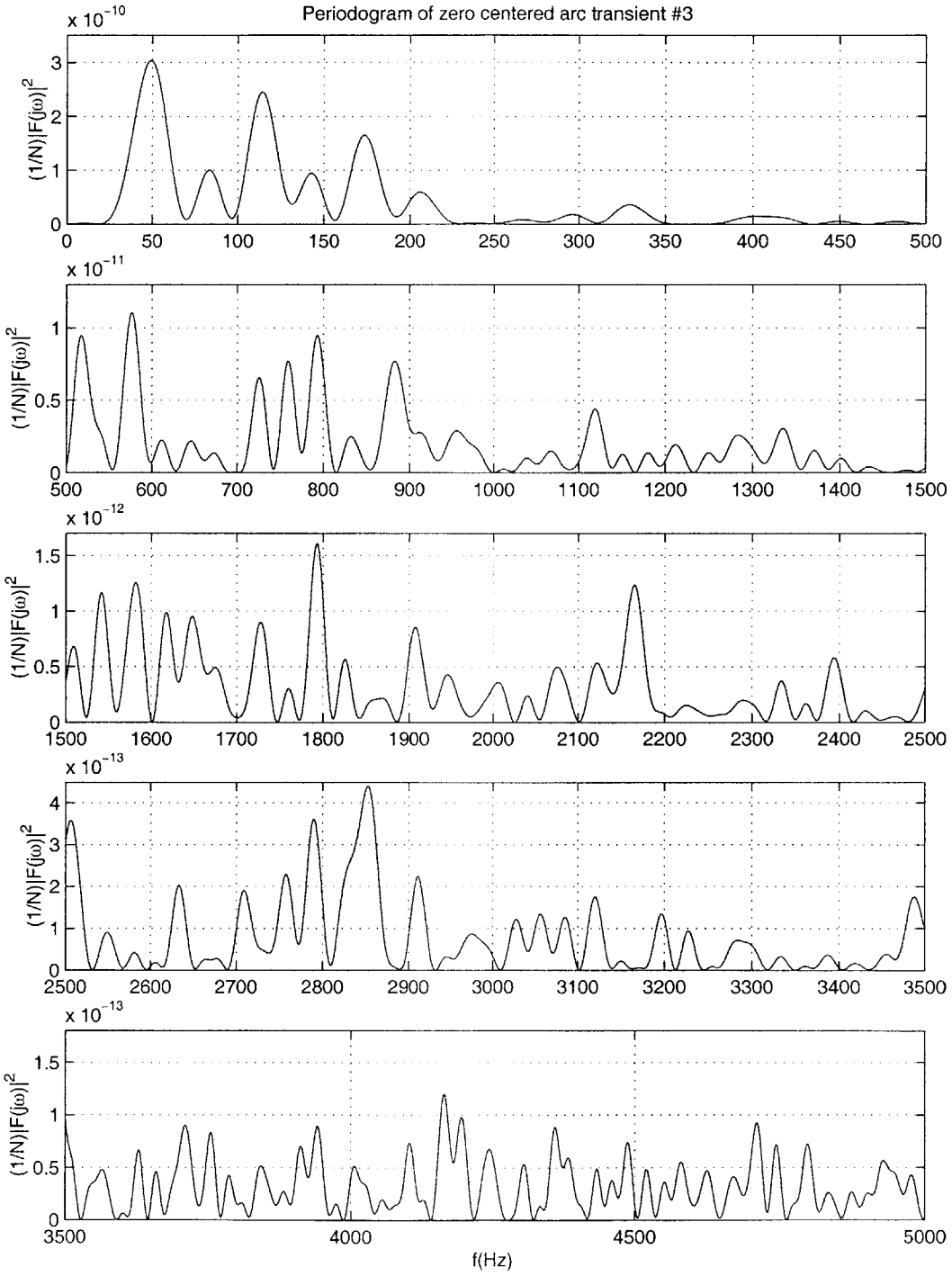
Periodogram of zero centered arc transient #3
x 10^-10
(1/N)|F(jω)|^2
0
50
100
150
200
250
300
350
400
450
500
x 10^-11
(1/N)|F(jω)|^2
500
600
700
800
900
1000
1100
1200
1300
1400
1500
x 10^-12
(1/N)|F(jω)|^2
1500
1600
1700
1800
1900
2000
2100
2200
2300
2400
2500
x 10^-13
(1/N)|F(jω)|^2
2500
2600
2700
2800
2900
3000
3100
3200
3300
3400
3500
x 10^-13
(1/N)|F(jω)|^2
3500
4000
4500
5000
f(Hz)

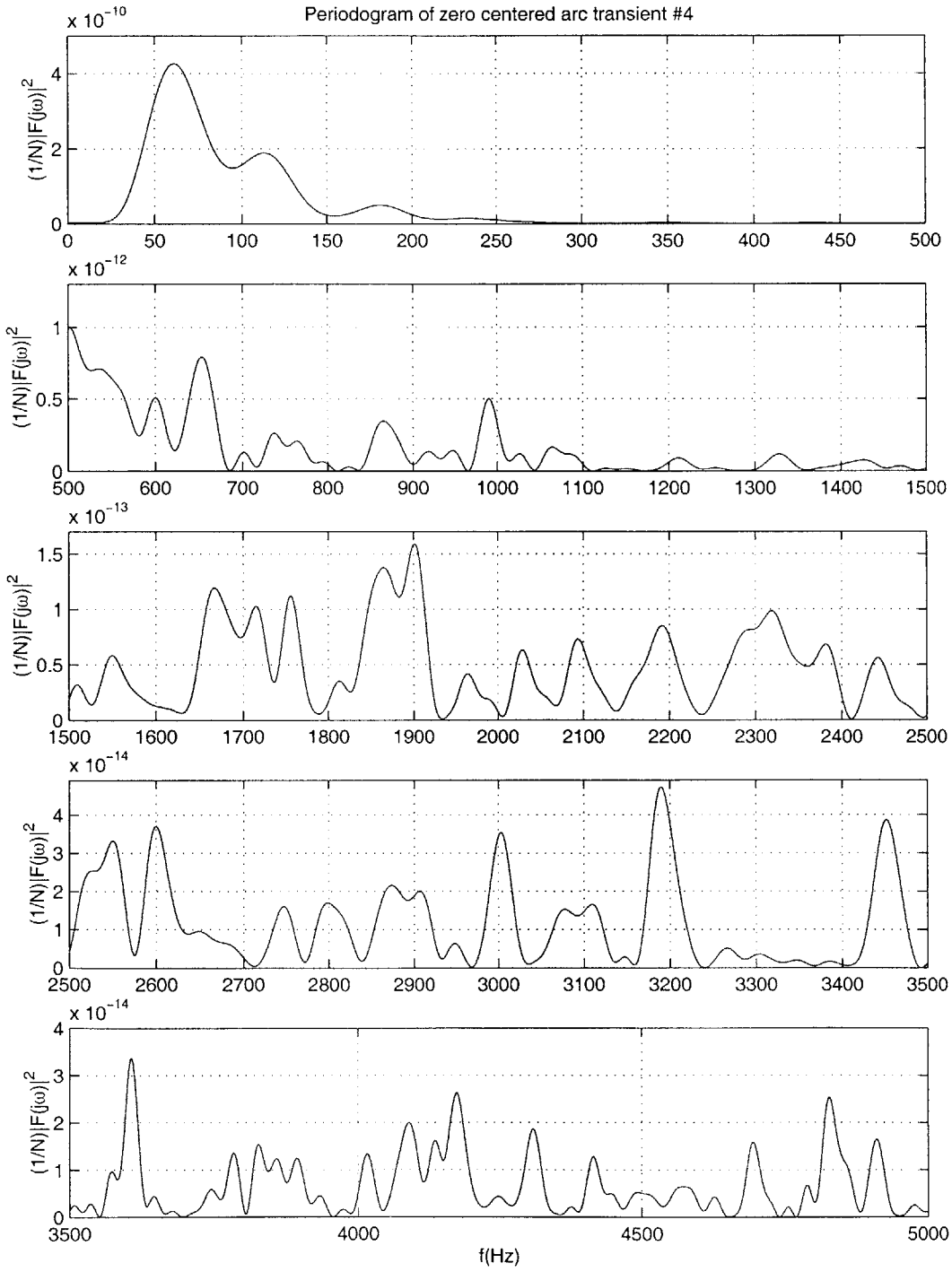
Periodogram of zero centered arc transient #4
x 10^-10
(1/N)|F(jω)|^2
0
50
100
150
200
250
300
350
400
450
500
x 10^-12
(1/N)|F(jω)|^2
0
0.5
1
500
600
700
800
900
1000
1100
1200
1300
1400
1500
x 10^-13
(1/N)|F(jω)|^2
0
0.5
1
1.5
1500
1600
1700
1800
1900
2000
2100
2200
2300
2400
2500
x 10^-14
(1/N)|F(jω)|^2
0
1
2
3
4
2500
2600
2700
2800
2900
3000
3100
3200
3300
3400
3500
x 10^-14
(1/N)|F(jω)|^2
0
1
2
3
4
3500
4000
4500
5000
f(Hz)

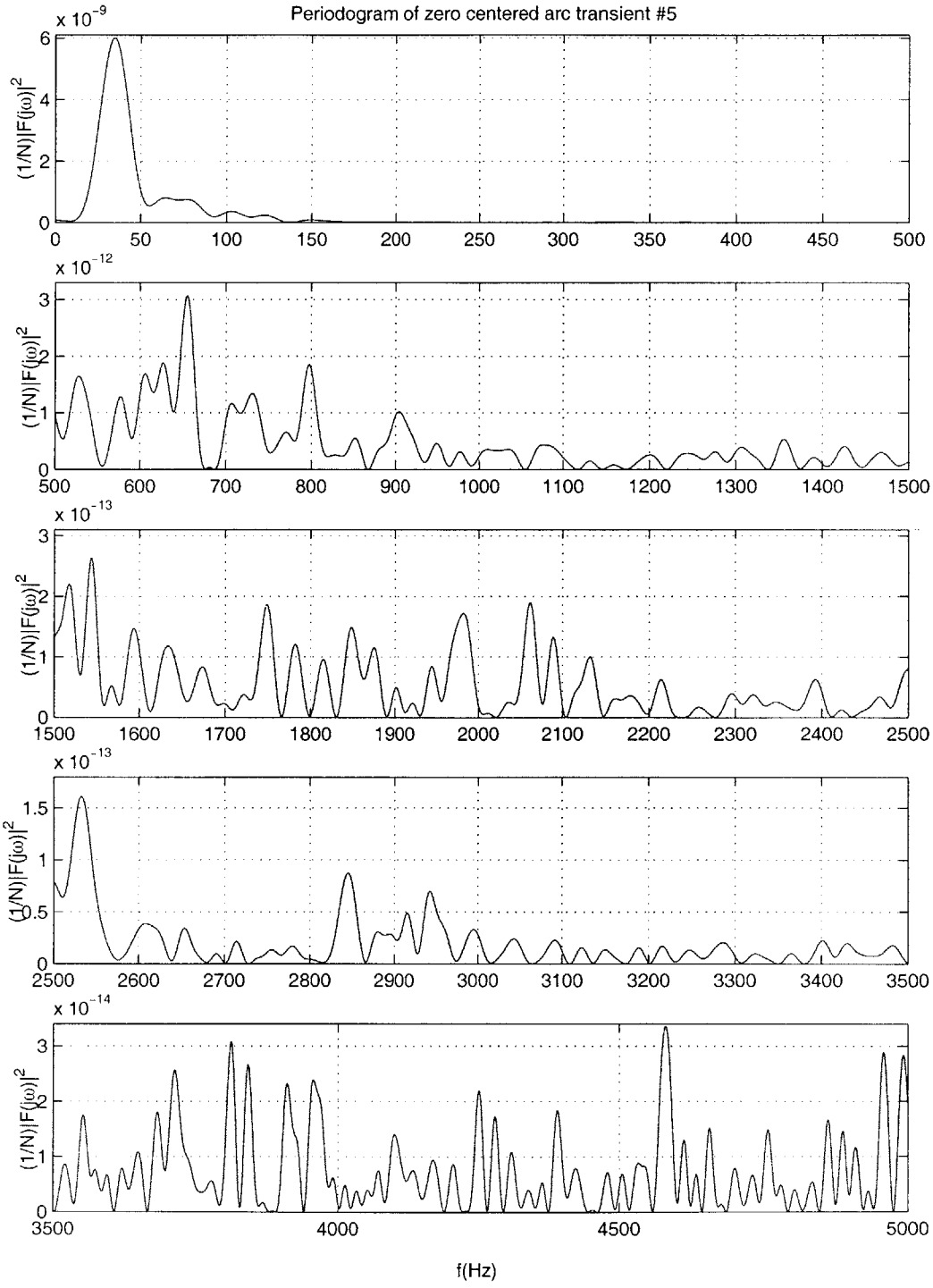
Periodogram of zero centered arc transient #5
x 10^-9
(1/N)|F(jω)|^2
0 2 4 6
0 50 100 150 200 250 300 350 400 450 500
x 10^-12
(1/N)|F(jω)|^2
0 1 2 3
500 600 700 800 900 1000 1100 1200 1300 1400 1500
x 10^-13
(1/N)|F(jω)|^2
0 1 2 3
1500 1600 1700 1800 1900 2000 2100 2200 2300 2400 2500
x 10^-13
(1/N)|F(jω)|^2
0 0.5 1 1.5
2500 2600 2700 2800 2900 3000 3100 3200 3300 3400 3500
x 10^-14
(1/N)|F(jω)|^2
0 1 2 3
3500 4000 4500 5000
f(Hz)

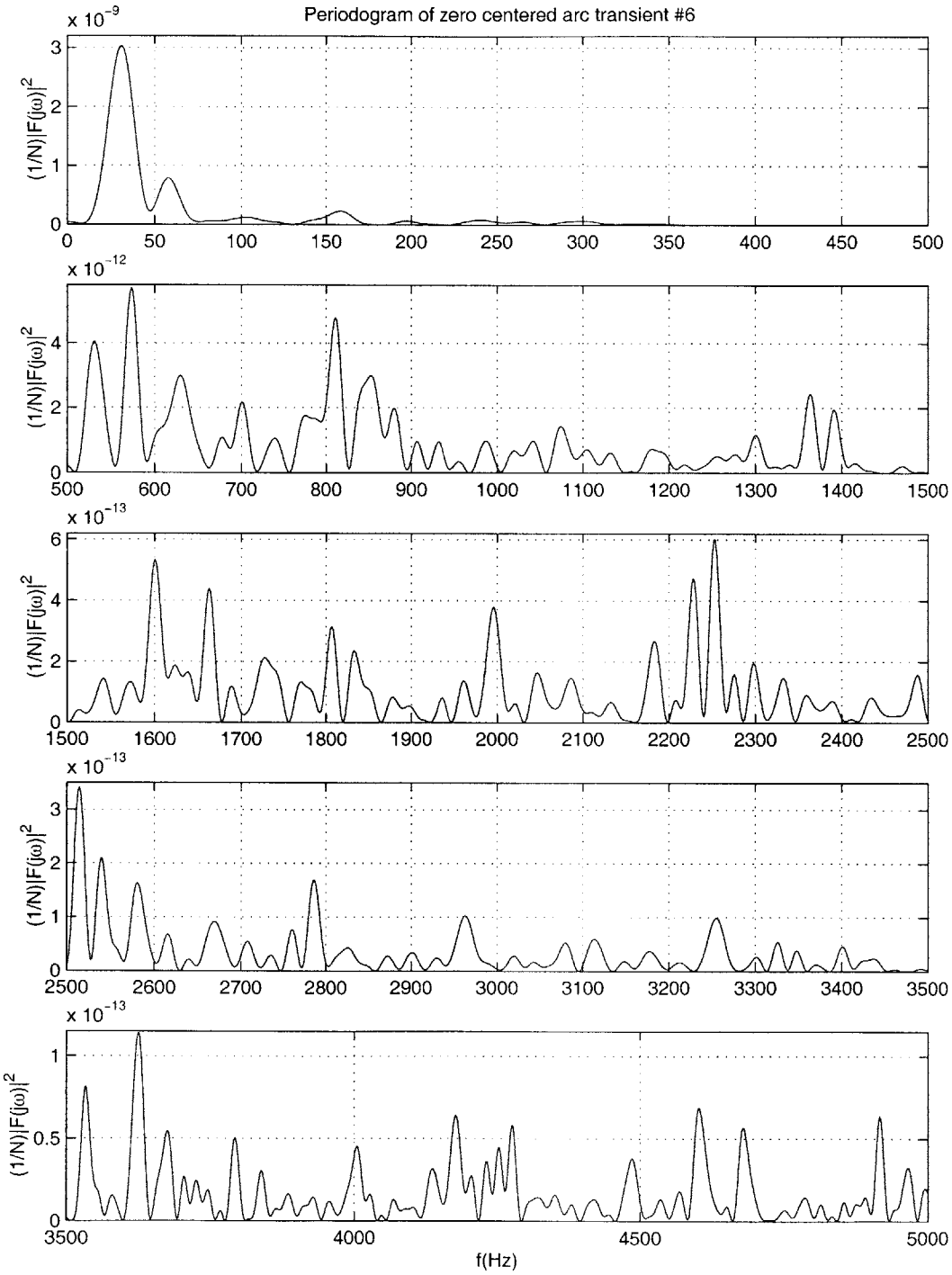
Periodogram of zero centered arc transient #6
x 10^-9
(1/N)|F(jω)|^2
0
50
100
150
200
250
300
350
400
450
500
x 10^-12
(1/N)|F(jω)|^2
500
600
700
800
900
1000
1100
1200
1300
1400
1500
x 10^-13
(1/N)|F(jω)|^2
1500
1600
1700
1800
1900
2000
2100
2200
2300
2400
2500
x 10^-13
(1/N)|F(jω)|^2
2500
2600
2700
2800
2900
3000
3100
3200
3300
3400
3500
x 10^-13
(1/N)|F(jω)|^2
3500
4000
4500
5000
f(Hz)

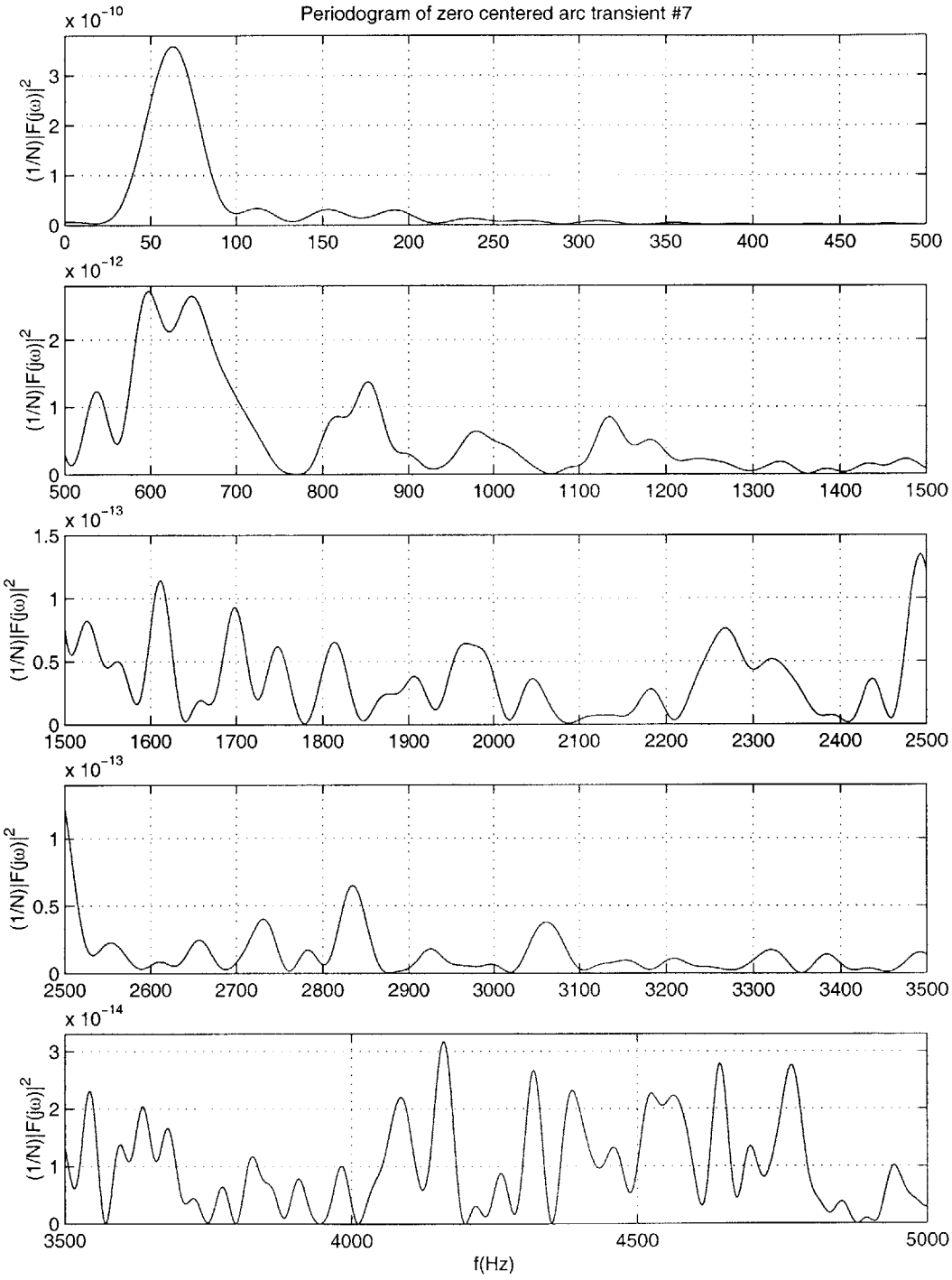
Periodogram of zero centered arc transient #7
x 10^-10
(1/N)|F(jω)|^2
0 50 100 150 200 250 300 350 400 450 500
x 10^-12
(1/N)|F(jω)|^2
500 600 700 800 900 1000 1100 1200 1300 1400 1500
x 10^-13
(1/N)|F(jω)|^2
1500 1600 1700 1800 1900 2000 2100 2200 2300 2400 2500
x 10^-13
(1/N)|F(jω)|^2
2500 2600 2700 2800 2900 3000 3100 3200 3300 3400 3500
x 10^-14
(1/N)|F(jω)|^2
3500 4000 4500 5000
f(Hz)

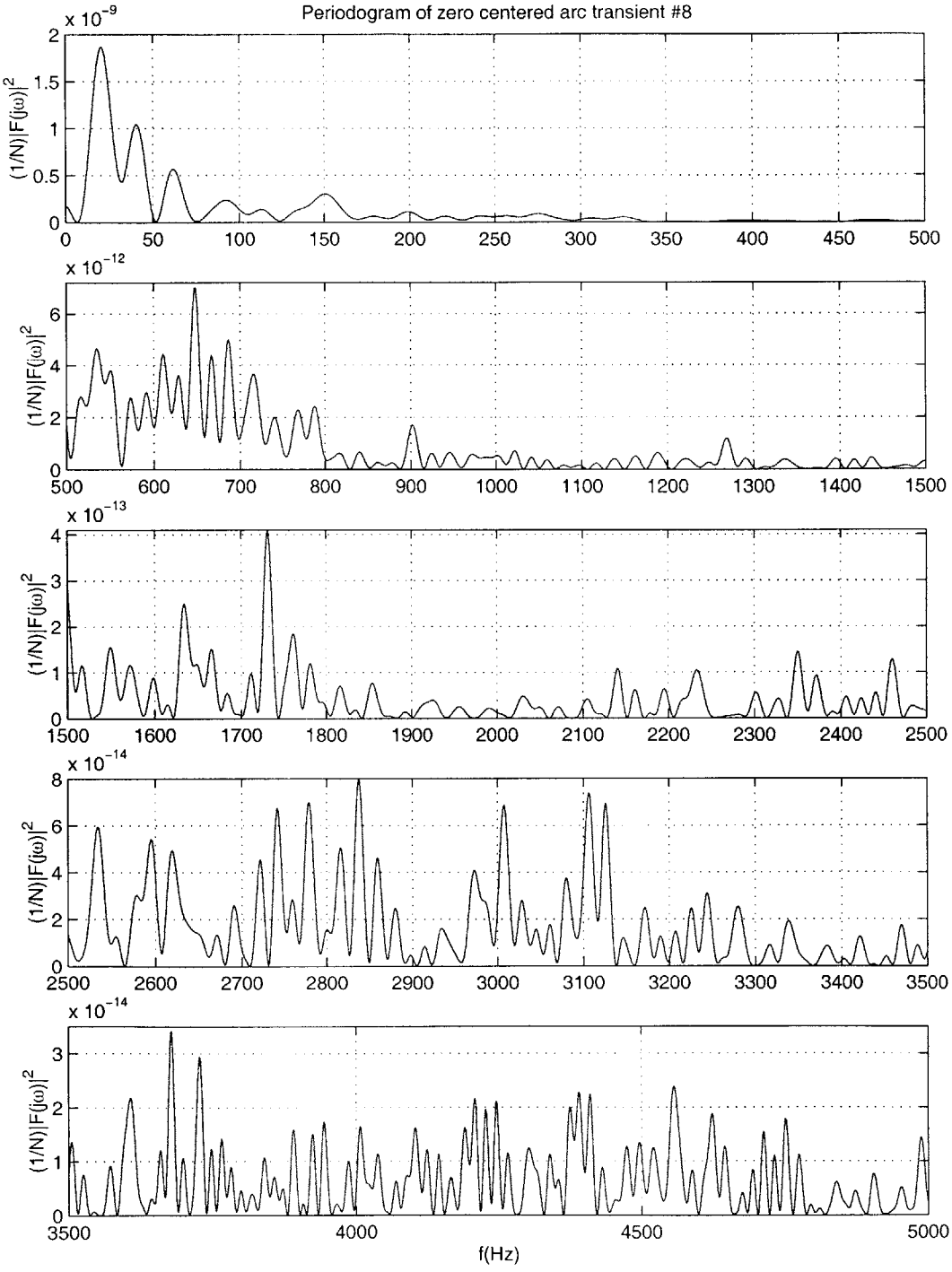
Periodogram of zero centered arc transient #8
x 10^-9
(1/N)|F(jω)|^2
x 10^-12
(1/N)|F(jω)|^2
x 10^-13
(1/N)|F(jω)|^2
x 10^-14
(1/N)|F(jω)|^2
x 10^-14
(1/N)|F(jω)|^2
f(Hz)

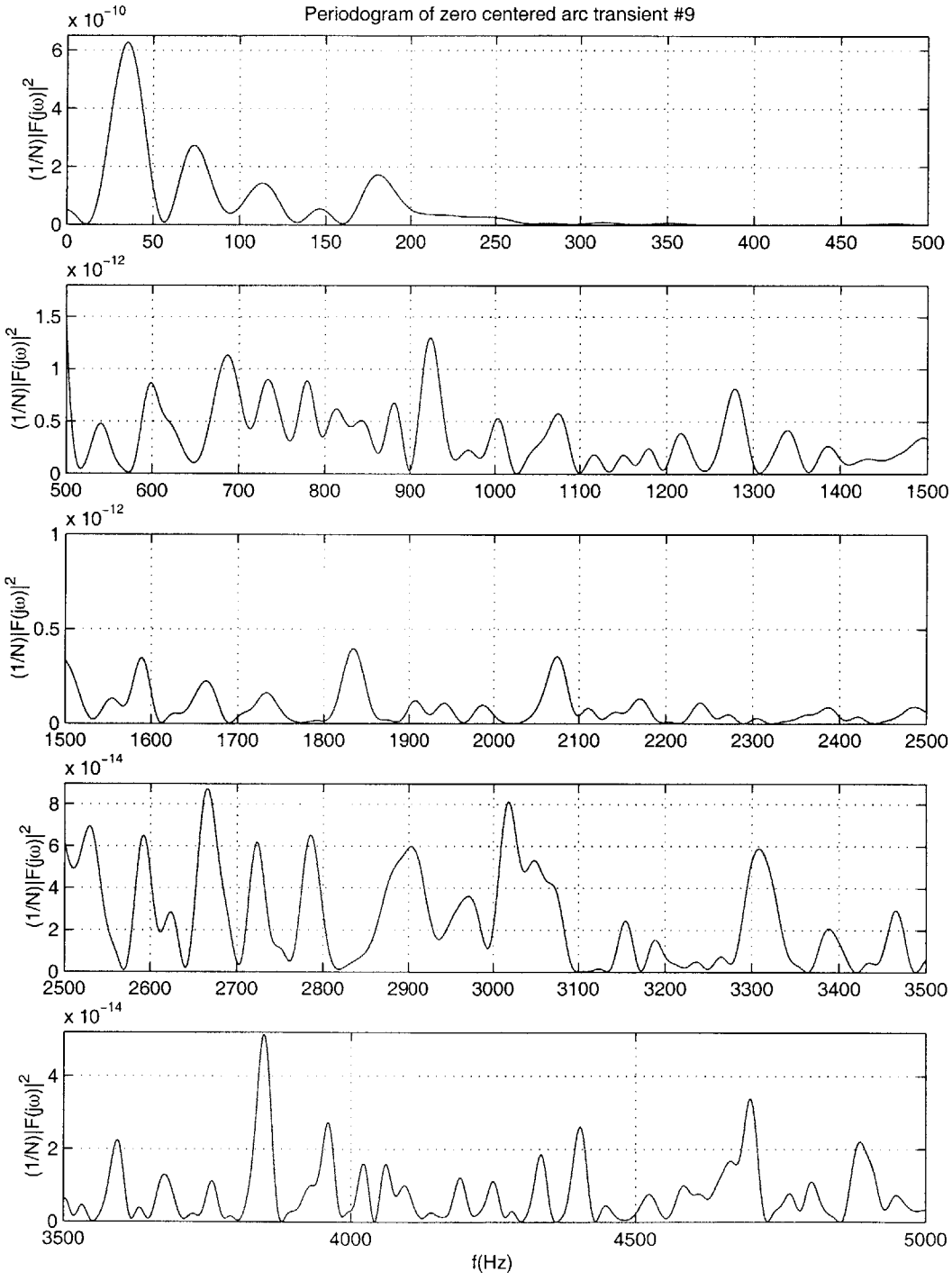
Periodogram of zero centered arc transient #9
x 10^-10
(1/N)|F(jω)|^2
0
2
4
6
0
50
100
150
200
250
300
350
400
450
500
x 10^-12
(1/N)|F(jω)|^2
0
0.5
1
1.5
500
600
700
800
900
1000
1100
1200
1300
1400
1500
x 10^-12
(1/N)|F(jω)|^2
0
0.5
1
1500
1600
1700
1800
1900
2000
2100
2200
2300
2400
2500
x 10^-14
(1/N)|F(jω)|^2
0
2
4
6
8
2500
2600
2700
2800
2900
3000
3100
3200
3300
3400
3500
x 10^-14
(1/N)|F(jω)|^2
0
2
4
3500
4000
4500
5000
f(Hz)

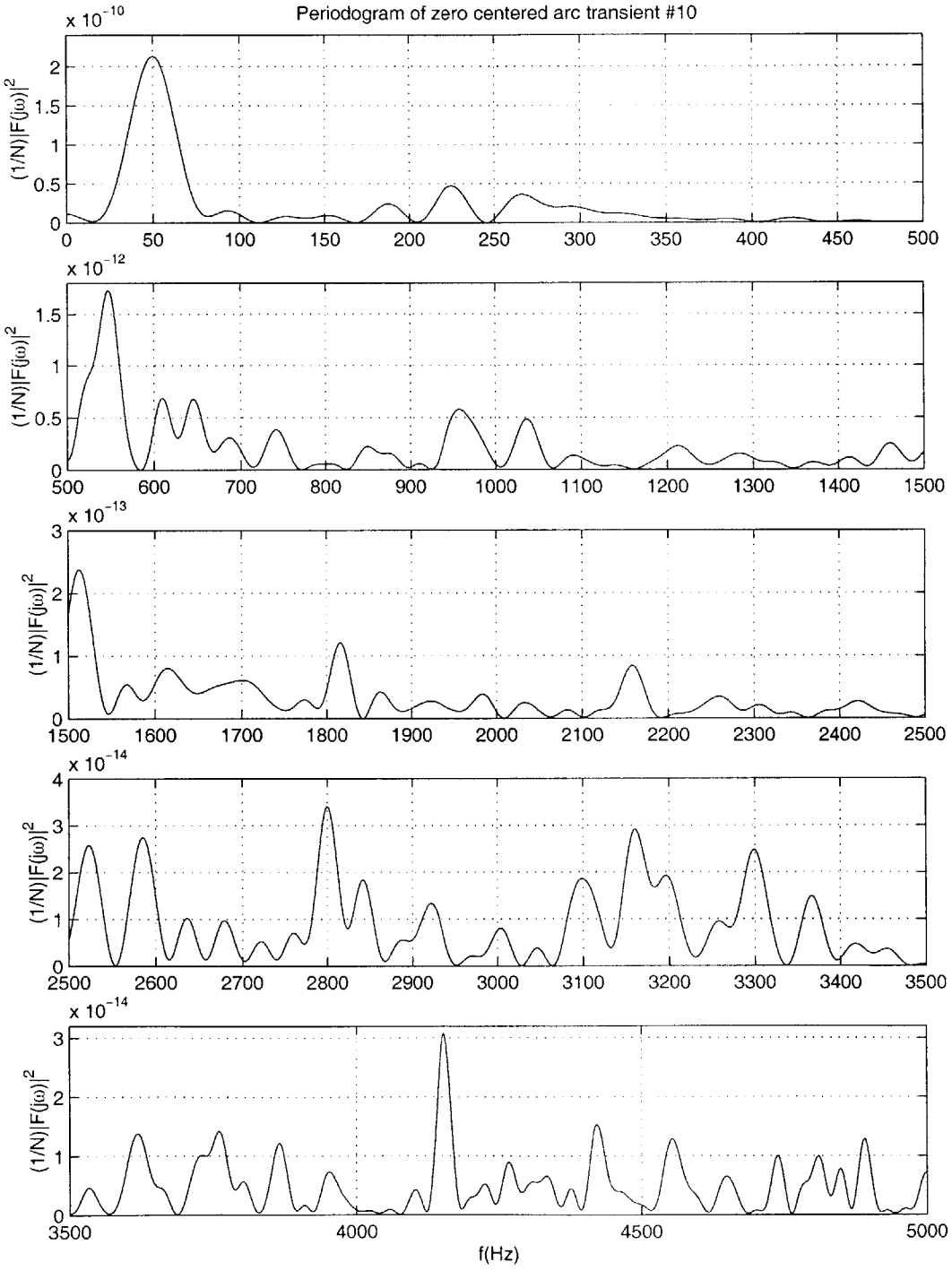
Periodogram of zero centered arc transient #10
x 10^-10
(1/N)|F(jω)|^2
0
0.5
1
1.5
2
0
50
100
150
200
250
300
350
400
450
500
x 10^-12
(1/N)|F(jω)|^2
0
0.5
1
1.5
500
600
700
800
900
1000
1100
1200
1300
1400
1500
x 10^-13
(1/N)|F(jω)|^2
0
1
2
3
1500
1600
1700
1800
1900
2000
2100
2200
2300
2400
2500
x 10^-14
(1/N)|F(jω)|^2
0
1
2
3
4
2500
2600
2700
2800
2900
3000
3100
3200
3300
3400
3500
x 10^-14
(1/N)|F(jω)|^2
0
1
2
3
3500
4000
4500
5000
f(Hz)

Appendix D

Ignition Bypass

In order to obtain circuit current measurements for many electrical loads, the ignition of the 1997 Mercury Sable had to be bypassed. In the off mode, only the door locks and head lights turn on. The accessory mode is needed to run the power windows, windshield wipers, and sunroof while the on mode is needed to simulate the start of the vehicle which includes running the radiator cooling fan and blinking dash lights.

An electrical system diagram was available but location of wires were not specified. It was therefore necessary to be able to turn the ignition key cylinder shown in Figure D.1. Using

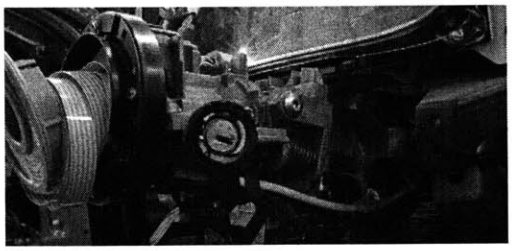

Figure D.1: Ignition key cylinder before bypass

a drill, a hole is drilled directly into the key hole as shown in Figure D.2. Once the drill

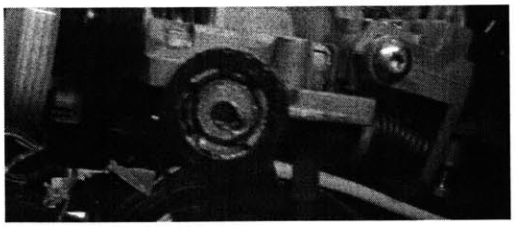

Figure D.2: Ignition key cylinder after drilling

reaches the edge of the cylinder, the cylinder is freed and a sturdy screwdriver can be used to turn the cylinder to the desired mode. Another method would be to attach a dent puller to the ignition cylinder and use the force of the puller to remove the cylinder.

Bibliography

[1] Kassakian, J.G., *Automotive Electrical Systems - The Power Electronics Market of the Future*, Proceedings of the IEEE Applied Power Electronics Conference and Exposition(APEC2000), Vol. 1, p.p 3-9, New Orleans, LA, February 2000

[2] Holm, R.,*Electric Contacts: Theory and Application*, 4th ed. New York:Springer-Verlag, Inc., 1967

[3] Wu, Alan N., *Investigation of Electric Arcs in 42-volt Automotive Systems*, M.Eng. Thesis, Massachusetts Institute of Technology, Department of Electrical Engineering and Computer Science, June 2001

[4] Russell, B.D., Mehta, K., Chinchali, R.P., *An Arcing Fault Detection Technique using Low Frequency Current Components - Performance Evaluation using Recorded Field Data*, IEEE Transactions on Power Delivery, Vol. 3, No. 4, October 1988

[5] Russell,B.D., Chinchali, R.P., Kim, C.J., *Behaviour of Low Frequency Spectra During Arcing Fault and Switching Events*, IEEE Transactions on Power Delivery, Vol. 3, No. 4, October 1988

[6] Russell,B.D., Chinchali, R.P., *A Digital Signal Processing Algorithm for Detecting Arcing Faults on Power Distribution Feeders*, IEEE Transactions on Power Delivery, Vol. 4, No. 1, January 1989

[7] Swift, G.W., Sultan, A.F., Fedirchuk, D.J., *Detecting Arcing Downed-Wires Using Fault Currnet Flicker and Half-Cycle Asymmetry*, IEEE Transactions on Power Delivery, Vol. 9, No. 1, January 1994

[8] Maroni, C.S., Cittadini, R., Cadoux, Y., Serpinet, M., *Series Arc Detection in Low Voltage Distribution Switchboard using Spectral Analysis*, IEEE Sixth International Symposium on Signal Processing and its Appications, Vol. 2, 2001

[9] Sidhu, T.S., Singh, Gurdeep, Sachdev, M.S., *Microprocessor Based Instrument for Detecting and Localizing Eelectric Arcs*, IEEE Transactions on Power Delivery, Vol. 13, No. 4, October 1998

[10] Bartlett, E.J., Vaughan, M., Moore, P.J., *Investigations into Electromagnetic Emissions from Power System Arcs*, International Conference and Exhibition on Electromagnetic Compatibility(Conf. Publ. No. 464), 1999

[11] Boksiner, J., Parente, M., *Power cable arcing fault detection system*, United States Patent 5,047,724

[12] Boksiner, J., Silverman E.J., *Arc Detection for Telephone DC Power Distribution Systems*, IEEE Telecommunications Energy Conference, 1993

[13] Keenan, J., Parker, M., *Arc Detectors*, Telecommunications Energy Conference, 1998

[14] Somerville, J.M., *The Electric Arc*, New York:John Wiley & Sons, Inc., 1959

[15] Schoepf, T.J., Rieder, W.F., *Consequences for Automotive Relays of a 42 VDC Power Network in Vehicles*, IEEE Transaction on Components and Packaging Technologies, Vol. 23, March 2000